EASA
European Aviation Safety Agency

Final Report EASA_REP_RESEA_2013_3

Research Project:

CODAMEIN III

Composite Damage Metrics and Inspection (high energy blunt impact) – 3rd phase

Intentionally left blank

Disclaimer

This study has been carried out for the European Aviation Safety Agency by an external organization and expresses the opinion of the organization undertaking the study. It is provided for information purposes only and the views expressed in the study have not been adopted, endorsed or in any way approved by the European Aviation Safety Agency. Consequently it should not be relied upon as a statement, as any form of warranty, representation, undertaking, contractual, or other commitment binding in law upon the European Aviation Safety Agency.

Ownership of all copyright and other intellectual property rights in this material including any documentation, data and technical information, remains vested to the European Aviation Safety Agency. All logo, copyrights, trademarks, and registered trademarks that may be contained within are the property of their respective owners.

Reproduction of this study, in whole or in part, is permitted under the condition that the full body of this Disclaimer remains clearly and visibly affixed at all times with such reproduced part.

		Hamburg (D)
Bishop GmbH Aeronautical Engineers		

Final Report

Department: Research Project: CODAMEIN III	Report No.: PBH100490A
Analysis type: Test / FEA Classification: CONFIDENTIAL	Project Reference: RBH100948A Customer Reference: EASA.2013.OP.12

Subject: **EASA.2013.OP.12 "Composite Damage Metrics and Inspection (CODAMEIN III)"**

Summary: This report presents the outcomes of the EASA CODAMEIN III research project. The main objectives of this project were, based on the outcomes of the EASA.2010.C13 CODAMEIN I and EASA.2011.NP.24 CODAMEIN II projects, to perform the last of a trilogy of investigations into low velocity high mass impact testing on a similar test panel representing hybrid fuselage structure of a CS-25 Aircraft, in order to improve the understanding of the influence of such impact damage. Three static load cycles were performed within the panel test using a test set up similar to CODAMEIN I and CODAMEIN II, but with changed boundary conditions and tie reinforcements. A stronger shear tie design resulted in the increased damage level. The outcomes of this research demonstrated a potentially significant safety threat of low velocity high mass impacts on composite aircraft fuselages beyond 82.1 kN of impact load, which may cause extensive internal structural damage without clear visual detectability on the external skin surface. Furthermore, the Finite Element Analyses showed good agreement with the testing results in terms of load vs. displacement curve, strain gauge reading and failure modes. Based on the findings of this research, recommendations for amending safety regulations for composite CS-25 fuselages are proposed.

Panel Storage: At the time of entry the CODAMEIN III panel is stored at Bishop GmbH, Blankenese Bahnhofstraße 12, D-22587, Hamburg, Germany.

Date: 02.12.2014	Prepared: Dr. D. Zou	Checked: P. Bishop		C. Haack	A. Bezabeh	Dr. R.Thomson	Approved: E. Isambert	Archive: W:\EASA_CODAMEIN_III_RBH100948 A\D_Documentation\1_Report\Final Report
Signature								

Distribution		Issue	Date:		N. Pages:		Changed pages:	Valid from/for:
P. Bishop	Bishop GmbH	A.	17.11.2014		110			A 350, B 787
Dr. D. Zou	Bishop GmbH	B.	27.11.2014		113			
C. Haack	Bishop GmbH	C.	18.02.2015		115			
A. Bezabeh	Bishop GmbH							
E. Isambert	EASA							
Dr. S. Waite	EASA							
E. G. Sanchez	EASA							
Dr. R. Thomson	ACS Australia							
Archive								

Table of Contents

Table of Figures

Department: Research	Date: 02.12.2014	Prepared: Dr. D. Zou	Checked: P. Bishop, C. Haack Dr. R. Thomson, A. Bezabeh	
				Page 3

List of acronyms

CODAMEIN	Composite Damage Metrics and Inspection
EASA	European Aviation Safety Agency
CS-25	Certification Specifications for Large Aeroplanes
UCSD	University of California San Diego
GSE	Ground Service Equipment
CFRP	Carbon Fibre Reinforced Plastic
UD	Unidirectional
DOF	Degree(s) Of Freedom
FE	Finite Element
Fr	Frame
ST	Shear Tie
Str	Stringer
kN	Kilonewton
µm/m	Microstrain
SG	Strain Gauge
LVDT	Linear Variable Differential Transformer
NDT	Non-destructive Testing
UL	Ultimate Load
LL	Limit Load
DBH	Internal Naming of Bishop GmbH Engineering Drawings

Acknowledgements

1. Introduction

1.1.   Background

Fiber-reinforced composite materials have wide-spread applications in light-weight aircraft structural components. In particular they are increasingly used in critical structure applications, e.g. wing box and fuselage pressure hulls. It is well-known that composites can be characterized by a high strength-to-weight and stiffness-to-weight ratio, but they can be easily damaged by transverse loads, such as those arising from indentation and impact loading (e.g. ground service vehicles). The aviation industry has acknowledged the risks associated with serious ground operation incidents and accidents. Consequences of these events result in aircraft damage, delays and financial cost to the industry [Mikulik, Haase 2012]. In 2000, the Airports Council International (ACI) reported that US$3 billion of losses were caused by airport ground vehicles colliding with aircraft, aircraft hitting each other or other objects around the airport. Narrowing down the focus to aircraft damage during ground operations, it has been reported that 50% of major damage has been recorded to be caused by baggage vehicles while 60% of minor damage was caused by collision of aircraft with ground vehicles. Billions of dollars in losses were caused by airport ground vehicles [Pringle 2010].

Moreover, the change from using conventional metallic alloys to composite materials must not compromise 'Acceptable Level of Safety'. Aircraft certification requires demonstration of the capacity of structure to carry ultimate load (UL) throughout the entire aircraft life with barely visible manufacturing flaws and in service damages and carry between UL and limit load (LL) for substantiated inspection periods with more substantial damages. The demand for sooner detection of damages that weaken the structure closer to LL capability, as described in EASA AMC 20-29 [EASA 2010] (see Figure 1), can be achieved by appropriately substantiated inspections throughout the entire aircraft life.

A source of concern is that blunt impacts could affect wide areas of structure and multiple structural elements, resulting in higher category damage, such as Category 5 damages, which should be obvious, reported, and requires immediate repair. Category 5 damage is considered to be outside the certification process. Therefore, it becomes necessary to clearly understand the boundaries between category 2/3 and category 5 damages respectively.
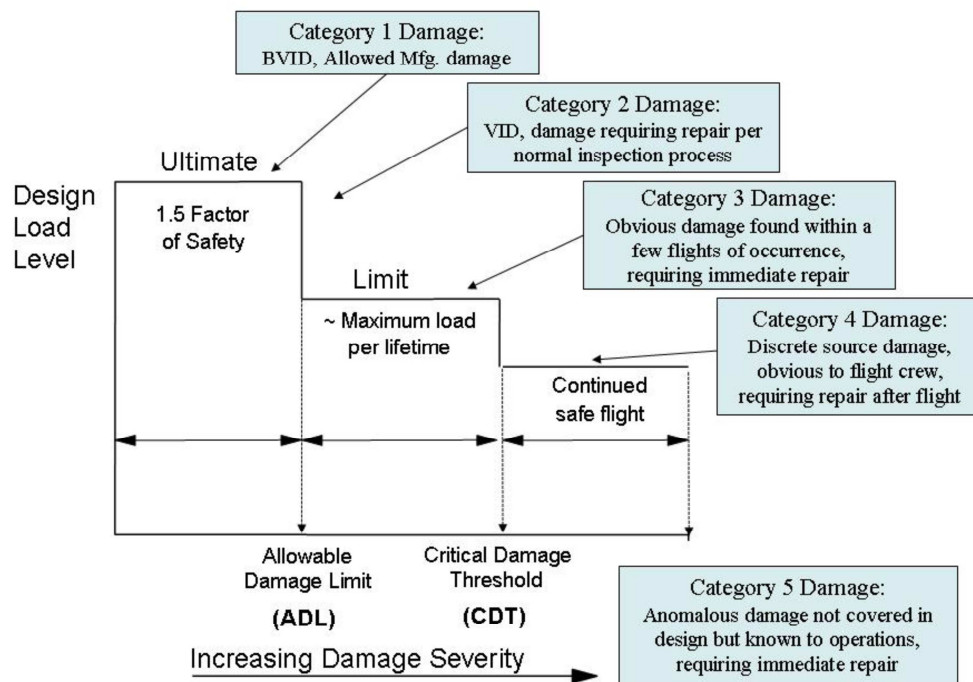
Figure 1. Schematic diagram showing design load levels versus categories of damage severity [EASA 2010]

With newly developed all-composite fuselage aircraft coming into service, more composite skin surface is likely to be subjected to such impacts. Therefore, blunt impact damage is of key interest, particularly which potentially leaves little or no externally visible detectable signs of damage and which involves large contact areas.

In order to address the difficulties of being able to predict and detect the damage resulting from blunt impact, and to evaluate its effect on structural performance, investigation of the development of impact damage is required.

EASA CODAMEIN Blunt Impact Focus. A comprehensive literature overview related to ground damages caused to aircraft at airports (e.g. during ground handling operations) has been performed in the CODAMEIN I project [Mikulik, Haase 2012]. Blunt impacts can result from various sources and involve a wide range of energy levels. Within the trilogy of EASA CODAMEIN projects, the main focus is the ground service equipment (GSE) impact. The initiation and progression of damage caused by a collision with a ground service equipment vehicle fitted with a rubber bumper was evaluated and a representative scenario for testing and numerical analysis has been performed to assess the boundary conditions for an impact test on a hybrid design fuselage panel.

1.2. Objectives

The main objectives of the CODAMEIN III (Composite Damage Metrics and Inspection) project are:

- To improve understanding of the formation of high energy blunt impact damage on hybrid composite metallic aircraft structures
- To investigate the significance to damage initiation, growth and detection resulting from possible design detail changes, i.e. for the purposes this study, a shear tie design change
- To investigate key impact parameters that increase the damage initiation level and produce significant impact damage with no or low visible damage to the impacted surface
- To correlate the structural performances of the panel with the full barrel by changing the flexibility of frame attachments, i.e. change the Boundary Conditions
- To perform the third test campaign for validating the finite element model and developing recommendations regarding composite-metallic structure damage tolerance and residual strength
- Damage tolerance assessment with focus on conditions related to loss of load carrying capability for certain damage levels

1.3. Summary of Previous Results

1.3.1. Outcomes of CODAMEIN I

Within the CODAMEIN I project, a hybrid design test panel (CFRP skin and stringer, metallic frames) was designed to provide a representative fuselage structure of a modern long range CS-25 airplane with a primary structure mainly made of composite material. The panel design was based on the same general lay-out of the test panels used in the UCSD research. Contrary to the full composite design (CFRP skin, stringers and frames) of UCSD's test panels that incorporate C-frames, the CODAMEIN I test panel used aluminum Z-frames. By performing Finite Element (FE) analyses of the test panel alongside a full fuselage barrel model, the boundary conditions for a suitable test were assessed. Physical properties of current GSE vehicles have been analyzed. Using reports of GSE-to-aircraft collision incidents, representative levels of the impact parameters were found. Since the high energy blunt impact of a vehicle, equipped with a rubber bumper, was considered to be a main threat for the generation of impact damage with low or no visibility on a composite aircraft fuselage, an impact case using a common circular GSE rubber bumper was chosen for investigation. A quasi-static test was performed by loading the panel in three cycles. The first load cycle was run until the first noticeable load drop, which was also highlighted by an audible event. Since A-scan inspection showed no delamination

in the skin, delamination in the shear tie radii was expected to be the first point of damage onset. The failure threshold energy for the first damage onset was 1270 J, which represents a vehicle with a mass of 2500 kg impacting the fuselage with a velocity of 1 m/s. The second load cycle was stopped when several shear ties in the panel centre showed significant radius cracking (see Figure 2), which accompanied a continuous softening of the panel. Besides the multiple shear tie damage, which was clearly visible in the loaded state and became invisible after unloading, no further damage was detected either visually or by A-scan.

Figure 2. Shear tie damage in CODAMEIN I 2nd load cycle [Mikulik, Haase 2012]

In the third load cycle, several shear ties failed, the centre frames came into contact with the centre stringers and the frames showed significant rotation. The third load cycle was stopped just before the estimated point of plastic deformation of the frames in order to prevent permanent deformation of the panel. A maximum energy of 2660 J was applied in the performed load cycles. The final inspection showed damage and failure of several shear ties as well as minor surface damage to the frames and stringers due to contact between those parts. The shear tie failure and stringer damage at frame 3 is shown in Figure 3. No delamination was detected in the skin and the stringers after the test.
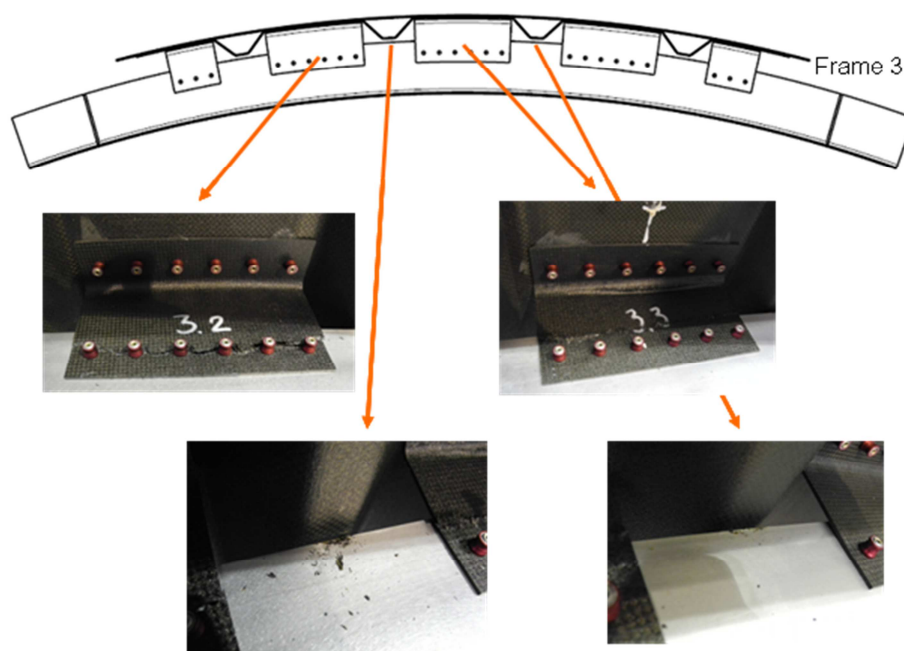
Figure 3. Shear tie failure and stringer damage in CODAMEIN I 3rd load cycle [Mikulik, Haase 2012]

1.3.2. Outcomes of CODAMEIN II

Following CODAMEIN I project, the CODAMEIN II tests delivered a broad platform of information which enabled a better understanding of the behaviour of the panel in the impact test. The general behaviour showed a high similarity to that recorded in the CODAMEIN I test. The first damage events were noticed at slightly lower loads than in the CODAMEIN I test. This might be caused by the increased boundary stiffness (the spring arrays with a stiffness of 8.5 kN/mm at each of the inner three frames in the CODAMEIN test, spring arrays with a stiffness of 9.5 kN/mm were used for all five frames in the CODAMEIN II test) or by small deviations between the two mainly identical test panel as the parts of the panel were manufactured in a manual process and assembled using Hi-Lok fasteners. The quality control revealed an improved precision of the CODAMEIN II panel, likely due to reported improvements in the manufacturing process as result of the experience from the previous manufacturing process. The modification of the boundary stiffness of the test set-up was done based on the results of simulations of an improved fuselage barrel model. The barrel model used represents an advancement of the existing model of CODAMEIN I including a representative inner structure which slightly increased the stiffness of the barrel model under impact loading.

Since EASA had stated the intention to use the test panel for CODAMEIN II again in another test, the target load and damage situation of the current test was reduced. Thus the stop criterion for this test was defined as the failure of shear ties which was expected to happen prior to any damage to other parts of the panel.

Based on the result of the CODAMEIN I test and the tests of UCSD, it was assumed that the expected shear tie failure would lead to contact between the stringers and frames. This event was expected to occur suddenly and with no possibility to be stopped. Therefore, in order to avoid any potential damage, especially to the stringers, it was decided to not continue loading up to shear tie failure.

Two static load cycles were performed within the panel test using a test set-up similar to the CODAMEIN I test, but with an increased boundary condition stiffness. A maximum impact energy of 1443 J was induced to the panel and local damage was generated in the centre shear ties. The damage onset threshold was found to be 970 J. Based on the outcomes of CODAMEIN I and the investigations of the University of California San Diego (UCSD), a typical damage sequence was anticipated which involved shear tie damage and failure as the first stage of damage.

The first load cycle was run up to a load of 39.5 kN and stopped at a damage event which caused a load drop of 1 kN. The only visible evidence of damage after the first load cycle was a crack in the radius of the centre shear tie no. 3.3 (see Figure 4) which covered ¾ of the width of the shear tie [Haase 2013].
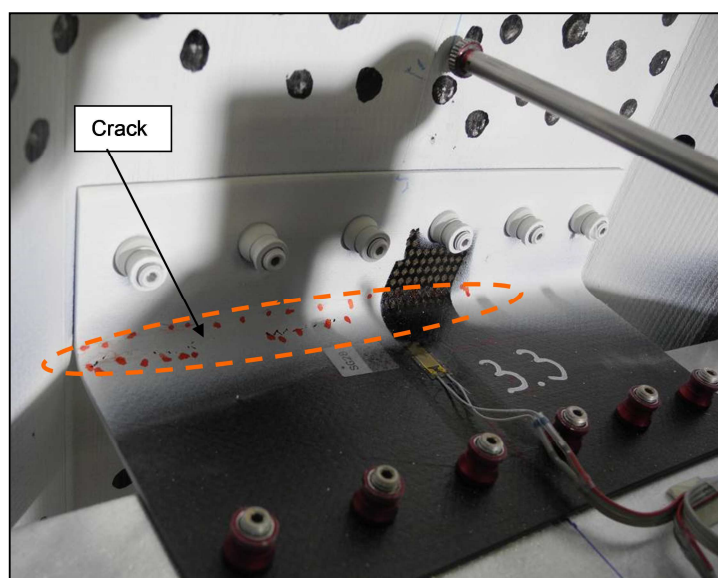
Figure 4. Damage after 1st load cycle: Crack in the centre shear tie no. 3.3 [Haase 2013]

The second load cycle was run up to a load level of 57 kN which corresponds to the maximum load of the second load cycle of the CODAMEIN I test. After exceeding the maximum load of the 1st load cycle,

damage onset and damage growth mechanisms were audible in terms of single cracking sounds or continuous cracking sounds which were assigned to the damage to the two centre shear ties ST 2.3 and ST 3.3 as well as ST 3.4. No load drop occurred prior to the maximum load of the 2nd load cycle. Figure 5 shows the panel inside at maximum load and the slight bending of the three centre frames is visible.
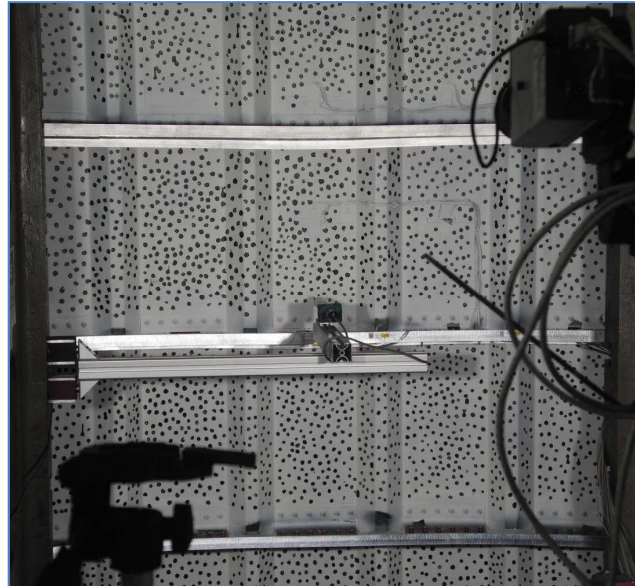
Figure 5. Panel inside at 2nd load cycle max. load [Haase 2013]

The distribution of the panel displacement in the impact direction is displayed at six load levels in Figure 6. At the maximum load of 57 kN, a displacement of 130 mm was measured. The damage event at maximum load resulted in a load reduction to approximately 54 kN, and then a further reduction to 50 kN as the center frame relaxed in torsion, resulting in the displacement distribution displayed in Figure 6.
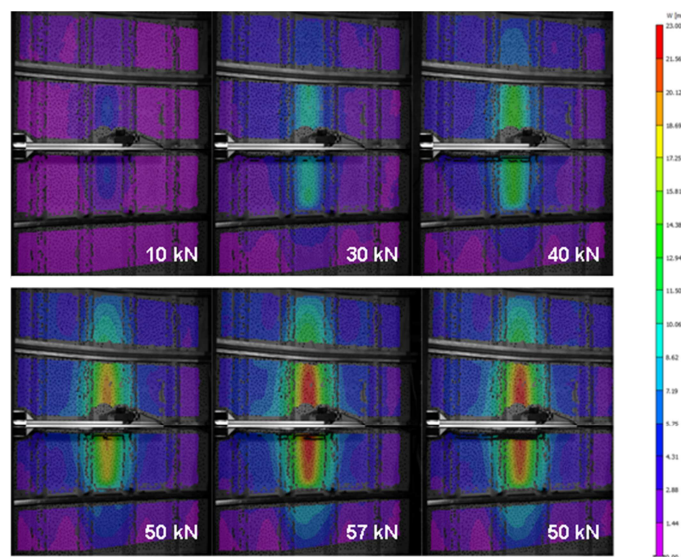
Figure 6. Panel displacement in impact direction (video correlation system): four load levels, max. load, unloading [Haase 2013]

After unloading the 2nd load cycle, the shear tie no. 2.3 exhibited initial cracking in the radius (see a. of Figure 7) along with delamination marks at the side of the radius (see b) of Figure 7). The crack in the shear tie no. 3.3 developed through the full width of the shear tie (see a) of Figure 8). Delamination was visible on both sides of the radius (see b) of Figure 8). The shear tie no. 3.3 also showed a crack along the entire width of the radius (see a) of Figure 9) and delamination of the radius (see b) of Figure 9). The delamination marks indicated delamination of multiple plies throughout the thickness of the shear ties and covering approximately the full radius curvature.
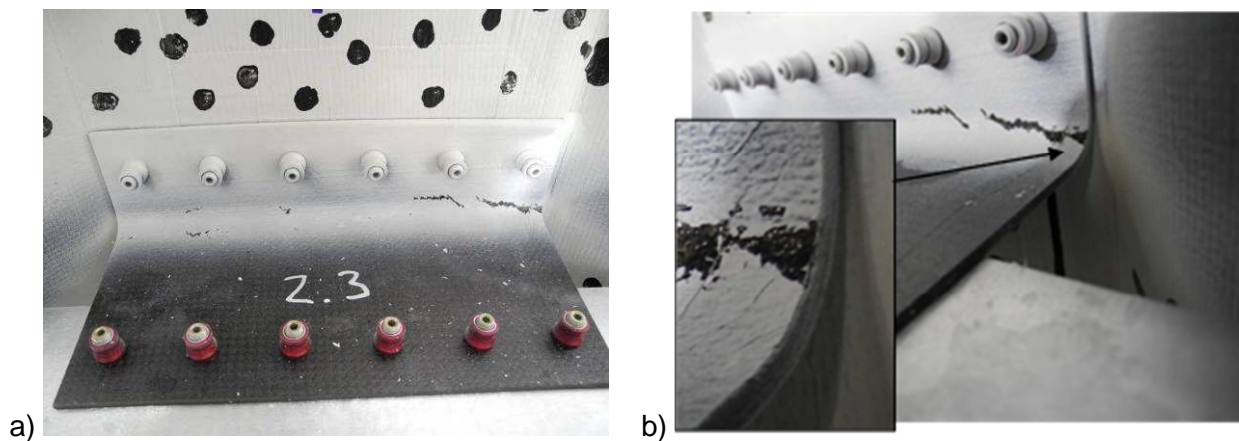
Figure 7. Shear Tie no. 2.3 after 2nd load cycle [Haase 2013]
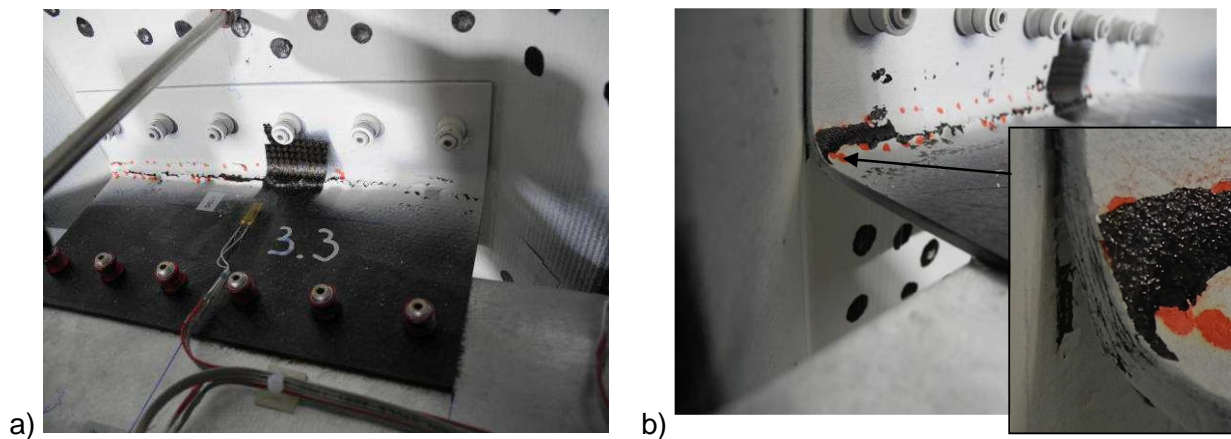
Figure 8. Shear Tie no. 3.3 after 2nd load cycle [Haase 2013]

a)   b)
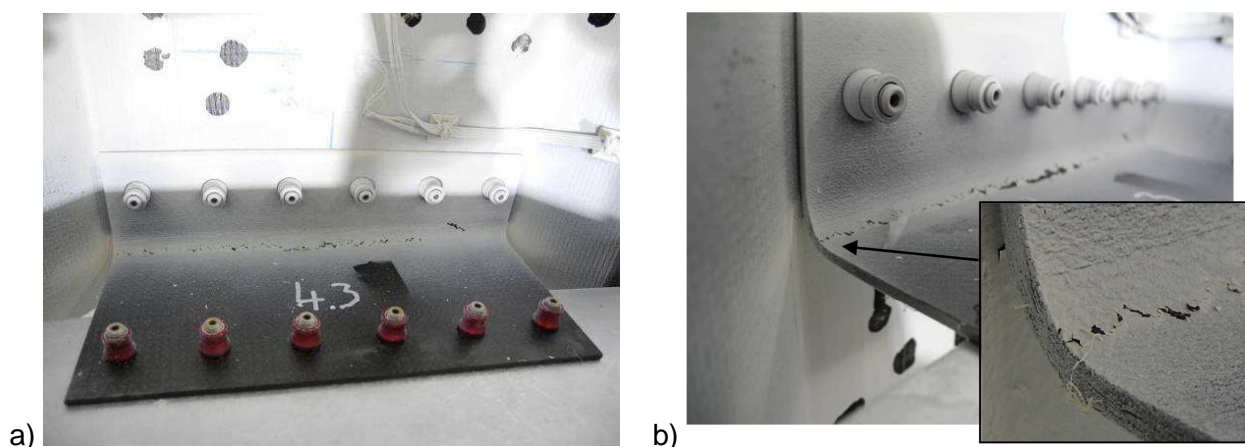
Figure 9. Shear Tie no. 4.3 after 2nd load cycle [Haase 2013]

1.4.   Results of the UCSD Research

The FAA-funded research work of Prof. Hyonny Kim's team at the UCSD uses a multi-step investigation of damage in composite fuselage structures caused by high energy blunt impacts. The aim of UCSD's research is to characterize blunt impact threats and locations and to understand damage formation and its relationship to visual detectability [Kim 2010], [Kim 2013]. Both quasi-static and dynamic tests have been performed on panels of differing sizes that are based on the part design concept which also influenced the design of the CODAMEIN I / CODAMEIN II / CODAMEIN III test panels. The design of UCSD's test panels incorporates a composite skin, composite omega stringers, composite C-frames and composite shear ties. The test panel types "stringer specimen" and "frame specimen" are illustrated in Figure 10.

Figure 10. UCSD "stringer specimen" and "frame specimen" [Kim 2013]

These two types of test specimens are summarized as below:

- Large Scale Specimen - Frame Specimen Frame01 (Quasi-Static Test) [Kim 2013]. The first stage quasi-static specimen involved a 3-frame curved test panel. Having four co-cured stringers, loading was applied over a distributed zone across a portion of the center of the specimen (on the skin between the two stringers), spanning from Frame 1 to Frame 2 as depicted in Figure 10. The upper attachments of the large scale specimens provide controlled rotational frame end via flexure plates and translational degrees of freedom (DOF) and the lower set of frame ends has the same controlled rotational stiffness, simulating the behaviour of the surrounding fuselage structure. More details can be found in Section 2.1.3.

- Large Scale Specimen - Frame Specimen Frame03 (Dynamic Test) [Kim 2013]. The second stage dynamic test specimen involved a larger 5-frame panel. The difference to the first-stage quasi-static specimen is the length of the panel in the longitudinal direction, the rest remained identical. The 3 inner frames are attached the same as the in first-stage quasi-static specimen and the 2 outer frames were simply supported at each end without any rotational stiffness constraint.

A load-displacement plot of a quasi-static indentation (Frame01) and dynamic impact (Frame03) tests and the typical damage of Frame01 specimen is shown in Figure 11.
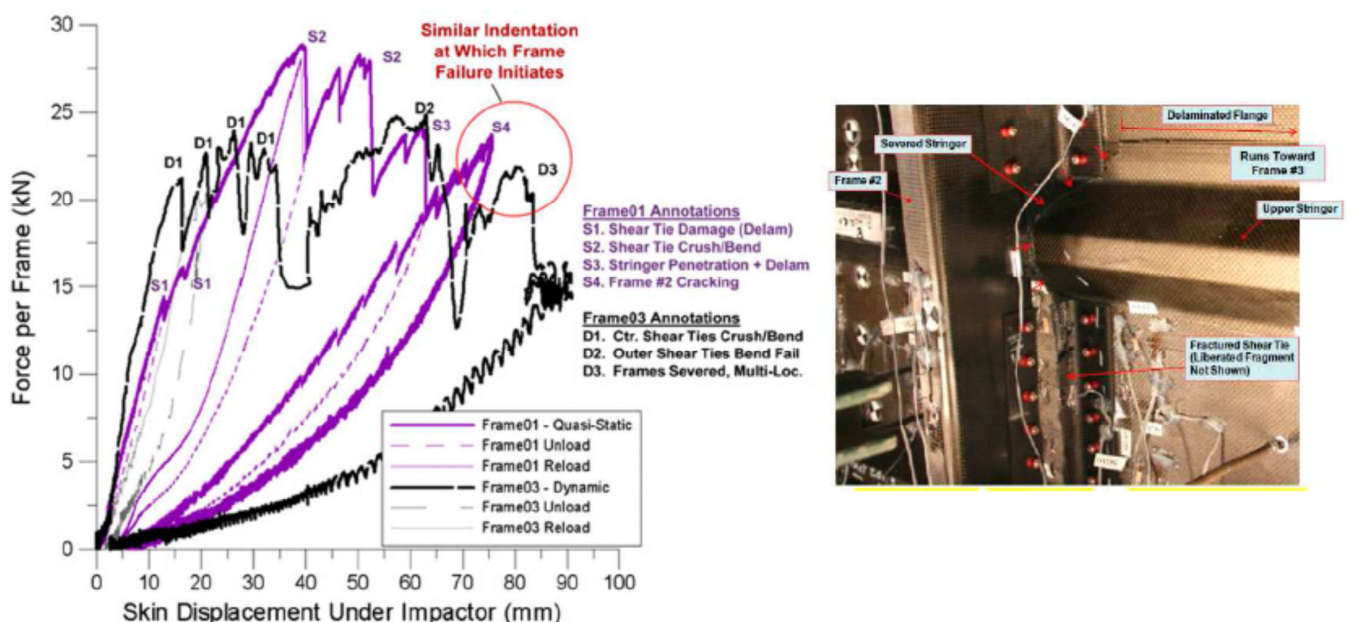
Figure 11. Force per frame comparison vs. skin displacement for quasi-static indentation (Frame01) and dynamic impact (Frame03) tests [Kim 2013].

The UCSD tests with rubber bumper impactors delivered valuable results regarding generation of significant damage with low or no visual detectability. A progressive failure process was established, which explains the single steps of local damage, stiffness reduction and load diversion (see Figure 12). The typical order of damage events of a 4-stringer 3-frame panel (Frame01) quasi-statically impacted by a rubber bumper between two stringers, first shows shear tie crushing, then delamination and multiple shear tie failure, followed by contact between the frames and the stringers due to the rotation of the frames. The test was stopped at the visible crack in one of frame webs.

The typical order of damage events of a 4-stringer 5-frame panel (Frame03) dynamically impacted by a rubber bumper between two stringers and across 3 frames, first shows a moderate crushing damage (bending failure) in the radius area of the shear ties directly under the impactor occurred, no delamination between the skin and stringers, then by rotation of the C-frame, scraping along the stringer, leading to failure of the outer set of six shear ties. The final fracture occurred near the boundary fixture joints with a combination of torsion, bending and shear. This failure is classified as a non-local failure since the failure locations were relatively far away from the impact contact region.
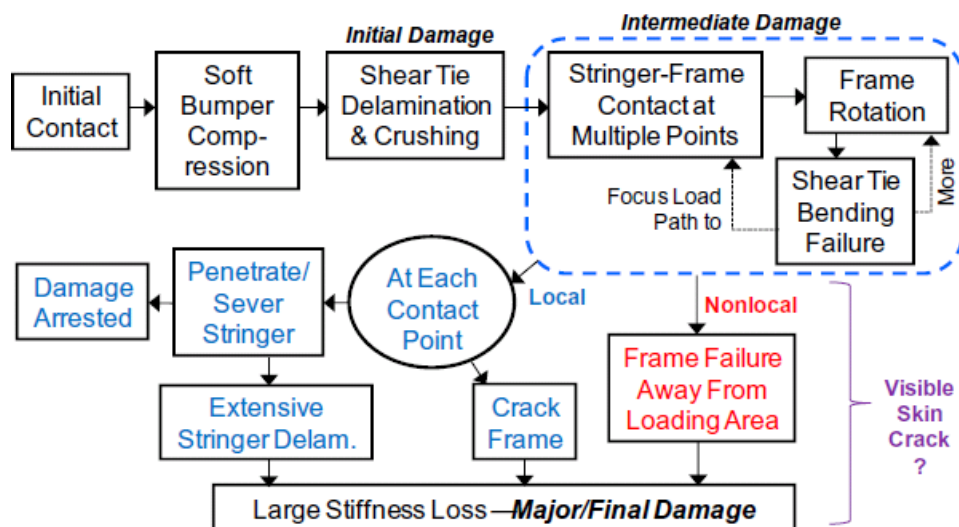
Figure 12. Damage Progression Process (Kim 2014)

2. Methodology

The methodology to assess the influence of high mass low velocity impact damage, and also the extent of formed damage, was applied to a five-frame, four stringer aircraft fuselage panel. This includes developing an understanding of failure modes, internal stresses, permanent damage level and degree of damage visibility. This will be achieved by a combination of experimental observation of the evolution of damage modes via different designs through the three project phases, the determination of the damage sequence, and analyses of these tests, which includes the validation of finite element models. The primary interest was to better understand the potential for damage with little or no visual detectability under this impact event. Moreover, the correlation between testing and analyses of blunt impact events will be established, especially on the representative boundary stiffnesses as determined from an analytical model of the full barrel.

Firstly, the re-use of the CODAMEIN II test panel apart from the shear ties was decided. Since an advancement of the FEA fuselage barrel model achieved in CODAMEIN II objectives and an increased stiffness of the barrel was expected as consequence of the involvement of more stiffening structure details, an increase of the test boundary stiffness was anticipated, compared to CODAMEIN I. Apart from the translational stiffness, the rotational stiffness plays an important role in determining the equivalence with the barrel model. The major design change to the test panel was to increase the thickness of the shear ties (from 2.5 mm to 5.28 mm) and extend boundary conditions to all five frames instead of three. A minor design change to the panel boundary was integrated to reduce the risk of undesired boundary failure of the panel. Based on the limitations in the FE representation that were found within CODAMEIN I, numerous new approaches and new feature integrations were planned for CODAMEIN II, such as the weak layers in the rivet line, cohesive surface implemented in the interfaces. Furthermore, with newly designed boundary stiffnesses and stronger shear ties in CODAMEIN III, more representative information about the test panel performance was generated, which covers the post-damage range.

Based on the results of CODAMEIN I & II and the investigations performed by UCSD, several general approaches were considered for CODAMEIN III. Since all activities conducted within in CODAMEIN projects and by UCSD present advantages and disadvantages, the approach with a maximum of comparability and flexibility was chosen. Therefore, CODAMEIN III methodology evolved through the previous experiments, modelling development and communication of results between Bishop GmbH and UCSD.

2.1.   Experiments

2.1.1.   CODAMEIN III Test Panel Design

The literature review and input from the UCSD were used to establish a credible baseline design for the hybrid test panel investigated in CODAMEIN III. The design is based on that of the CODAMEIN II test panel [Mikulik, Hasse 2012], i.e. in accordance with recent CS-25 aircraft design principles, and the configuration used in the UCSD work. The UCSD and the CODAMEIN I / CODAMEIN II test panels [Hasse 2013] have a similar level of complexity and were comparable due to the similarity of the majority of parts and materials. Furthermore, the stiffnesses of the frames were matched, although being of differing section and materials. The test panel configuration was chosen to represent the structure local to lower fuselage door cutouts, whilst not representing the details very local to the cut-out edge, as shown in Figure 13. This is relevant regions for this investigation since the hybrid fuselage design might be used in this region, including locally in an otherwise full composite design, where the investigated type of damage occurs under static high energy blunt impact.
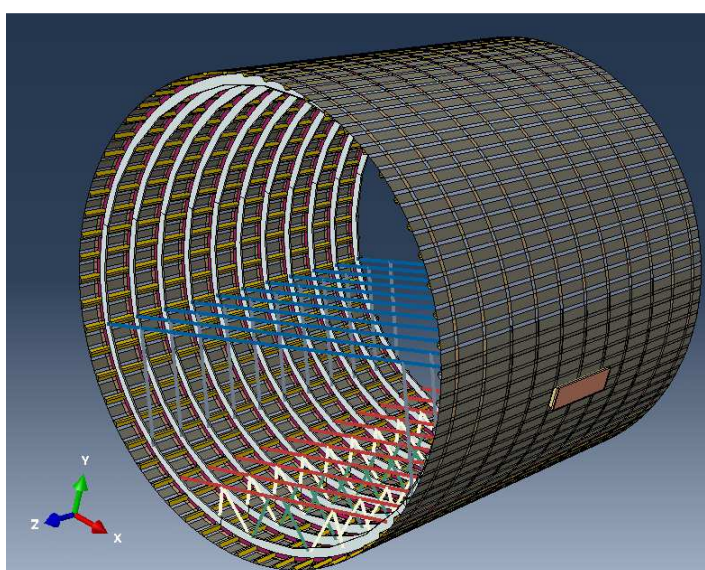
Figure 13. Full barrel FE model

Based on the knowledge of the shear ties being the parts to most likely fail first, the CODAMEIN II test was stopped after the second load cycle around 57 kN of actuator force in order to avoid further damage. The CODAMEIN I test showed that sudden multiple shear tie failure led to immediate contact between frame and stringer in the third load cycle. Therefore, the CODAMEIN III test panel was that used in CODAMEIN II (following NDI confirmation that no damage existed) except for use of replacement of the shear ties. A design with stiffer shear ties is introduced for the CODAMEIN III panel in order to investigate potentially different failure modes, in line with UCSD.

The panel configuration was approximately 1930 mm in the axial direction by 1830 mm in the circumferential direction and was of CFRP skin, four co-cured CFRP omega-stringer, five Aluminium Z-frames and L-shaped CFRP shear tie constructions. An overview of the panel design for CODAMEIN III is shown in Figure 14.
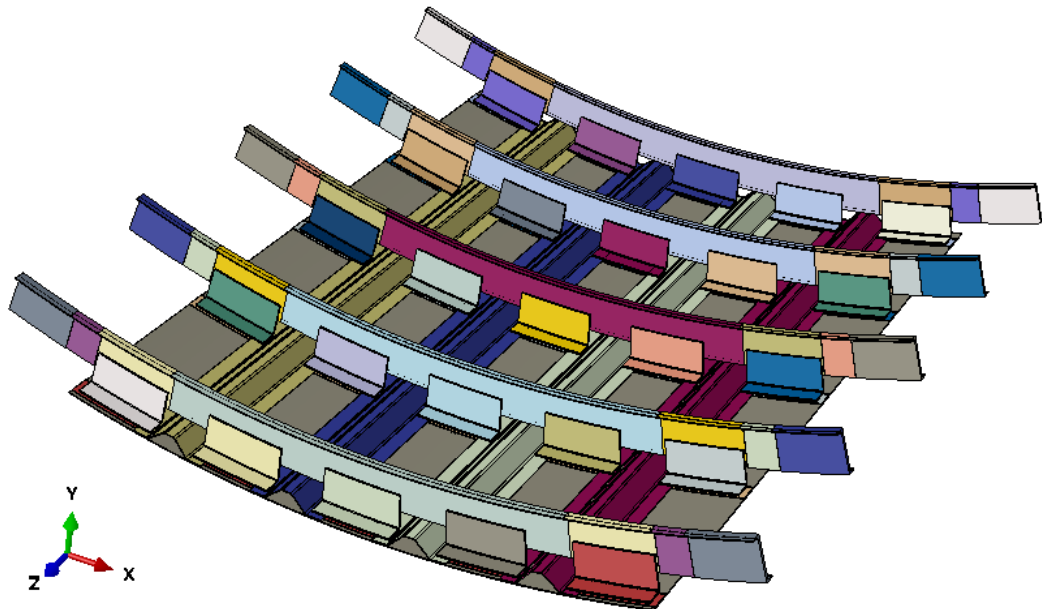
Figure 14. Overview of the CODAMEIN III panel

Skin and stringers are made from aerospace grade carbon fibre reinforced epoxy unidirectional tape (X840 Z60 12k) and plain weave fabric (X840 Z60 PW) prepreg, procured from Cytec Industries Inc. The Z-frames were manufactured from Aluminium 7075-T6 and Hi-Lok fasteners were used to attach the shear ties to the skin, the stringer feet and the frames. Shear ties (clips) are made of T800H-39002D PW prepreg from Toray Industries since it was difficult to obtain the previous material plain weave fabric (X840 Z60 PW) prepreg of Cytec Industries in short time and at reasonable expense. However, a comparable material T800H-39002D PW was selected and it has been used in primary structures of aircraft. Advantages arising from using T800H-39002D compared to X840 Z60 are listed below:

- Excellent value and with short deliverable time

Disadvantages are mainly:

- Elastic modulus and strengths are weaker
- Available average roll size was approximately 95m², but only 45m² was required.

Stacking sequences of all composite parts are summarised in Table 1. The skin panels have sixteen unidirectional layers with fabric on each side. The stringers have 14 UD plies with fabric on each side, while the shear ties consist of 24 fabric plies. The laminates are quasi-isotropic and symmetric.

Table 1. CODAMEIN III: Part Composite Lay-ups

Skin (Cytec)		Stringer, Shim (Cytec)		Shear tie (Toray)	
Material type	Orientation	Material type	Orientation	Material type	Orientation
Fabric	0	Fabric	0	Fabric	45
UD	0	UD	0	Fabric	0
UD	45	UD	45	Fabric	45
UD	90	UD	-45	Fabric	0
UD	-45	UD	90	Fabric	45
UD	0	UD	45	Fabric	0
UD	45	UD	-45	Fabric	45
UD	90	UD	0	Fabric	0
UD	-45	UD	0	Fabric	45
UD	-45	UD	-45	Fabric	0
UD	90	UD	45	Fabric	45
UD	45	UD	90	Fabric	0
UD	0	UD	-45	Fabric	0
UD	-45	UD	45	Fabric	45
UD	90	UD	0	Fabric	0
UD	45	Fabric	0	Fabric	45
UD	0			Fabric	0
Fabric	0			Fabric	45
				Fabric	0
				Fabric	45
				Fabric	0
				Fabric	45
				Fabric	0
				Fabric	45

The properties and ply thickness of the materials are reported in Table 2.

Table 2. The material properties of T800H-39002D PW and X840 Z60 PW (UD)

	X840 Z60 PW prepreg of Cytec	T800H-39002D PW prepreg of Toray	Cytec X840 Z60 UD
Young's Modulus (GPa)			
E_{11}	80	69	168
E_{22}	80	66	8
E_{33}	13.8	-	-
Poisson's Ratio			
v_{12}	0.06	0.06	0.27

v_{23}	0.37	0.1	-
v_{13}	0.5	-	-
Shear Modulus (GPa)			
G_{12}	6.5	4	6
G_{21}	4.1	4	6
G_{33}	5.1	-	3
Lamina Thickness (mm)			
Ply Thickness	0.208	0.22	0.1422
Density (g/cm³)			
Lamina Density	1.6	1.51	1.76
Strength (MPa)			
(S_{11}) Tensile	992.8	963	2800
(S_{11}) Compressive	772.2	671	1620
(S_{22}) Tensile	-	883	55
(S_{22}) Compressive	-	600	220

As not all relevant material parameters of the used material were known, several properties such as the shear modulus and the fracture toughness of the composite materials had to be estimated using data of similar materials.

The CODAMEIN III testing aims to increase the shear tie stiffness and strength, while remaining representative of CS25 configuration. The stiffness and the strength of the new shear ties shall equalize the early failure of the shear ties and enable a more expectable distribution of damage threat to the other components of the panel.

2.1.2.   Comparison between the CODAMEIN II and III Test Panel Designs

The CODAMEIN III panel is generally similar to the CODAMEIN II panel. It integrates a major design change by including stronger shear ties (doubling the thickness) in order to investigate the potential for changes to the extent and modes of damage. Moreover, a minor design change at the panel boundary was incorporated, i.e. reinforcement of the boundary region of the frames. The CODAMEIN III testing expected to reach a higher level of panel deformation compared to the CODAMEIN II test. To ensure the equal flexibility of the frame attachments, the boundary stiffnesses were added to all five frame ends instead of three. An overview of the panel designs for CODAMEIN II and CODAMEIN III is shown in Figure 15.
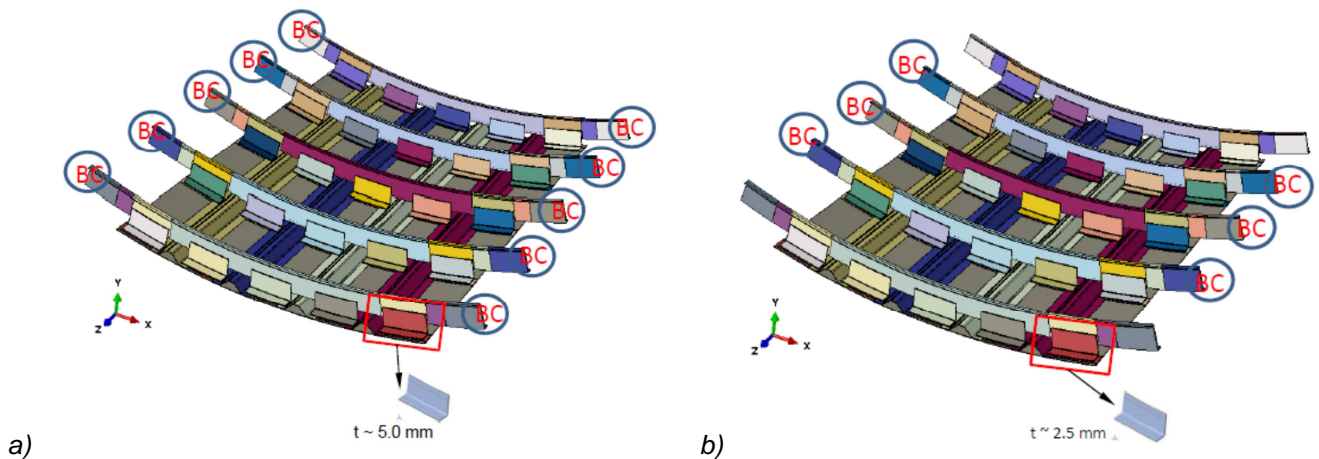
Figure 15. Overview of panels: a) CODAMEIN III panel; b) CODAMEIN II panels

Figure 16 shows the boundary conditions in top view of the CODAMEIN II panel and axial view of the CODAMEIN III panel. For CODAMEIN II panel, the axial rotations are allowed in both frame ends. In the boundary conditions of CODAMEIN III panel, the axial rotations are controlled in such a way that the overall behaviour of the panel is comparable to the full barrel. The calculated rotational stiffness boundary conditions are added to both frame ends as highlighted.

b)
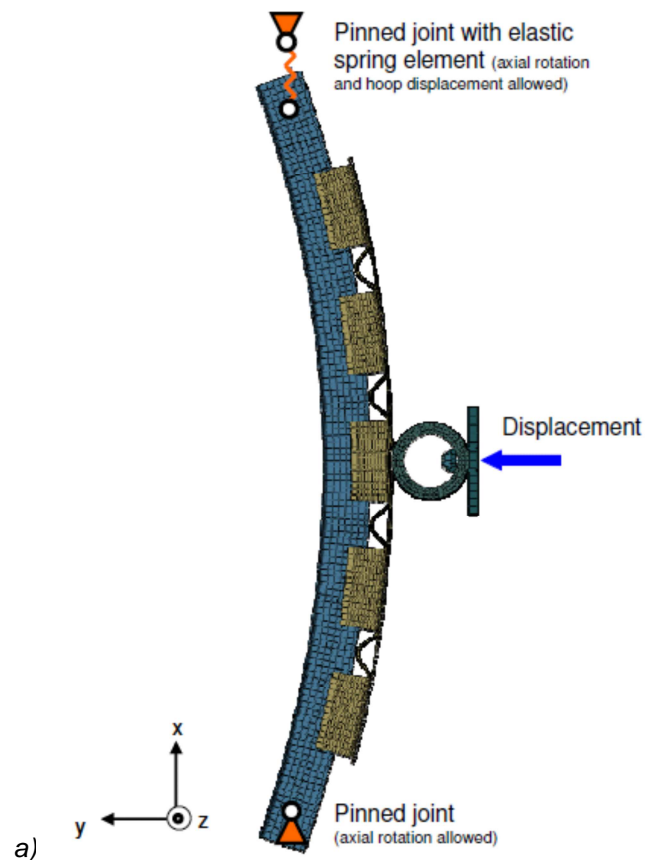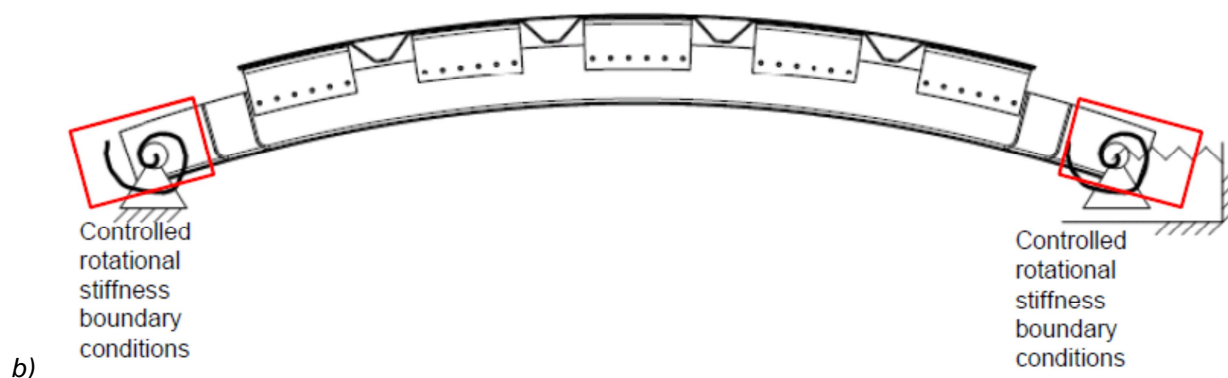
Figure 16. Boundary conditions: a) CODAMEIN II panel (top view); b) CODAMEIN III panel (axial view)

Moreover, the frame end region was modified for both CODAMEIN II & III panel, compared to CODAMEIN I panel. The frame web thickness was increased in three steps (see Figure 17) towards the ends. Thus the frame end was reinforced more gradually with the intention of preventing local failure, without adversely influencing the results of the tests.
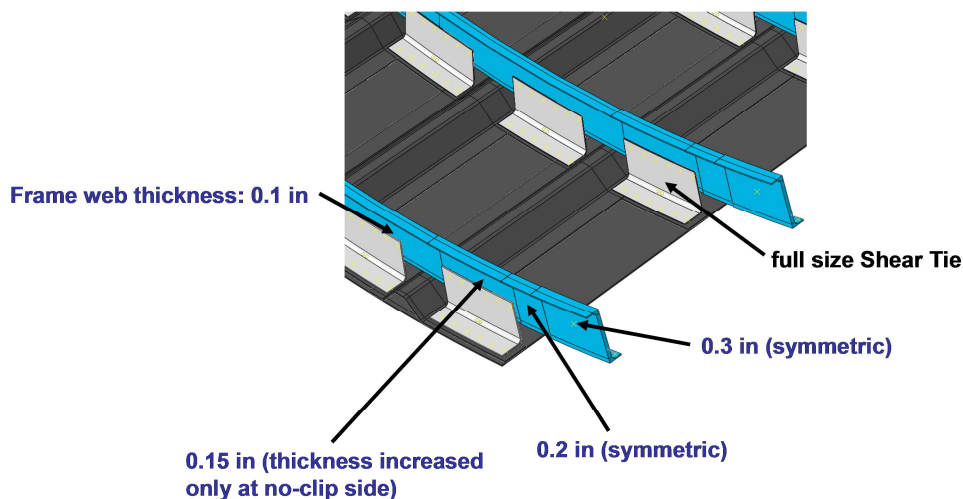
Figure 17. Frame end reinforcement details [Hasse 2013]

Possible consequences of the shear tie design change might be the promotion of higher damage level upon shear tie failure initiation. The definition of the controlled rotational stiffness boundary conditions were supported by Prof. Hyonny Kim, who leads the associated investigation at UCSD, thus ensuring that the complementary relationship and value was maintained between the two project processes. The

composite frames of the UCSD test panels are clamped in a controllable rotational stiffness to 3 frames out of five, while there were no restraints on the remaining 2 frames.

2.1.3. Similarity to the UCSD Test Panel Designs

The test panel design of CODAMEIN I and CODAMEIN II is based upon the component design of UCSD test panels. The UCSD performed numerous tests on specimens of different sizes and levels of detail which imply a size similar to the CODAMEIN I / CODAMEIN II panel. A set of standard components has been used for all performed tests. Thus the material, lay-up and cross section of the test panel's skin, stringers, frames and shear ties were maintained throughout the impact testing program. The size of the test panels, the number of involved components and the boundary conditions has all been evolved. Figure 18 shows the UCSD test panel types, "stringer panel" and "frame panel".
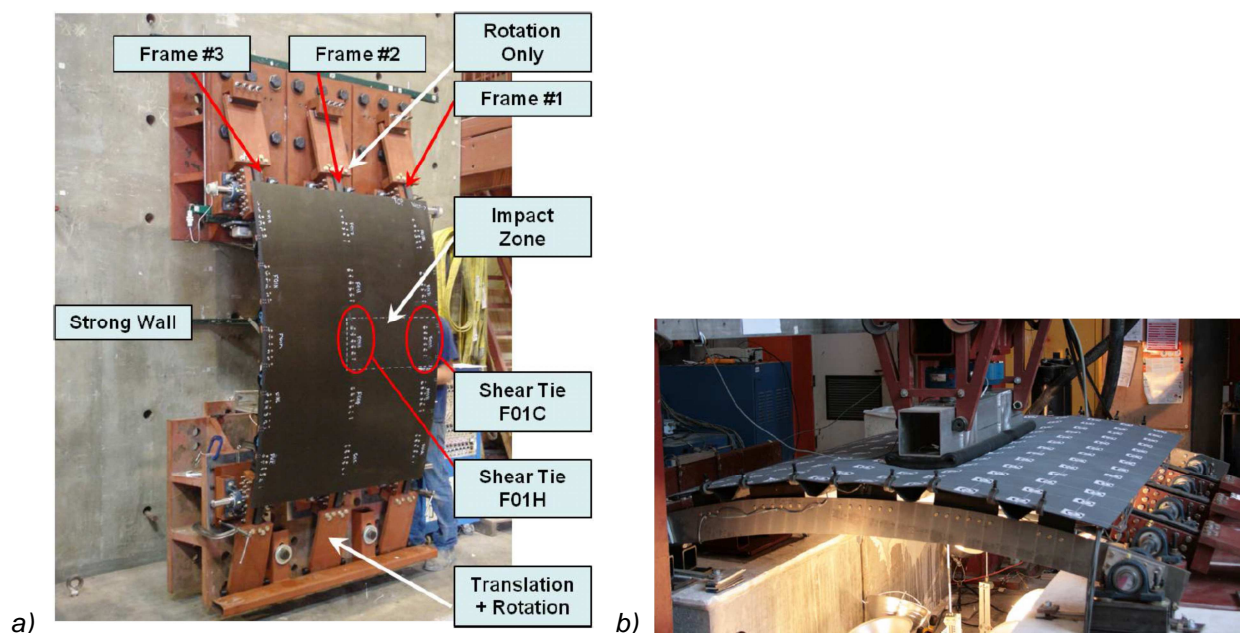
Figure 18. UCSD investigated panels: a) Stringer Panel; b) Frame Panel [Kim 2013]

All the UCSD test panels incorporate composite C-frames. Instead, the trilogy of CODAMEIN test panels uses Aluminium Z-frames. The Z-frame, which was chosen for the CODAMEIN I and CODAMEIN II panels to create a hybrid design panel, as displayed in Figure 19. This picture also shows the composite C-frame which UCSD uses for its comparable investigation on a full composite fuselage design.
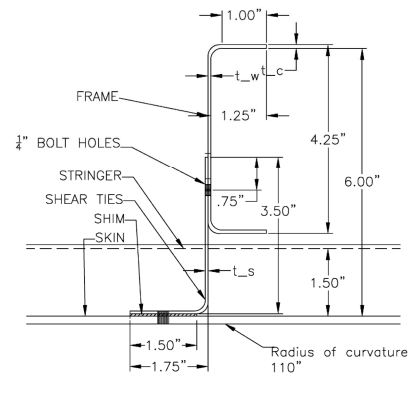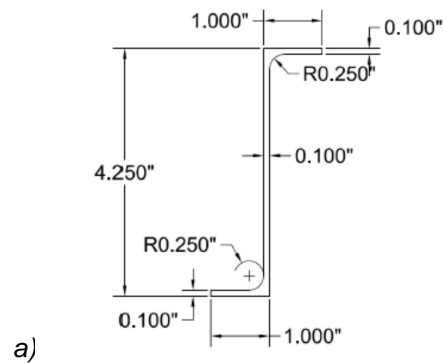
Figure 19. Frame shape and geometry: a) Z-Frame section of CODAMEIN III panels; b) UCSD C-Frame section [Kim 2011]

The geometry of the composite omega-stringers and composite L-shear ties, which are identical for the UCSD test panels and the CODAMEIN I / CODAMEIN II panels, are shown in Figure 20.
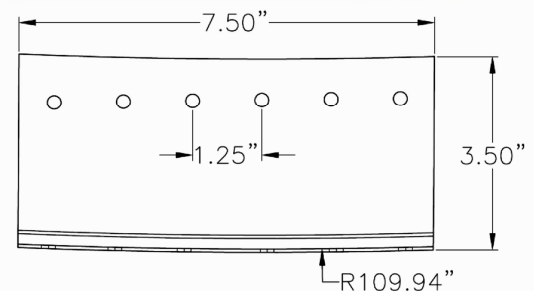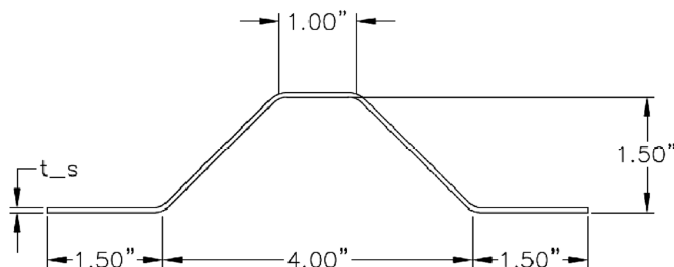
Figure 20. Omega Stringer Section, L-Shear Tie [Kim 2011]

2.1.4. Manufacturing

As mentioned before, EASA stated the intention to not damage the CODAMEIN II panel apart from shear tie failures. The CODAMEIN III panel was taken directly from CODAMEIN II panel. The manufacturing of the CODAMEIN II panel was based on the procedures of the CODAMEIN I panel manufacturing, with high similarity to the manufacturing of the UCSD large test panels (see [Haase 2013]). The skin was made using hand lay-up. The four stringers were laid up on the skin using silicon cores, and co-cured in an autoclave according to the manufacturing specification.

The shear ties were laid up using an aluminum mold (see Figure 21) and cured in the autoclave. The measurement of one shear tie at the various locations is shown in Figure 22.

Figure 21. Shear ties on the aluminum mold
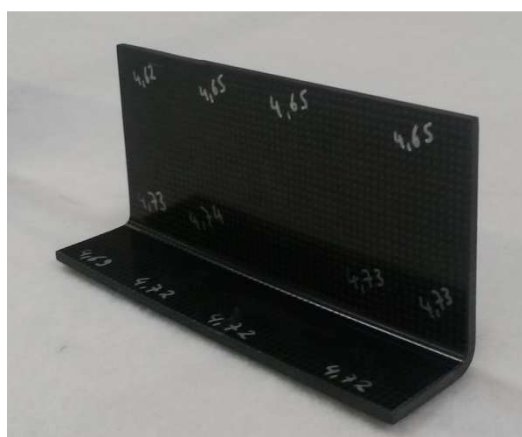
Figure 22. Different locations for measurements on shear tie

According to the measurements conducted on the 24 shear ties, the average thickness for the shear tie is 4.7 mm which is slightly less than the nominal thickness 5.28 mm due to manufacturing. The aluminum frames were machined using a CNC machine. Hi_Lok fasteners were used to attach the shear ties to the skin and to the frames as shown in Figure 23.

Figure 23. Fastener Attachment of Shear Ties

2.1.5.   Test Method

Three test methods (Dynamic Impact Test System (DITS), Crash Impact Test and displacement controlled test) were discussed in CODAMEIN I report [Mikulik, Haase 2012]. Evaluating all aspects of the different test methods, the quasi-static displacement controlled test was selected for the three series of CODAMEIN tests. This method was in agreement with the existing research program and due to enhanced control of test parameters and simple damage monitoring solutions, involved relatively low project risk.

2.2.   Model Development

The development of the test panel model for the high mass low velocity impact is presented step by step, in order to determine the buckling of the shear ties, damage initiation and failure modes in the post shear tie failure stage. FE models were created using Abaqus software. The Abaqus 6.13 CAE pre-processor and Python scripts were used to generate the models. Two different FE models were generated: the test panel and a section of a complete fuselage barrel. Numerical simulations of the blunt impact by a rubber bumper were conducted using the explicit dynamic solution.

In the preliminary stage of CODAMEIN I project, a fully elastic FE model was created, which did not contain any material failure models, plasticity, degradation of properties nor failing part connections. The objective of the first analysis was to determine the generic elastic behaviour of the panel and the barrel FE models. These models also assisted in determining the energy level of the impact and investigating the required boundary conditions for the panel in order to replicate the behaviour of the full barrel FE model.

Based on the numerical models of CODAMEIN I which were generated to simulate the stiffness of the hybrid structure, the detail level has been increased in several ways in the CODAMEIN II project. While an implicit integration scheme was used in CODAMEIN I, an explicit integration was adopted in CODAMEIN II to better deal with the high levels of non-linearity. A numerical model of the test panel as well as several additional FE models were generated and advanced throughout the project to deliver the desired test simulation data and information on parameter sensitivity.

One main objective of CODAMEIN III was the development of a numerical model that permits the simulation of the investigated impact case and which predicts the sequence of structural damage that is caused by the impact. Such a model can be used to predict further load cases, different panel designs or different materials in future work. This objective is achieved by investigating the rotational stiffness effects on the structural behavior.

2.3.   Communications with UCSD

EASA has indicated that UCSD's research on impact of composite structures is of significant interest and could run in parallel to the UCSD study, for the benefit of all concerned. The FAA-funded research work of Prof. Hyonny Kim's team at the UCSD uses a multi-step test/analysis pyramid approach to the investigation of damage in composite fuselage structures caused by high energy blunt impacts. The aim of UCSD's research is to characterize blunt impact threats and locations and to understand damage formation and its relationship to visual detectability [Kim 2013]. Both quasi-static and dynamic tests have been performed on panels of differing sizes that are based on the part design concept which also influenced the design of the CODAMEIN I / CODAMEIN II / CODAMEIN III test panels. The UCSD's test panel design has included composite skins, composite omega stringers, composite / aluminum C-frames and composite shear ties. Two test panel types "frame specimen" and "stringer specimen" were investigated. The first configuration "frame specimen" is primarily focused on damage development to the circumferential frame members and their connection to the skins. The second configuration "stringer specimen" is focused on damage formation to the stringers and their connection to the skins, i.e., representing localized impacts occurring between frames. Due to the differences in test panel designs used by Bishop and UCSD, the result comparisons are made between the failure modes and permanent damage levels following the quasi-static testing at the specimen level for comparable design features.

3. Finite Element Modelling and Analyses

3.1.   Description of the Finite Element Model

The finite element model is developed for the current numerical analysis with the FEA package (ABAQUS) employed in order to investigate the non-linear structural behavior. One of the main objectives of CODAMEIN III was to develop a numerical model that permits the simulation of the investigated impact case and subsequent impact damage formation and damage sequence. Similar to the CODAMEIN II simulation technique, an explicit integration was adopted in CODAMEIN III to deal with the high non-linearity. The FE panel model is illustrated in Figure 24.
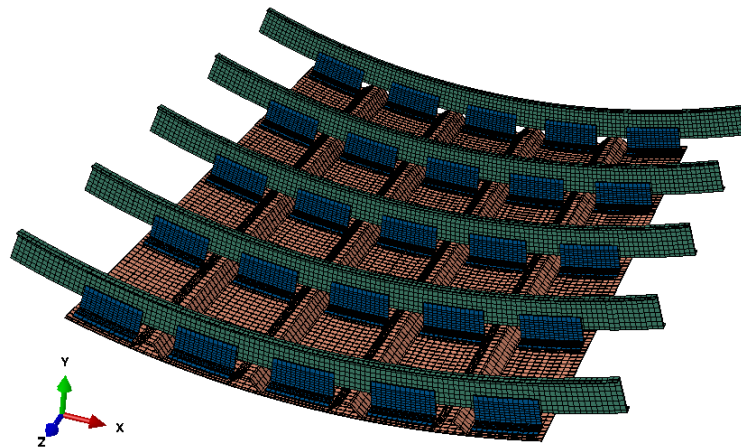
Figure 24. CODAMEIN III panel FE model

Moreover, as documented in CODAMEIN II report [Haase 2013], to reach a higher geometrical detail level, the basic element type of the model was changed from Shell to Continuum Shell. This modelling approach permits an improved geometrical precision, reduces inaccuracies due to section offsets and provides through-thickness outputs. Linear continuum shell element type SC8R were used for all composite parts and the frames. The impactor structure was meshed using linear solid element type C3D8R, and the rubber bumper was meshed using linear solid element type C3D8I with incompatible modes. Incompatible mode elements C3D8I are first-order elements that are enhanced by incompatible modes to improve their bending behavior. In addition to the standard displacement degrees of freedom, incompatible deformation modes are added internally to the elements. The primary effect of these modes is to eliminate the parasitic shear stresses that cause the response of the regular first-order displacement elements to be too stiff in bending. Moreover, incompatible mode elements such as C3D8I can overcome the issue of shear locking. However, they are sensitive to element distortions, which may make them much too stiff and less useful because it is difficult not to distort the elements in real-life finite element modeling.

The element mesh size was chosen in order to provide sufficient analysis accuracy, based on an appropriate element dimension ratio and an optimal match between the meshes of the parts connected in the assembly. These conditions were in opposition to aim to achieve the maximum possible element size in order to allow for reasonable solution times.

The finite element mesh size is approximately 20 mm by 20 mm for skin panels, stringers, and consists of 54727 elements and 108955 nodes. As the shear ties were found to be the most critical parts in the previous stages of CODAMEIN I & CODAMEIN II, they are modelled with a finer mesh 15 mm by 8 mm and with introduction of the bending radius which is key region regarding damage and failure. Table 3

summarizes the detail level of the FE models of three phases of CODAMEIN in terms of element types and numbers.

Table 3. Finite element model details: CODAMEIN I, CODAMEIN II and CODAMEIN III

Number of elements	CODAMEIN	CODAMEIN II	CODAMEIN III
S4R	15443	0	0
C3D8I, C3D8R	5538	14831	14831
SC8R	0	39896	39896
Total	20981	54727	54727

The specific materials used for the CODAMEIN III panels are listed in Table 4.

Table 4. Materials of the CODAMEIN III panel

Material	Usage
Cytec X84-Z60 UD 12k Tape	Skin, Stringers
Cytec X840-Z60 PW Fabric	Skin, Stringers
Toray T800H-39002D PW Fabric	Shear Ties
Al 7075-T6	Frames
Rubber NBR	Bumper

In particular, two layers of continuum shells were used to allow prediction of delamination damage instead of shell elements. The shear ties are connected to the stringer foot and frame by fasteners in the test panels. The rivet connection of the shear ties to the skin and the frames was modelled using 1D fastener elements. The failure of fasteners in tension or shear was also integrated although fastener failure did not occur in the tests of CODAMEIN I, CODAMEIN II or in the FE analyses.

The fasteners attaching the shear ties to the skin were replaced by local tie constraints (DOF equalization of node pairs) to reduce the tendency of elements within the shear tie feet to undergo hourglassing modes that caused delamination. The fasteners that attached the shear ties to the frames were modelled using connectors. The connector type definition "Cartesian+cardan" allows the assignment of properties in all DOFs. For the representation of the fasteners, translational elasticity as well as axial and shear strengths were defined. The frame parts of the CODAMEIN III model are depicted in Figure 25. The geometrical detail level of the frames was kept the same as the CODAMEIN II model which involved the improved reinforcement at the frame ends and the increased bending stiffness of the frames.
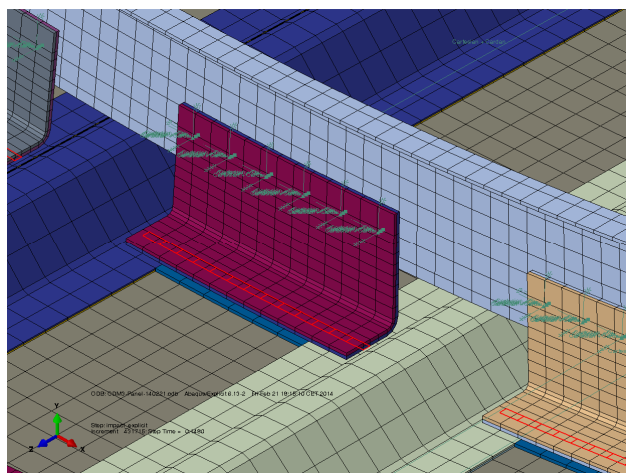
Figure 25. Connections of shear tie to stringer and frame

Furthermore, the techniques and methodologies used previously to predict delamination in the skin, stiffener and shear tie layers and between the co-cured skin and stiffeners, whereby two element layers through the thickness, were combined using a cohesive zone model. By the definition of a cohesive surface contact between the two layers, physical delamination was enabled. The connection of the parts that were co-cured during the manufacturing was represented by a cohesive surface definition that allowed for delamination. Delamination is expected to initiate when a damage variable reaches the critical value. The advancements of the panel FE model based on CODAMEIN I & II test and FE analysis results used the Hashin damage criterion to develop intralaminar damage and degradation. The investigations of the number of frame attachments, boundary stiffness, and shear tie stiffness are discussed in the current section.

3.2. Results and Discussions of CODAMEIN II Panel Response

3.2.1. Influence of Frame Attachment

In this part, the influence of the number of frames fixed to the test fixtures was evaluated by FEA. The previous CODAMEIN I & CODAMEIN II test and all associated FE analyses were performed using a three-frame attachment. The FE model of CODAMEIN II panel was established to make this comparison since it is more convenient to validate the FE model by the already performed tests. A further FE model with a five-frame attachment was simulated to compare with the common panel with only three-frame attachment. This analysis indicated no significant deviation of the global load-displacement due to the different number of frames attached, as displayed in the load-displacement chart in Figure 26. The deviation of the displacement at the first load drop is most likely overestimated since the FEA used a low

output frequency and the two peak points lay on adjacent output points while the real peak points have less offset.
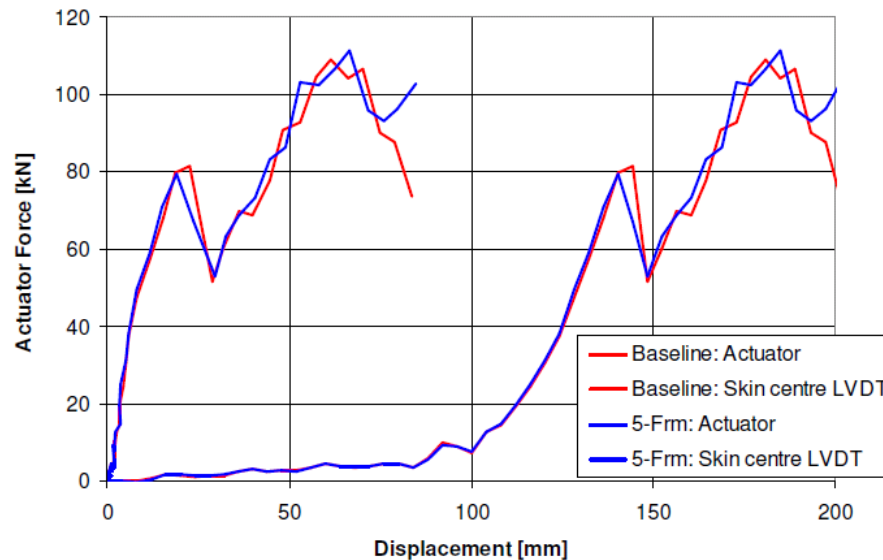
Figure 26. Load-shortening curve CODAMEIN II: 3-frame vs. 5-frame attachment [Haase 2013]

3.2.2. Boundary Stiffness

The CODAMEIN II test showed a very small influence of the boundary stiffness on the panel response. The compression of the test fixtures was found to be very low at the different spring stiffnesses while the effect of the boundary longitudinal rotation which was not restrained in the CODAMEIN I / CODAMEIN II test set-up, was more significant. It was proposed to use different test fixtures in CODAMEIN III tests that provide longitudinal rotational stiffness. A model with five attached frames was analysed, the basic translational stiffness (9500 N/mm same as CODAMEIN II) at one end of all frames and also added rotational stiffness (5000 N-mm/radian) on both ends of all frames. These test fixtures correspond to the test set-up that was used by Prof. Kim's group at the UCSD to perform impact tests with all-composite panels. As the rotation of the frame ends becomes more critical at a higher panel deformation, the translational stiffness dominates at low panel deformation, and the global stiffness increases against the base configuration at higher loads as displayed in Figure 27. In the later CODAMEIN III panel analyses, this rotation stiffness is used as the baseline and more sensitivity studies on this value will be conducted in section 3.4.2. The hoop displacement at the test fixture and the rotation are the main issues to correlate with the ones from full barrel analysis.
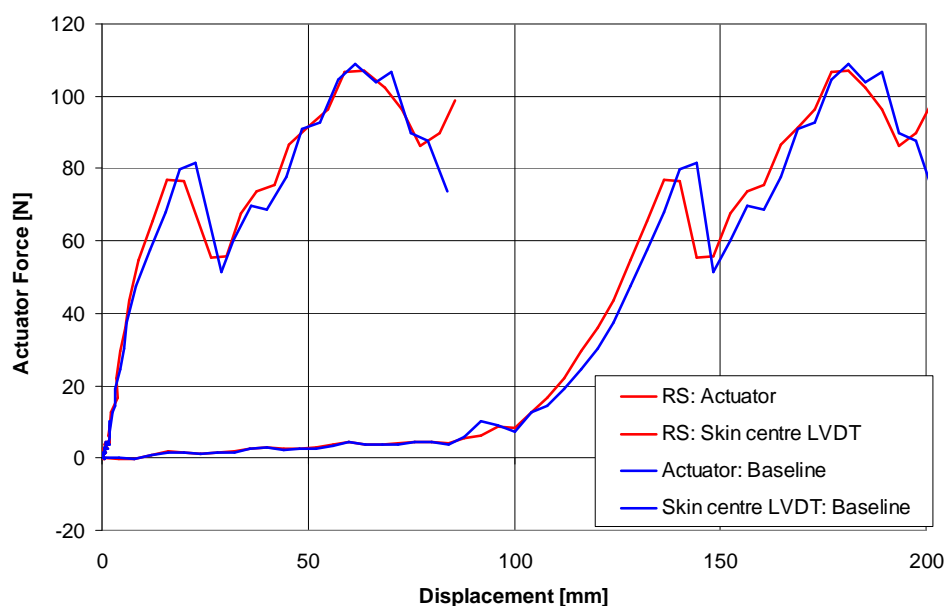
Figure 27. Load-displacement: Basic set-up and 5-Frm attachm.+ rotational stiffn. [Haase 2013]

3.3. Comparison of Panel and Barrel Response

3.3.1. CODAMEIN II vs. CODAMEIN III Barrel Response

As shown in Figure 13, the full barrel model which incorporates the new shear tie design was similar to CODAMEIN II barrel model. Additional structure, such as floor beams and load struts, increased the stiffness of the barrel exposed to the blunt impact located in a position $21°$ below the horizontal axis. This impact position on the lower fuselage is both a likely position where ground service equipment such as belt loaders might impact the fuselage and a position of maximum distance to the reinforcing inner structure which permits high indentation and thus the risk of creation of impact damage with low visibility. The design change of shear ties has been implemented into the current barrel model and the displacement versus time curve is compared with CODAMEIN II barrel model as illustrated in Figure 28. The barrel FE model was fixed in all DOFs at remote edge nodal points. The impactor mass of 2000 kg was modelled as a rigid plate attached to the rubber bumper whose impactor velocity was 1.39 m/s.
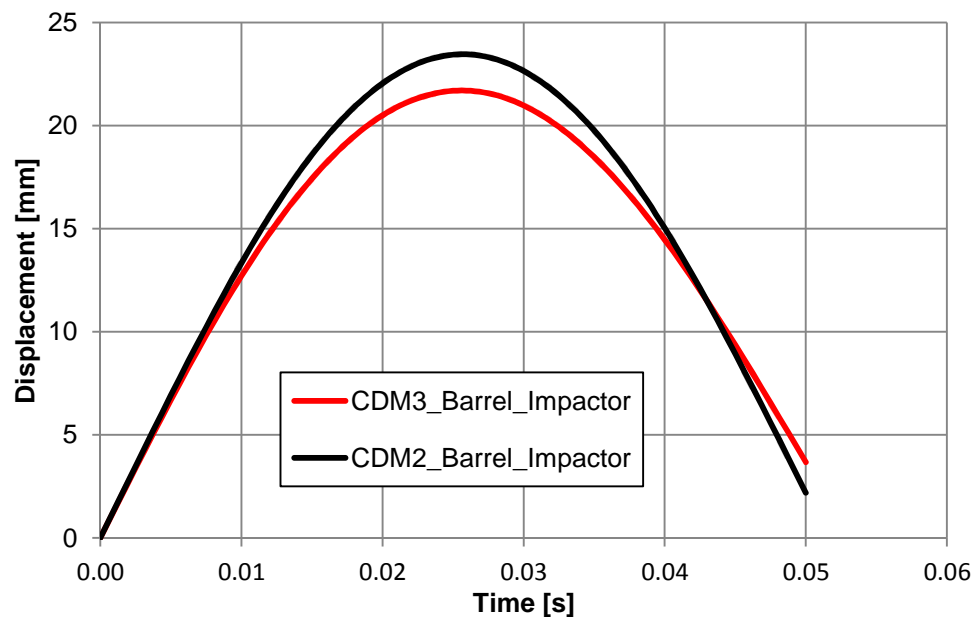
Figure 28. Displacement – time curve: CODAMEIN II vs. CODAMEIN III

Moreover, the load-shortening curve of the barrel models from CODAMEIN II & CODAMEIN III is displayed in Figure 29 and the corresponding reference node on the skin is illustrated in Figure 30. It indicates the impactor actuator displacement was close to the local displacement on the skin, and it is not consistent with the results from the panel which showed clear deformation of the impactor rubber. For this reason, the displacement of the skin is considered as a reference in the later sensitivity study.
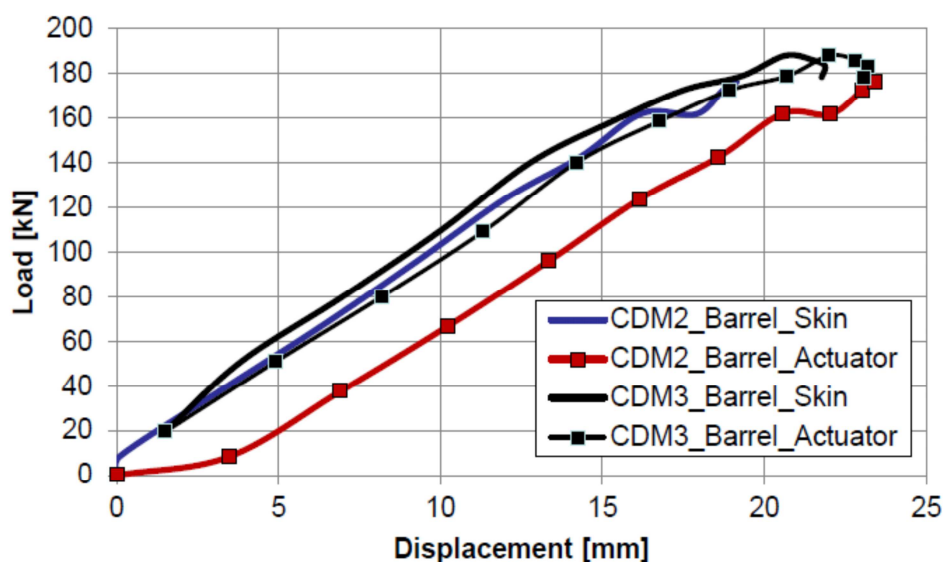
Figure 29. Load-displacement curve of barrel models: CODAMEIN II vs. CODAMEIN III
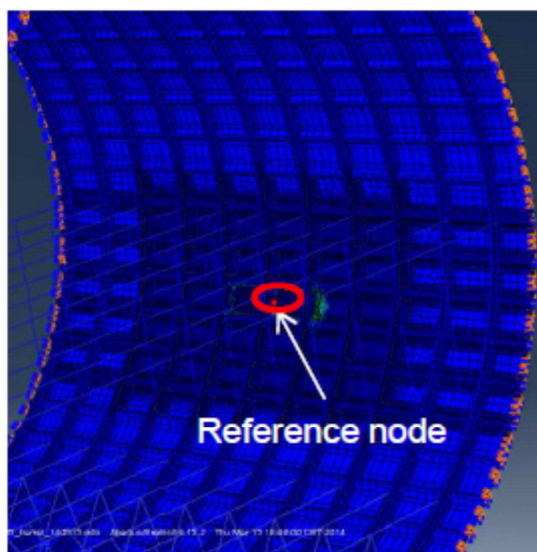
Figure 30. Reference node on the skin of CODAMEIN III barrel

According to what had been reported in CODAMEIN II, the improved barrel model which includes the inner structures indicated an increase of elastic stiffness approximately 12% compared to the empty barrel in CODAMEIN I [Mikulik, Haase 2013]. Even though there is shift due to number of data points in the data, the stiffnesses of CODAMEIN II and CODAMEIN III barrels are comparable.

3.3.2.   Comparison between the CODAMEIN III Panel and Barrel

The load-displacement curves from the baseline panel configuration (described in Section 3.2.2) and the barrel is depicted in Figure 31. It shows that the barrel is significantly stiffer than the panel. The panel boundary conditions need to be modified to more closely match the barrel stiffness. It is noted that the translational stiffness is determined not to change from CODAMEIN II test panel as it is important to limit some parameters in order to clarify the influence of the added rotational stiffness.
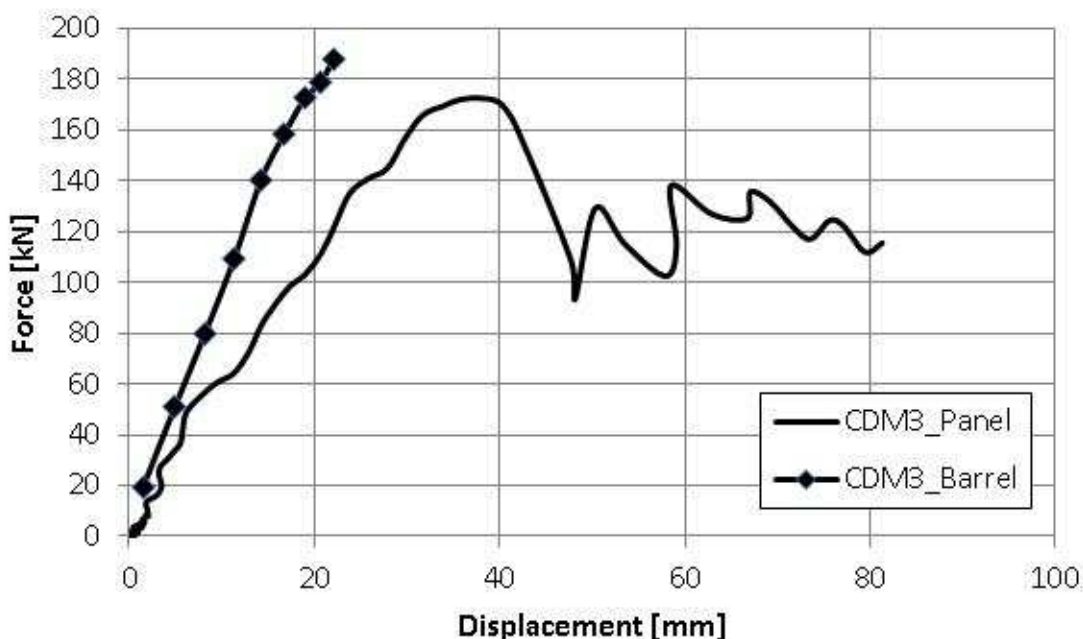
Figure 31. Load-displacement curve: panel vs. barrel in CODAMEIN III

3.3.3. Comparison of the three CODAMEIN Panels

The load-displacement curves of the three panel models are described in

Figure *32*. The comparison of the predicted peak loads for each of three stages of CODAMEIN is reported in Table 5. As reported in CODAMEIN I documentation [Mikulik, Haase 2012], the accuracy of the FE models was limited to approximately 30 kN when the test panel's behaviour became non-linear due to damage growth since no failure criteria were implemented in the FE models. Nevertheless, the panels from three stages of CODAMEIN were able to predict a similar stiffness in the pre-damage phase. It can be observed that the first load drop of the CODAMEIN III panel was higher than that of CODAMEIN II panel, mainly due to the stronger shear tie design.
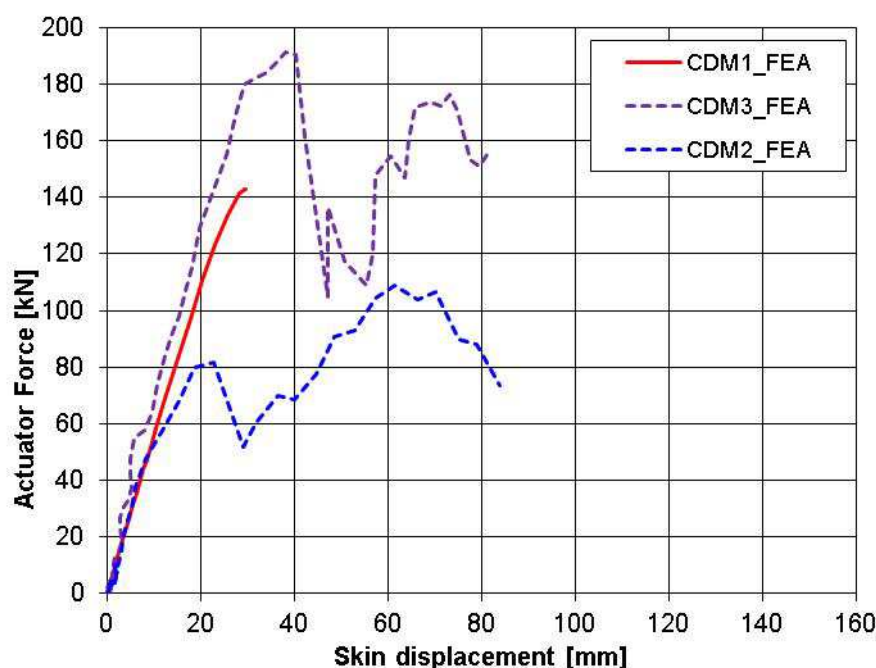
Figure 32. Load-displacement curve comparison: CODAMEIN I, CODAMEIN II, CODAMEIN III panels

Table 5. Predicted peak loads among CODAMEIN projects

Project	CODAMEIN I	CODAMEIN II	CODAMEIN III
Predicted peak load	143 kN	83 kN	191.5 kN

3.4.   Further Development of CODAMEIN III Panel Response

Similar to CODAMEIN II simulation, the impactor loading of CODAMEIN III panel was simulated dynamically with a velocity of 1 m/s while the test was performed under quasi-static loading. The determination of the impact velocity was based on evaluation of the dynamic effects and the computation time. The influence of the dynamic loading was previously determined to be acceptably low [Haase 2013]. To simulate the loading phase, the impact velocity was defined as a constant initial condition with velocity of 1 m/s held for 0.2 s, which resulted in an impactor displacement of 200 mm.

The permitted mass scaling factor is another factor which can influence the computation time. The most critical regions for damage onset and progression are the section radii of the stringers and shear ties within the model where no simplification was done. Since the resulting mesh of the model still required a prohibitively large solution time, mass scaling was allowed at low magnitude. The mass scaling function in ABAQUS allows for an automatic increase of mass for the elements that are most critical for the

solution minimum time increment. The factor and type parameters are defined in the model to scale the masses of only the elements whose element stable time increments are less than the value assigned. During the current analyses, the mass scaling factor was held below 5 which means the mass of some elements in the shear tie and stringer radii was increased by a maximum factor of 5 throughout the entire analysis. Using this approach, the computation time could be reduced to approximately 54 hours on 4 CPUs for a panel analysis.

Additional investigations, in terms of different material properties of shear ties, rotational stiffness boundary conditions and bumper material parameters, summarised in the following section, were incorporated.

3.4.1. Materials

The boundary conditions of the panel analyses were chosen to represent the test set-up as illustrated in Figure 33. Boundary conditions were defined at the ends of the five frames and coupling constraints with reference points represented the steel fittings at the frame ends. At the frame support where the frames were attached to test fixtures by a bolted connection in the test set-up, the boundary rotational stiffness was permitted and defined on the fitting reference point. It is noted that the rotational stiffness (5000 N-mm/radian) is used in the current section as a reference to compare.
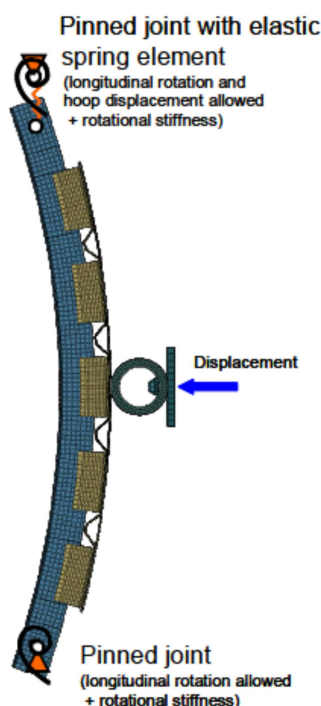
Figure 33. Basic set-up: 5-frame attachments and rotational stiffness

In the current study, the material properties were investigated in order to compare the material T800H-39002D PW and X840 Z60 PW on the new shear ties. The load-displacement curves are illustrated in Figure 34. In addition, the reasonable variations in the material properties (an increase of 5% in the elastic stiffness of shear tie, 10% in strength of the composite material, 25% damage progression of the composite material as reported in Table 2) were investigated to determine the effect of these variations and the load-displacement curves are depicted in Figure 35. The deviation of the peak load is most likely exaggerated since the FEA used a low output frequency and the two peak points lay on adjacent output points while the real peak points have less offset. The parameters of the test panel FE model that had the most significant influence on its response to the blunt impact loading, will be simulated in the later sensitivity study in section 3.4.2. Those parameters include mass scaling, strength of the adhesive surface, damage progression of the adhesive material, stiffness of the rubber bumper and impactor mass. As mentioned earlier, an increase of 5% in the elastic stiffness of shear tie, 10% in strength of the composite material, 25% damage progression of the composite material is introduced to the models presented in Figure 34 and Figure 35.
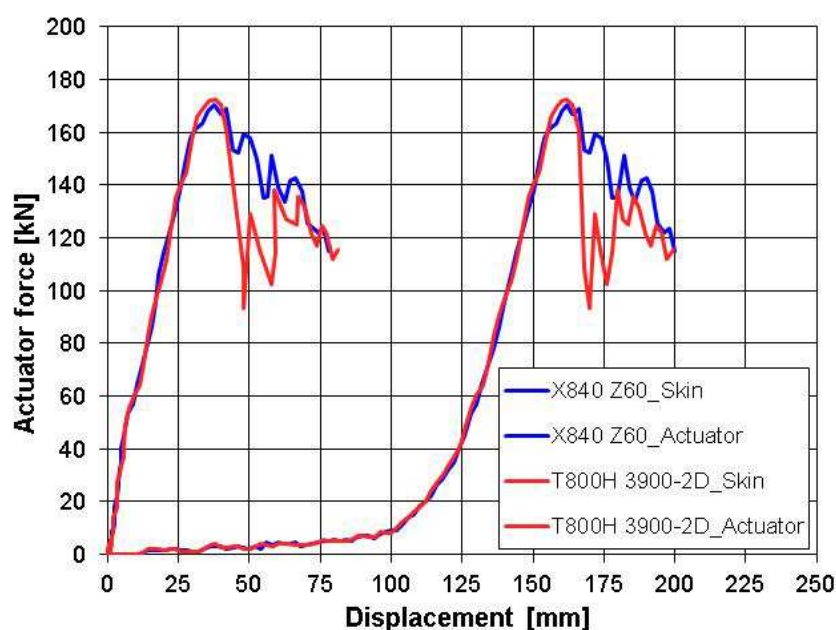
Figure 34. Load-displacement curve: different materials comparison
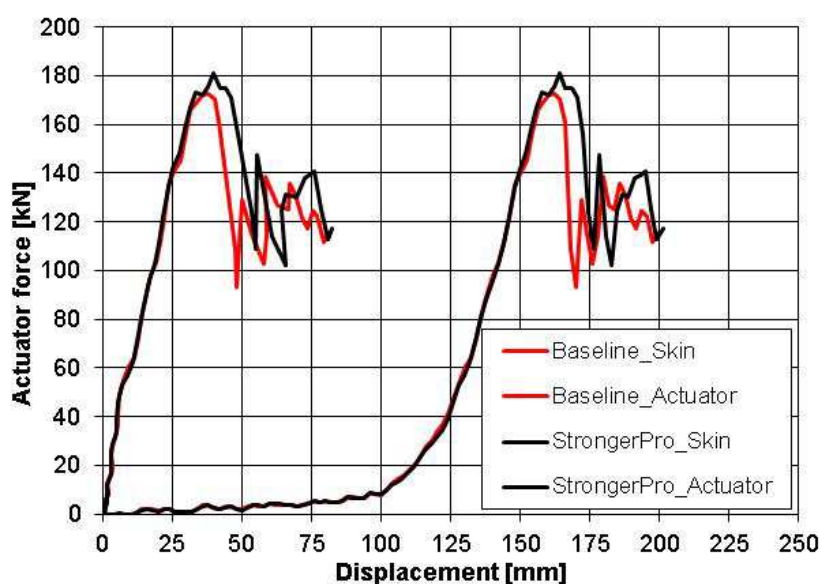
Figure 35. Load-displacement curve: baseline and stronger material comparison

3.4.2. Boundary Conditions

As mentioned in CODAMEIN II project, the results of sensitivity studies were used for the further improvement of the numerical model of the test panel, e.g. the potential impact of modifications to component design, the materials used, and boundary conditions can be assessed relative to likely changes in the characteristic damage sequence.

The boundary conditions for the current panel design are critical to ensure that the panel response replicates the behaviour of a full barrel. Due to the low velocity of the ground service equipment represented by the experiments, a quasi-static response is triggered in the panel structure. In this case, boundary conditions play a significant role in the panel response. Boundary conditions have to be carefully designed in order to allow correlation of data from a substructure panel specimen to the full barrel. In the current study, the investigated rotational stiffness and recommended rotational stiffness are reported in Table 6.

Table 6. Boundary stiffness values in CODAMEIN III panel

Source / Name	Rotational stiffness (N-mm/radian)	Rotational stiffness (in-lbf/deg)	Translational stiffness (N/mm)
Baseline	5.0 e3	-	9500
40tBaseline	2.0 e5	-	9500
UCSD	6.48 e8	100000	9500
Proposed value	7.45 e8	115000	9500
Final value	1.36 e8	-	9500

UCSD had performed an iterative process to determine the appropriate value of boundary stiffness such that boundary displacements and frame rotation are equivalent. The same procedure should have also been followed to match the hoop-direction and rotation displacement between the panel and the full barrel. As UCSD stated, doing so would achieve equivalence, thereby making results measured from the panel applicable to the full barrel. The displacements and rotations will be taken from the centre frame (Fr 3.) of the panel (see Figure 36) and the centre frame of the impact region of the full barrel.
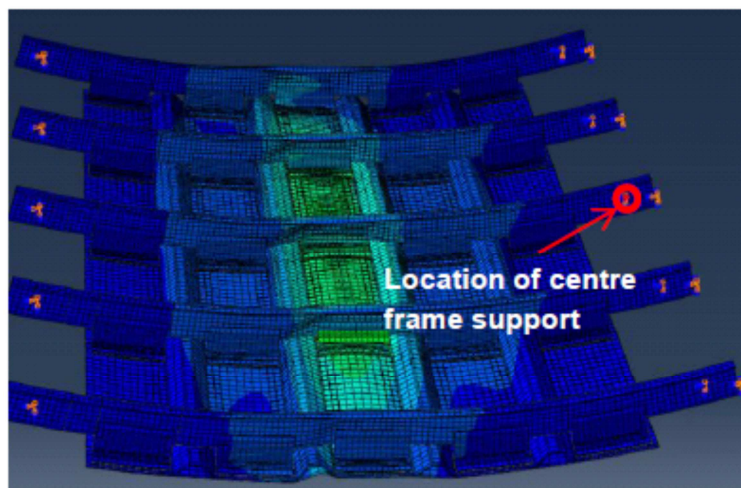
Figure 36. Reference frame in the panel

Figure 37 and Figure 38 display the predicted frame hoop displacement and rotation with respect to skin displacement caused by the impactor, for different values of rotational stiffness. It can be observed that the panel, in the case of lower rotational stiffness, exhibits much larger hoop displacement at the higher indentor displacement than the full barrel. This is because of the low in-plane displacement constraint at the boundaries result in the bending moment distribution across the span of the panel which is different from the full barrel model. However, the higher rotational stiffness matches rotation angle better than the barrel model. In this case, a proper representation of the boundary stiffness values plays an important role in obtaining equivalence.
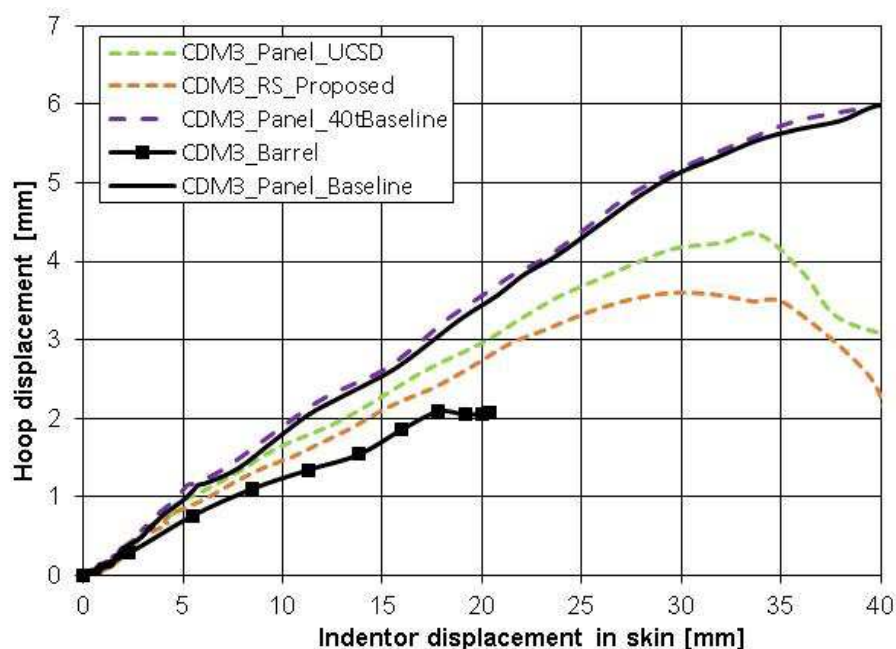
Figure 37. Hoop displacement for different rotation stiffness of panel and full barrel model

From Figure 37, the hoop displacements with UCSD value also correlates better than the others compared to the full barrel model. It should be noted the indentation on the skin is shown up to 40 mm but the stiffness mentioned is determined by the data collected from only the initial linear deformation range. As shown in Figure 38, it can be seen that the UCSD rotational stiffness (5000 N-mm/radian) and 2.0 e5 N-mm/radian (40 times baseline value as a trial value) yields rotation displacements that match closely with the full barrel model. The rotation at the centre frame predicted in the panel with the increased rotational stiffness value correlated well with the barrel.
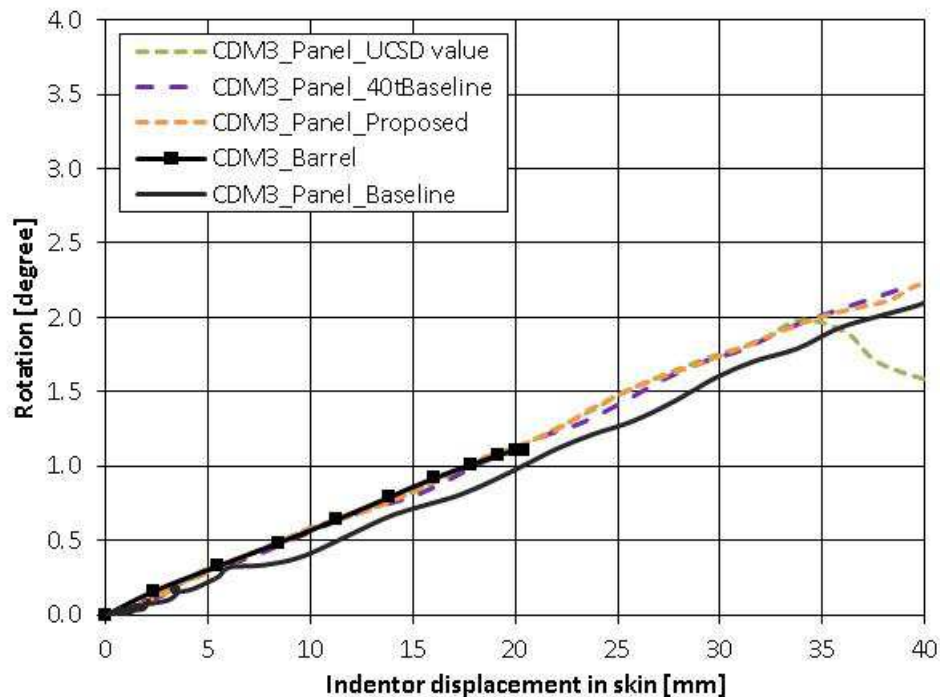
Figure 38. Rotation at the support location of panel and full barrel model

Moreover, the overall stiffness of the panel is also an important factor to reach the appropriate representation of the barrel in the aircraft-level. The stiffness of the panel with UCSD value [Kim 2010] is 4% higher than the baseline model reported in Table 6. From documentation of CODAMEIN II, the inclusion of the cargo floor in the full barrel model resulted in an increase of elastic stiffness of approximately 12% compared to the empty barrel. However, the UCSD barrel model reported in [Kim 2010] neglected the floor structure, and the panel deformation was compared with this. From the rotation and hoop displacement comparison, the panel with UCSD value matches closer to the full barrel behavior than others.

From Figure 31, the panel behaved less stiff than the full barrel model. Therefore the rotational stiffness equal to 7.45 N-mm/radian (115 in-lbf/deg), which is 15% increment of UCSD rotational stiffness value, is recommended to use in the test fixture design. As seen in Figure 39, the influence of rotation stiffness is more significant since it leads to the increased stiffness of the panel in the linear phase. In this case, it results in a complementary role that the added rotation stiffness affects not only the high load level as described in CODAMEIN II documentation, but also the overall stiffness. It is important to note that the high load level is defined where damage has been initiated. Compared to previously predicted load-displacement curve, the current proposed value is applied to the model, incorporating the measured ply thickness after manufacturing shear ties. The nominal ply thickness of 0.22 mm was used for the previous sections, while the measured ply thickness of 0.1958 mm is implemented to the current and

future study. This may also explain the difference between the predicted peak loads summarized in Table 5 and the predicted peak load 202 kN in Figure 39.

Due to the manufacturing test fixture capability of the testing department, the rotational stiffness is limited to approximately 1.36 e8 N-mm/radian (18 percent of the proposed value). It is noted that the finite element analysis model with the final rotational stiffness value is then compared with the testing result in the following chapter.

As seen from the FE results, the higher rotational stiffness seems to match the full barrel better. Therefore the completely clamped boundary conditions are applied to both 5-frame ends to avoid any rotational movement. In the low load level range below 50 kN, the clamped boundary condition behaved in a similar way to the controlled rotational stiffness boundary conditions. Based on these investigations, on one hand, it can be concluded that the case with no rotational stiffness would represent the lower bound of panel stiffness. On the other hand, the case with completely constrained rotations would represent the upper bound of panel stiffness. The actual rotational constraint required to represent the full barrel stiffness lies between these two bounds.
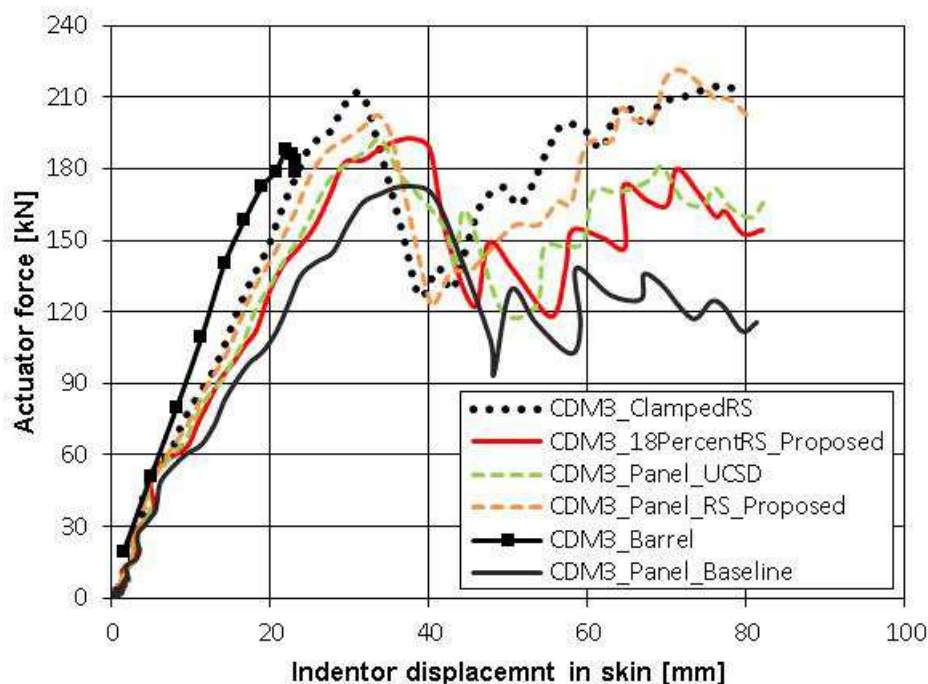
Figure 39. Load-shortening curve comparison

3.4.3. Rubber Bumper Modelling

The finite element representation of the rubber bumper is expected to have significant influence on the behaviour of the impacted panel. Since the complete modelling of the rubber bumper proved to be complicated, a simplified pre-compressed part was used in CODAMEIN I. The circular section of the bumper was expected to completely close at a relatively low load level. In order to avoid convergence issues and avoid the use of an extremely fine mesh required for such hyperelastic simulation, a decision was made to model the bumper as a representative flat section. The mesh of the original D-shaped bumper section and the flattened bumper shape are shown in Figure 40.
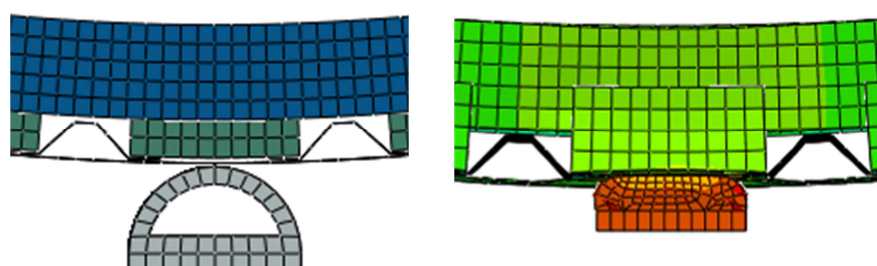
Figure 40. Mesh of the rubber bumper section: D-shape, flattened shape [Mikulik, Haase 2012]

The limitations of this simplification are the missing simulation of the impact phase prior to the complete compression of the bumper in which both the bumper and the panel get deformed. Furthermore, the contribution of the bumper attachment tooling on its inside to the load distribution could not be covered by the simplified bumper modelling. Within CODAMEIN II, a solution for the modelling of the undeformed rubber bumper was found. The inner attachment tooling consisting of a steel plate and two bolts was integrated in the model. The inclusion of the bumper compression phase enabled a comparison of the whole impact process with the test. The final representation of the rubber bumper is shown in Figure 41 in the undeformed state and as a cut view of the meshed and deformed combination with the panel.
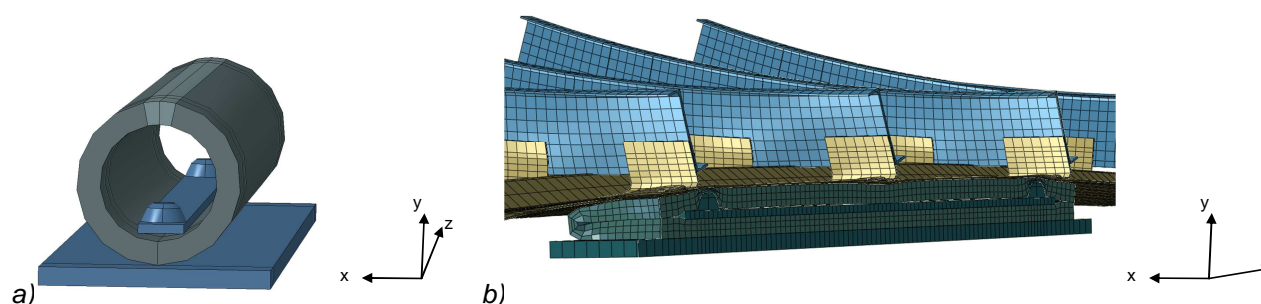
Figure 41. Rubber bumper assembly: a) geometry; b) cut view of the meshed deformed state [Haase 2013]

It was stated that the rubber bumper was integrated in the numerical model with a high detail level that implied the attachment structure and the simulation of the bumper compression process. As no bumper material tests had been performed within this project, its material was simulated in a simplified way, using a stiffness that enabled compression behavior similar to the test observations. The main parameters that govern the formation of impact damage were assessed in a sensitivity study. One reference node is taken from the bumper to measure the deflection of the bumper. Three different values of elastic modulus were investigated for the current study and the results are presented in Figure 42. The results indicate that the bumper material parameters influence only slightly how the panel structure reacts to the bumper.
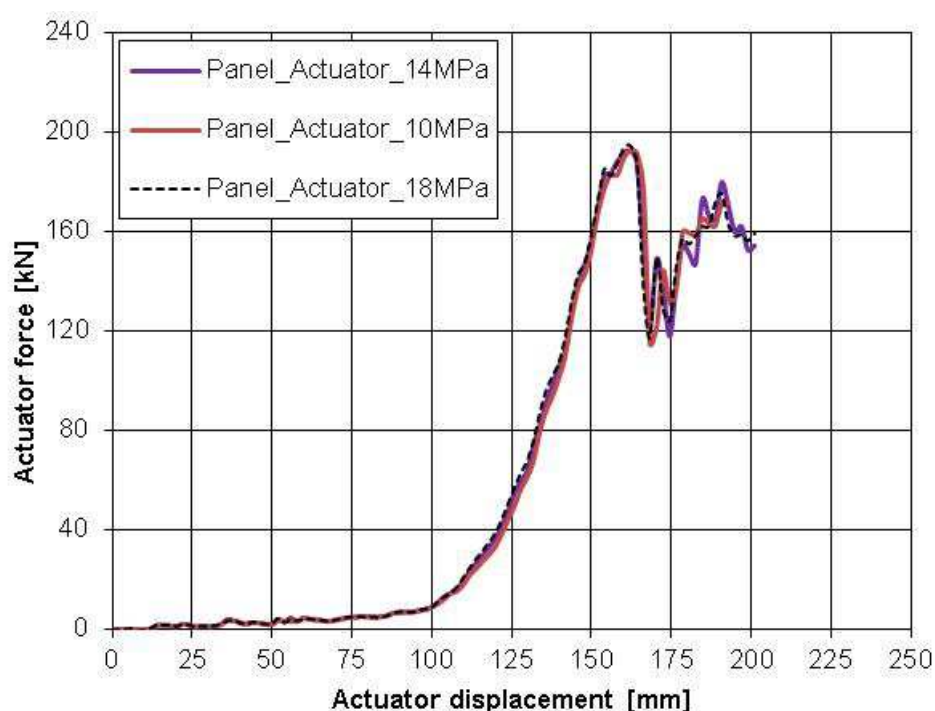
Figure 42. Rubber bumper material properties investigation

4. Experiments Description

The test specimen was designed at Bishop GmbH, supported by EASA and UCSD, as described elsewhere in this document. Figure 43 illustrates the scenario of interest, where a GSE with a long cylindrical bumper makes contact against the side of an aircraft fuselage. The fuselage structure is generally composed of longitudinal stringers and circumferential frames, and several circumferential frames are subject to the interior portion of the long bumper during impact event, while the near-end portions of the bumper would involve biaxial bending response. The near-end zone of the barrel, under the transverse shear developed in the stringers and the end-effect of the bumper where large bending stresses and interlaminar shear can result in visible skin cracking. A quasi-static testing method is used in the current experiment.
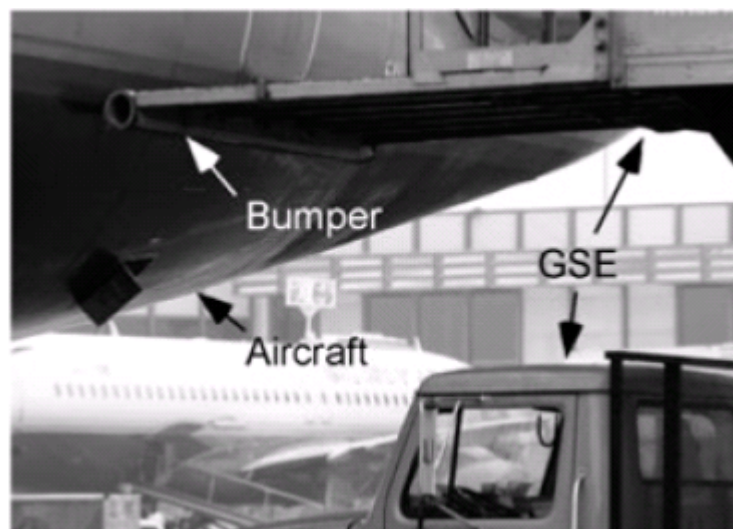
Figure 43.Conceptual view of the interested scenario of GSE [Kim, 2013]

A large stiffened composite panel test specimen (1.93 * 1.83 m) and newly designed shear ties were manufactured at San Diego Composites and Luratec, respectively. The curved specimen was designed using wide-body aircraft fuselage construction design principles, with four co-cured longitudinal omega-stringers and five aluminum Z-shaped cross-section circumferential frames mechanically-fastened to the skin via five L-shaped shear ties (angle brackets) per frames. Specimen materials have been described in Section 2.1.1. The tested sample was the same as used in CODAMEIN II, and prior to performing the actual test, the previously damaged shear ties were replaced. The new shear ties and rivets are depicted in Figure 44 according to the shear tie replacement. The shear ties were bolted to the skin using six 11.1 mm Hi-Lok HL18 PB8-7 alloy countersunk shear head bolts and HL70-8 aluminum collars (see details in Figure 45). The interior three frames were also mechanically fastened to the shear ties via six 7.94 mm Hi-Lok HL18 PB8-7 countersunk fasteners and the exterior two frames used the shear ties via six 11.1

mm Hi-Lok HL18 PB8-5 alloy countersunk fasteners. A gap of 7 mm existed between the stringer and frames, as depicted in Figure 46.

Figure 44.Shear tie replacements [Hernandez 2014]
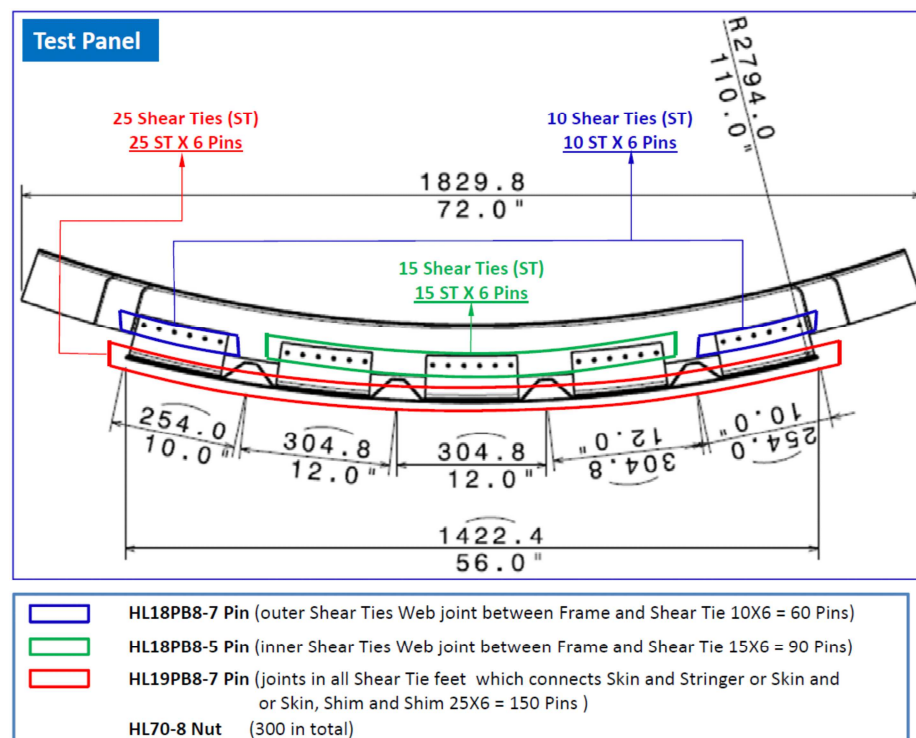
Figure 45.Pins used in shear tie replacements
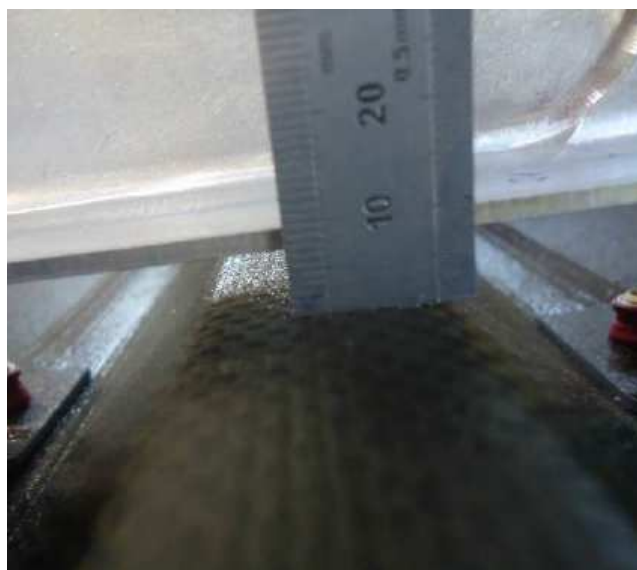
Figure 46. Distance between the stringer and frame

The main components of the CODAMEIN III test panel (skin, frame, Omega-stringer, L-shear tie) are displayed in Figure 47.
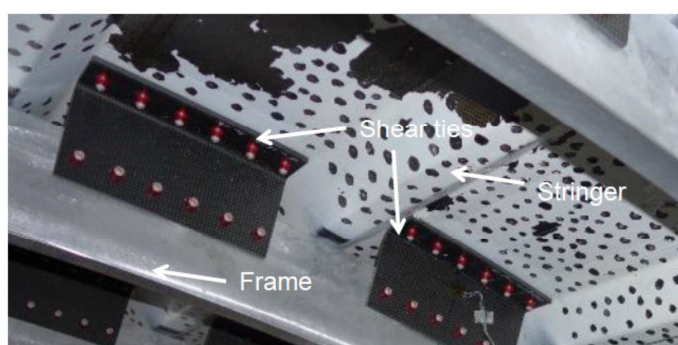
Figure 47. Panel components: Skin, assembled components (shear tie, frame, stringer)

4.1.   Test Set-up and Test Fixtures

The specimen was tested in the Applus LGAI test lab in Bellaterra (near Barcelona) in Spain. The specimen was secured to strong walls (see Figure 48) via a bolted connection at the frame ends to the pivoting boundary condition fixtures. Controlled rotational stiffness of 1.36 e8 N*mm/radian is provided to each frame end via flexure plates. Both frame ends had the identical rotational stiffness, but it was free to translate in the hoop direction (horizontal in Figure 48) in one of the two frame ends via spring-based sliding plates. The rotational stiffness at the frame ends was determined by using a series of finite element analysis models, comparing the behavior of the smaller panel test specimen to a full aircraft barrel with inner structure, and adding rotational stiffness to the former to achieve an equivalent

response in terms of stiffness, hoop displacement, rotation and bending stress as the full barrel, as described in Section 3.4.2.

The specimen was quasi-statically loaded under a displacement-controlled hydraulic actuator using an original equipment manufacturer rubber cylindrical bumper mounted to the fixture shown in Figure 48. It has only one load cell and the main components of the test set-up are illustrated in the right side of Figure 48. The bumper dimensions are 178 mm outer diameter, 127 inner diameter and 1000 mm length.
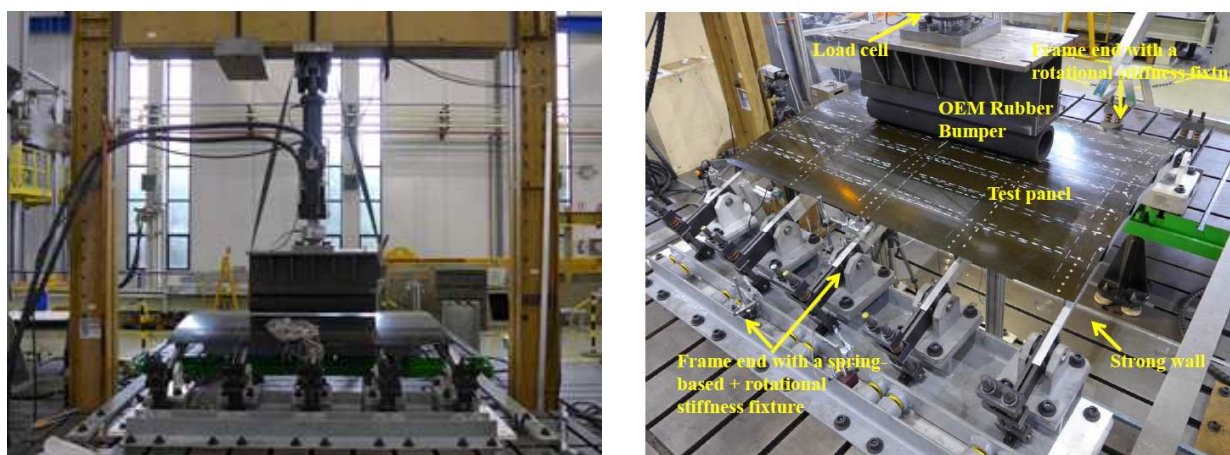
Figure 48. CODAMEIN III test set-up (left); main components (right)

The two different types of test fixtures, which attach the five frames, are shown in Figure 49.
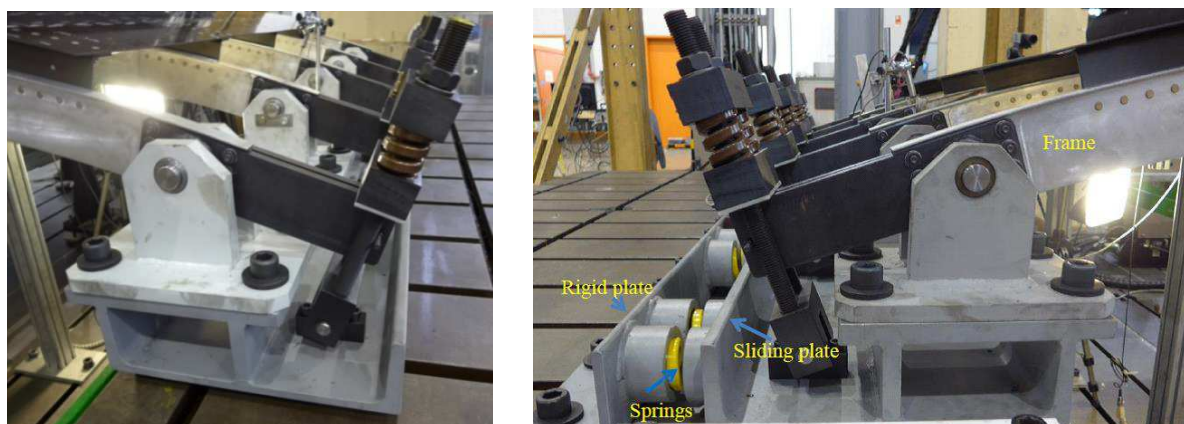
Figure 49. Frame attachments: pinned fixture with fixed rotational stiffness (left), pinned fixture with hoop direction springs and fixed rotational stiffness (right)

The springs in the test fixtures are the same as the CODAMEIN II test. After having used spring arrays with a stiffness of 8.5 kN/mm at each of the inner three frames in CODAMEIN I test, spring arrays with a stiffness of 9.5 kN/mm were used for the inner three frames in the CODAMEIN II test and for the five frames in the CODAMEIN III test.

4.2. Loading Methodology

The specimen was quasi-statically indented directly on the skin between two stringers and cross 3 frames over the area, as highlighted in Figure 50.
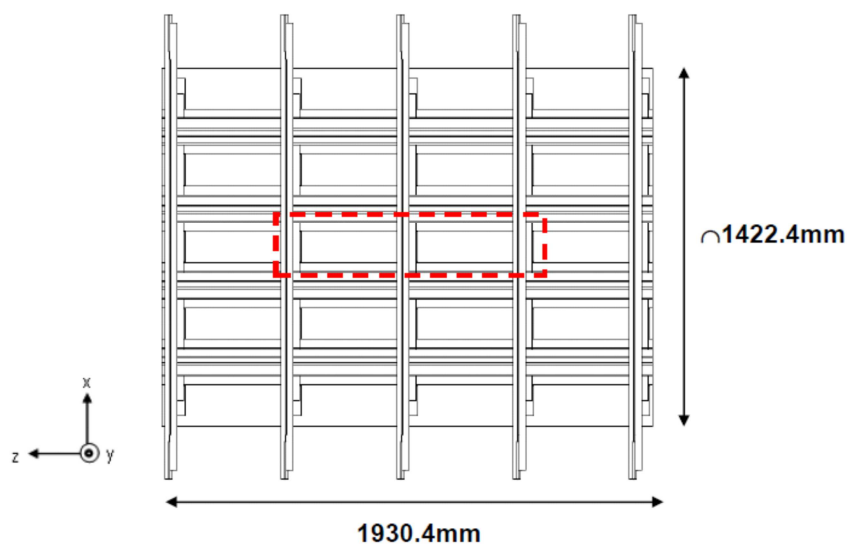
Figure 50. Impact area on the test specimen

A maximum of three separate load cycles was planned according to test plan [Zou 09/2014], as illustrated in Figure 51.
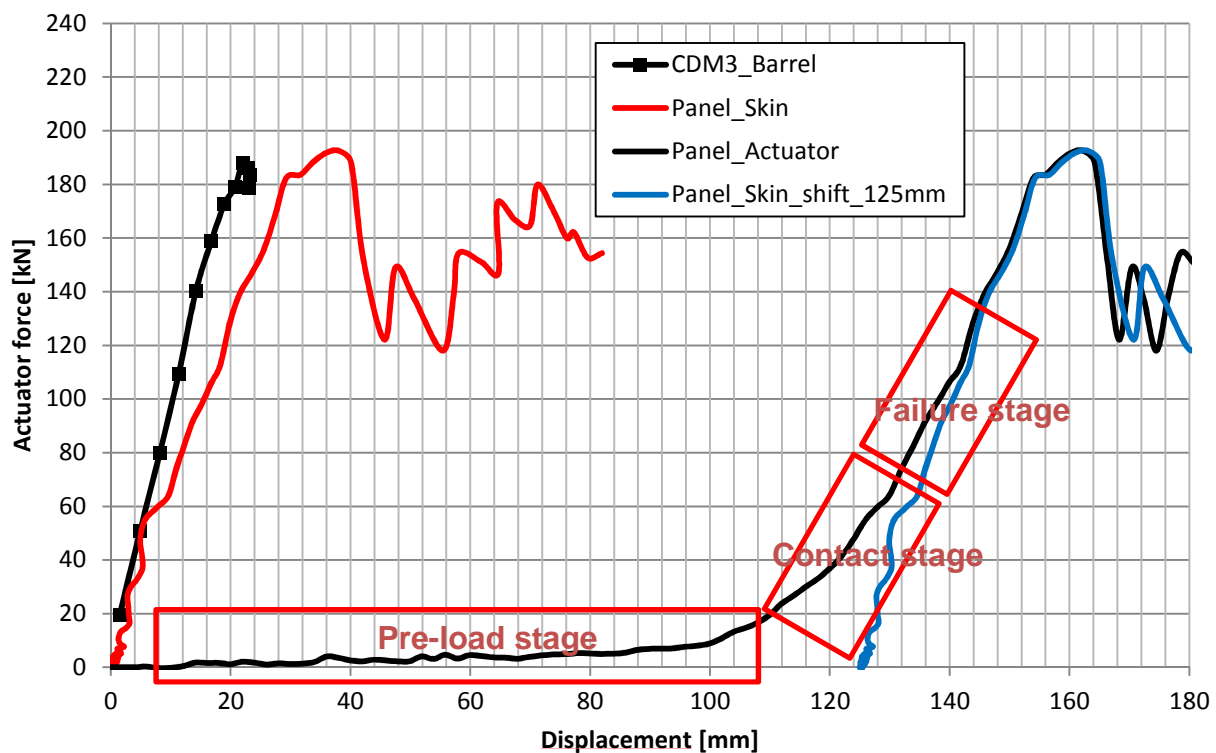
Figure 51. Loading methodology

These load cycles were intended to be completed in steps defined by the following visual or audible events:

- Load cycle 1: First loud crack noise / first measured load drop / damage initiation / instability indicated by buckling (up to contact stage of inner metallic part of the impactor)
- Load cycle 2: Visual or acoustic damage of shear ties or stringers / frame-to stringer contact / excessive rotation of the frames / damage propagation measured by a number of load drops (up to contact stage or failure stage)
- Load cycle 3: Shear tie or stringer failure / excessive rotation of the frames (up to collapse)

The displacement–controlled loading was completed in accordance with the basic scheme in Figure 52.
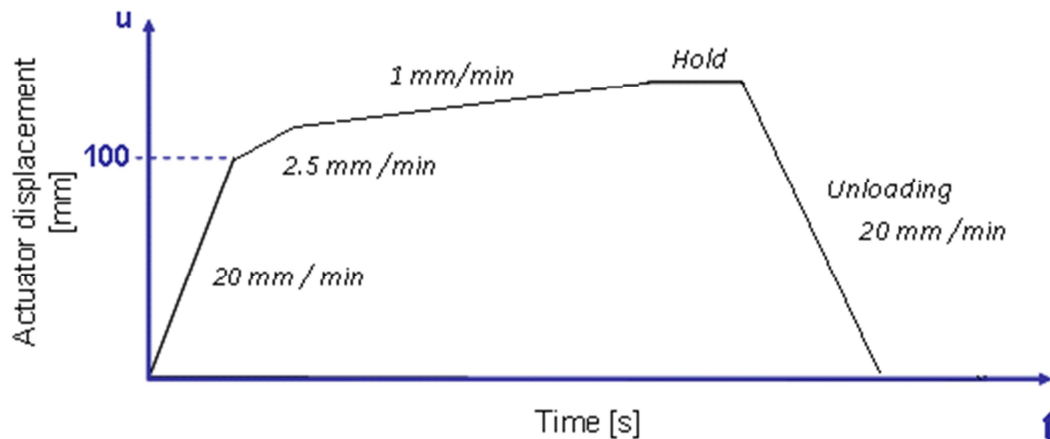
Figure 52. Loading scheme

The pre-test was performed to check whether all the strain gauges and LVDT were active, and the test was setup correctly. During the first loading phase in which the rubber bumper was not fully compressed, the actuator was moved with a velocity of 20 mm/min with 5 stops. At a displacement of 100 mm where the rubber bumper was close to be fully compressed, the loading rate was lowered to 2.5 mm/min for 4 stops. The loading was stopped at defined load steps to capture snapshots with the video correlation system. The testing was controlled completely by the actuator displacement, especially at the last loading stage, each step was loaded by only 1 mm/min. The online strain gauge readings were captured accordingly. The test stops were manually controlled in response to visible drops in stain gauge values at the shear ties. At the maximum actuator displacement, which was defined by the respective maximum load of the first failed shear ties or by an expected damage event, the loading was held for documentation of the panel state, before unloading with a velocity of 20 mm/min.

4.3.   Instrumentation

The following instrumentation was used in the quasi-static loading test.

- 1 Load Cell at the hydraulic actuator
- 10 LVDTs to measure displacements and rotations plus the actuator displacement gauge
- 30 Strain Gauges at the skin, a stringer, the centre frame and two shear ties
- 2 Video Cameras on the panel inside and outside

Figure 53 shows the positions of the used LVDTS, at which hoop displacements (LVDTs 1, 2, 5, 6, 8, 9, 10) and rotations (LVDTs 3, 4, 7) were recorded.

Side View   Inside View
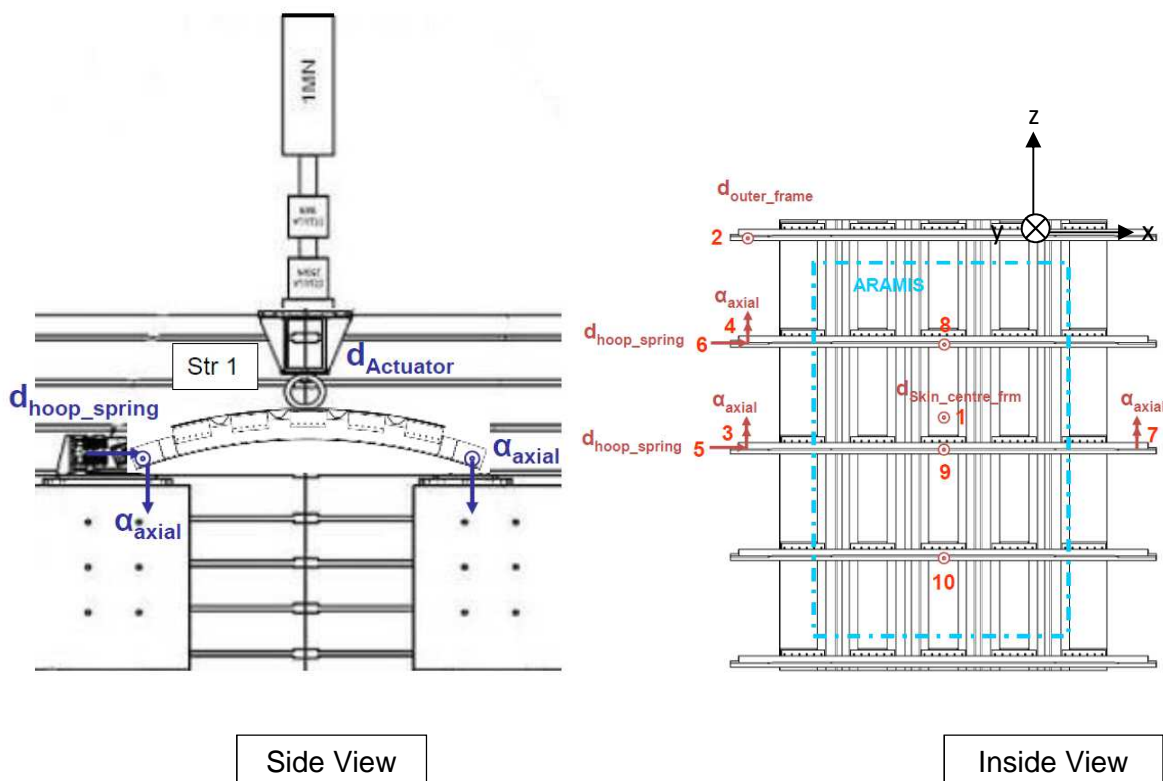
Figure 53. LVDT positions for displacement and rotation

Locations of the LVDTs installed in the test set-up are displayed in Figure 54 a): LVDTs 1, 8, 9, 10; b): LVDT 2, c) LVDT 7; d) LVDTs 3-6).
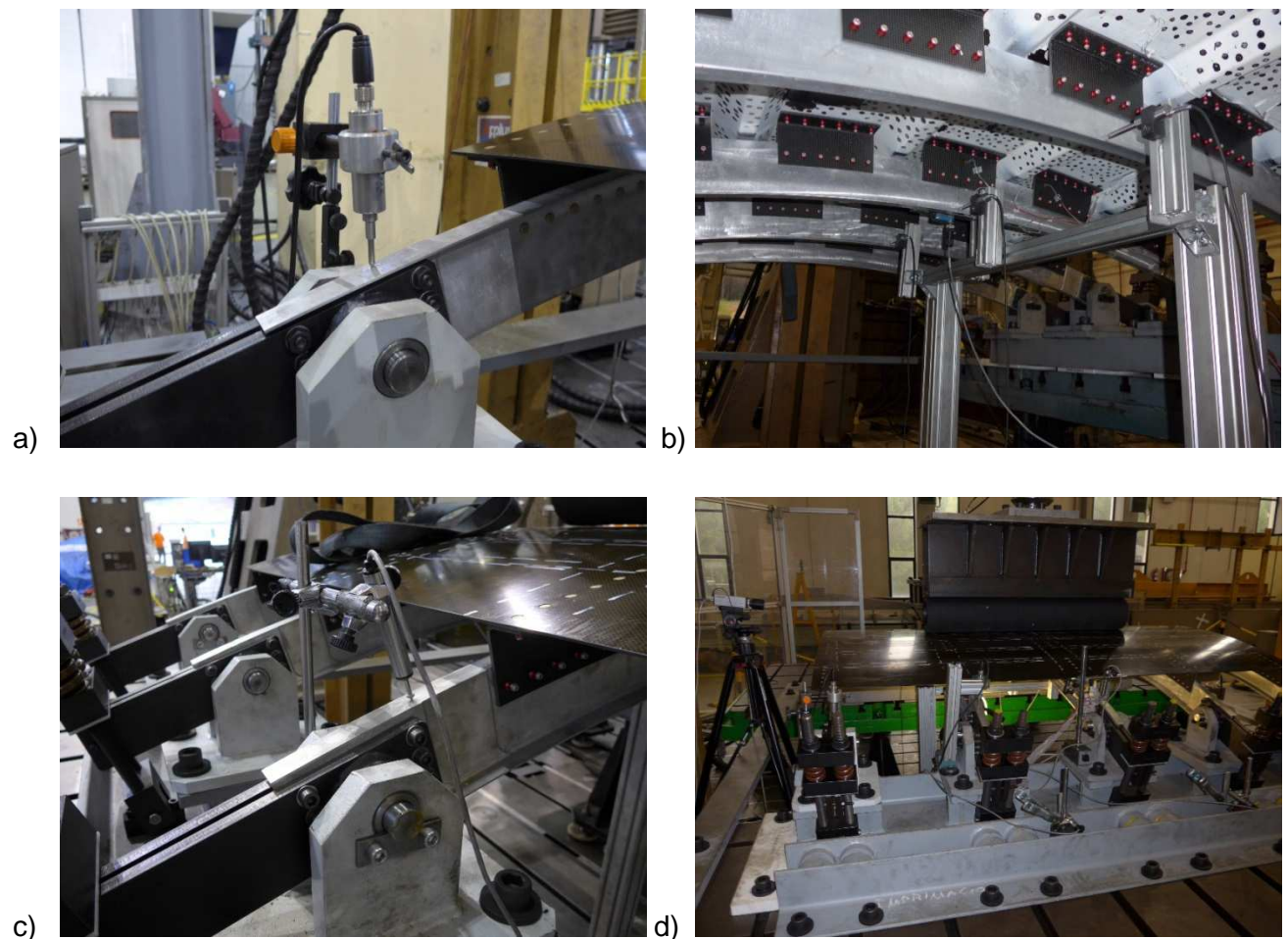
Figure 54. LVDTs in the test set-up: a) LVDTs 1, 8, 9, 10; b) LVDT 2, c) LVDT 7; d) LVDTs 3-6

The positions of the 30 strain gauges are depicted in Figure 55 and Figure 56. These figures also show the channel numbers of the strain gauges. On the skin and the stringer no. 3, strains could only be measured on the panel inside. For the frame and shear tie strain gauge positions, each two channels were applied on both sides of the part to obtain information about bending. In case of marked sets of two strain gauges at one defined position, the numbering follows the rules below.

- Skin: 1st SG circumferential, 2nd SG axial
- Frame: 1st SG on the inside (radially), 2nd SG on the outside (radially)
- Shear ties: 1st SG on the non-frame side, 2nd SG on the frame-side
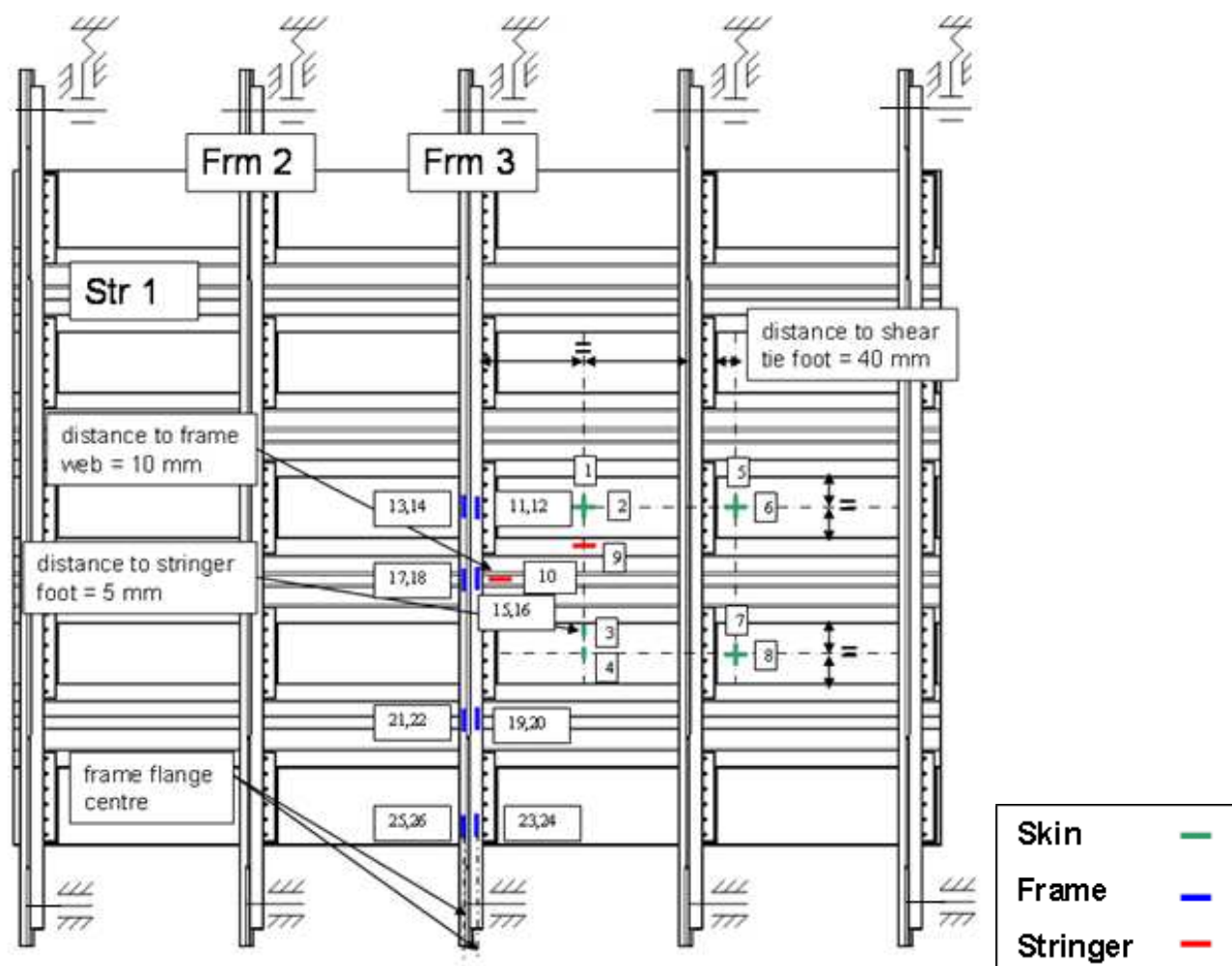
Figure 55. Strain Gauge positions: inside view
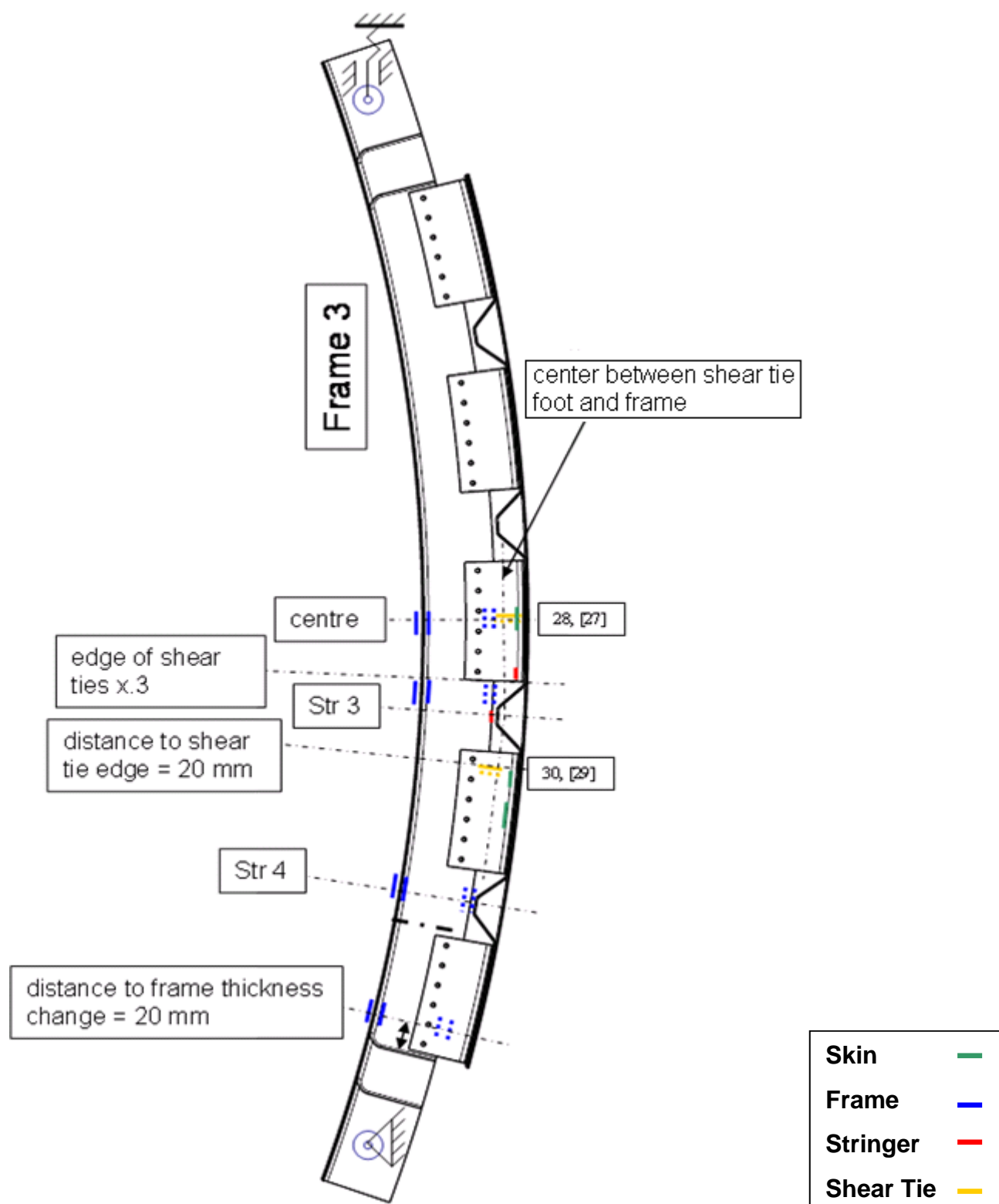
Figure 56. Strain Gauge positions: axial view

Figure 57 shows the strain gauges on the test panel. The skin channels have been covered for the paint preparation of the panel; the inner frame channels at each frame position are clearly visible.
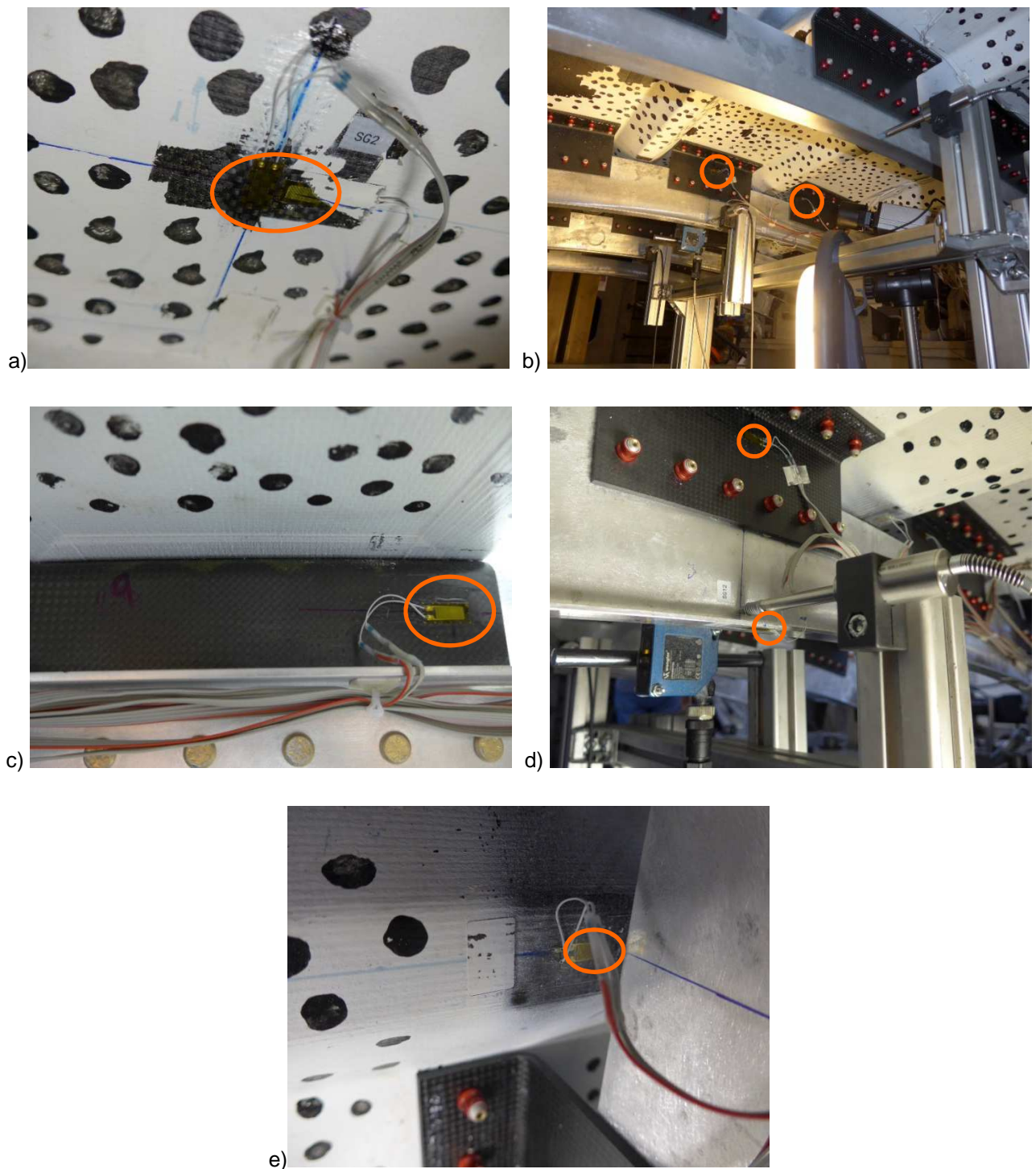
Figure 57. Strain Gauge positions on the panel: a) Strain gauge 1,2; b) Strain gauge 27,29;c) Strain gauge 28;d) Strain gauge 13, 14; e) Strain gauge 9 on the stringer foot.

Two video cameras were used to capture the structural behaviour of the panel internal structure and the bumper impact on the skin as shown in Figure 58. The video camera inside the panel captured mainly the two center shear ties since they were expected to fail first.

Figure 58. Video cameras location

The second video camera was used to record the movement of the rubber bumper. A combined recording showing the camera views in one video was provided by the test lab.

4.4. Results

Three Load Cycles (LCs) were performed separately according to the loading methodology in Figure 51. As mentioned before, the occurrence of damage events were detected by listening for audible cracking sounds and by observation of drops in the measured load/strain. At a significant drop in measured strain, the loading was held, careful observations were made and the panel was relaxed and loaded again to check if the components were damaged or not.

The first load cycle was stopped at the actuator displacement of 110 mm (27.6 kN), due to the observation of significant buckling in the center shear ties. The second load cycle was run up to the actuator displacement of 126 mm (66.3 kN) when a loud noise was heard. The final load cycle reached 154 mm (133.6 kN) where the center shear ties were not able to carry any more load and further cracking was heard.

The test stop criteria for this test was the point at which the shear ties start to fail, whilst other failure modes could occur, but the panel structure was still capable of sustaining more load.

After a discussion between Bishop and EASA representatives after the second load cycle, about the possibilities and risks of continuation of the test, it was decided to perform further load until the complete failure of shear ties. From CODAMEIN II test, the shear ties failed at a load level of 57 kN which is the maximal load of the 2nd load cycle of CODAMEIN I test. With the stronger shear ties in CODAMEIN III test panel, it was expected that the shear tie failure would initiate at a higher load level. Based on the result of the CODAMEIN I test and the tests of UCSD, it was assumed that the shear tie failure would lead to contact between the stringers and frames. This event was expected to occur suddenly. Therefore, in order to avoid potential damages of the frame, especially to the stringers, it was decided to continue loading up to shear tie failure, accepting that contact between the frames and stringers was likely to occur. After the final load cycle, and withdrawal of the impactor, the panel relaxed fully to its original pre-test profile. Except of one small scratch the skin surface outside was found to be fully intact, while most of the shear ties at the impactor location had been cracked and the outer flange of the metallic frames had deformed plastically.

At the positions where strain gauges were applied to both sides of a part (the frame and shear ties), the bending strains were calculated by the following equation:

$$E_{Bending} = (E_{Inner} - E_{Outer})/2 \qquad \text{(Equation 1)}$$

4.4.1. Load Cycle 1

The first load cycle was run up to an actuator displacement of 110 mm (27.6 kN) and stopped at a buckling event at the shear tie during elastic stage. There was no visible evidence of damage nor auditable damage noise during the first load cycle. The load-displacement curve is shown in Figure 59.
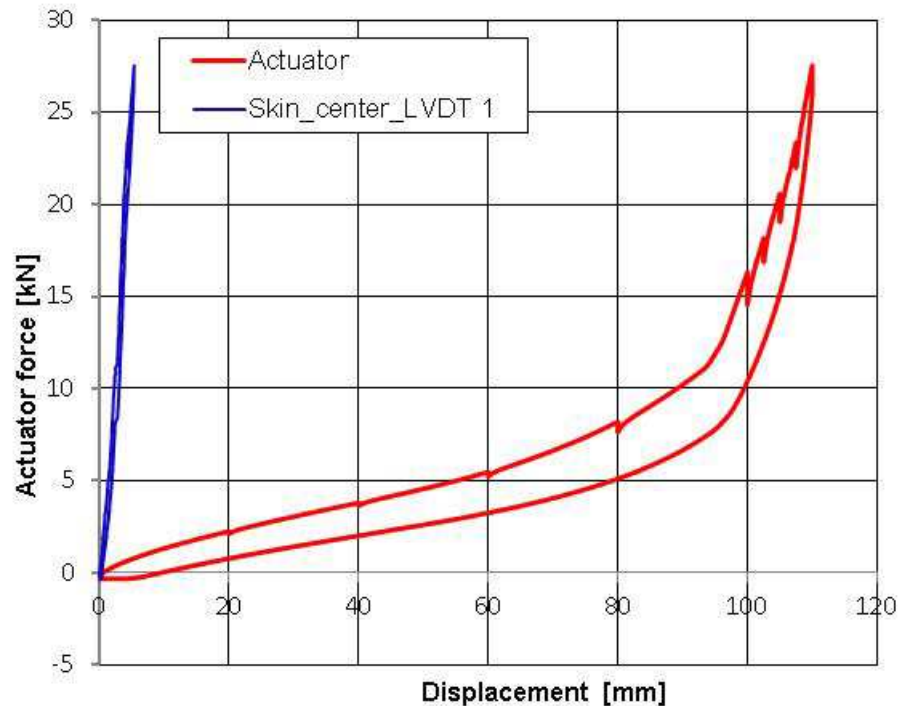
Figure 59. Load-displacement curve: skin & actuator displacement vs. actuator force (LC1)

The readings of the strain gauges in the shear tie web are displayed in Figure 60, and the sudden reversed change of stiffness in strain gauge 27 indicates that the buckling of the shear ties occurred at approximately 110 mm of the actuator displacement. At this stage, the bumper was in contact with the skin panel, but still not fully compressed.
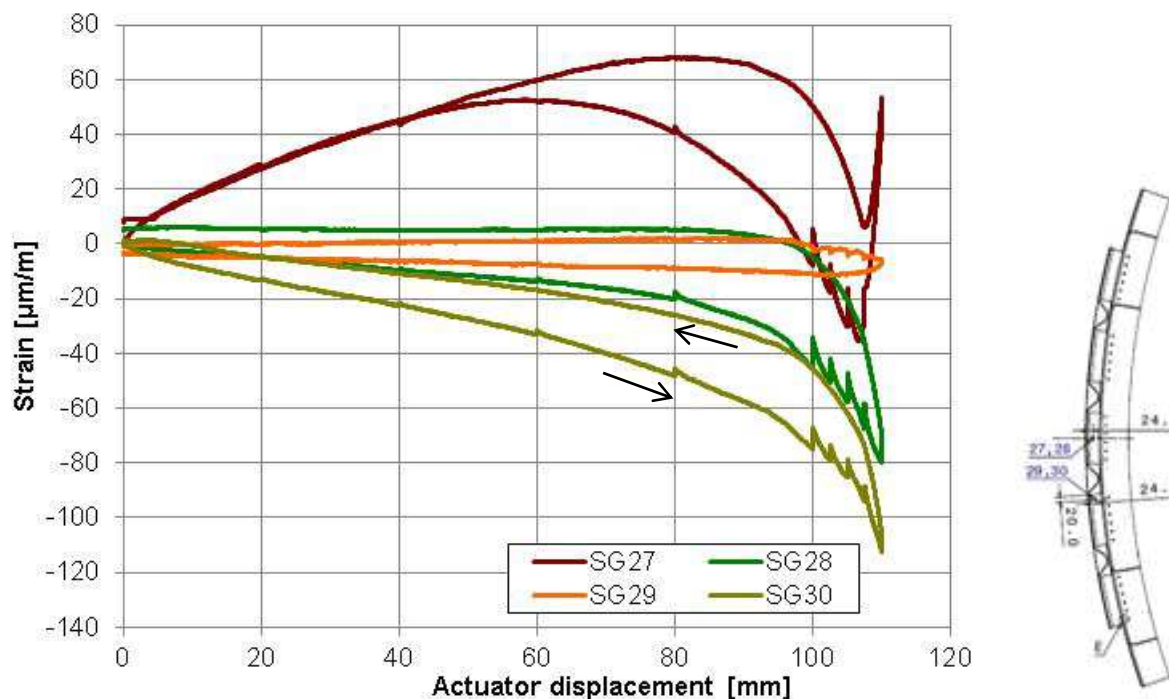
Figure 60. Shear tie strain gauges: strain vs. actuator displacement (LC1)

4.4.2. Load Cycle 2

The second load cycle was run up to an actuator displacement of 126 mm (66.3 kN) which is higher than the maximum load 57 kN of the second load cycle of the CODAMEIN II test. The load-displacement response is depicted in Figure 61.
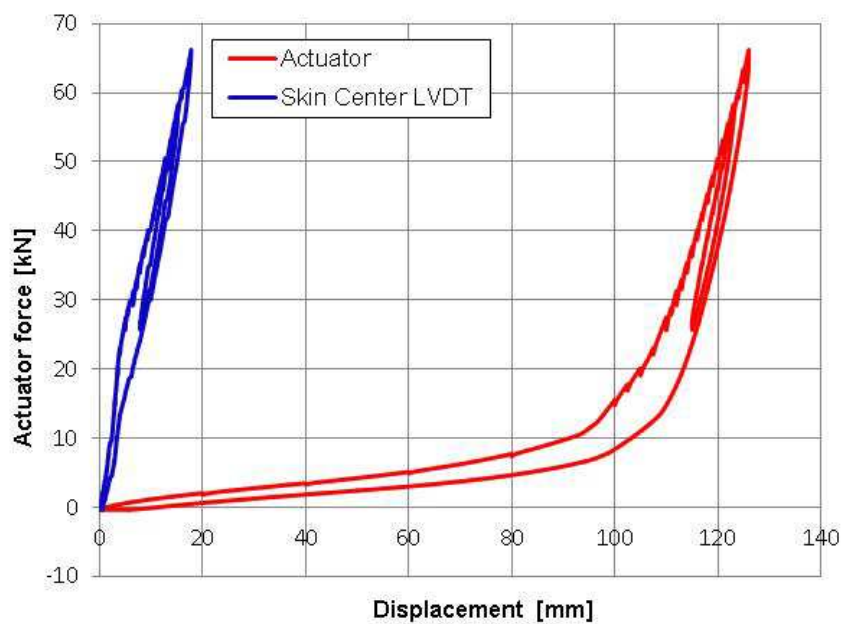
Figure 61. Load-displacement curve: skin & actuator displacement vs. actuator force (LC2)

Figure 62 shows the skin dent level under maximum load. The deformed bumper over its full length was not in full contact across the whole lower surface due to the steel joint between the steel plate and the bumper.

Figure 62. Bumper in contact with panel at 2nd load cycle max. load

At the actuator displacement of 113 mm, the bumper seems to be in full compression with the skin panel. The linear stage appeared because the impact loading was transferred through the bumper to the panel. Noise was heard at the displacement of 120 mm (58.4 kN) and the clicking noise continued until the displacement of 126 mm (66.3 kN). However, no damage on the internal panel was detected by visual inspection and NDT inspection. The damage onset of shear ties was expected.

The readings of the load cell, of the LVDTs and of the strain gauges were all documented. The LVDT 8, 9, 10 readings are displayed in Figure 63. It is noted that the LVDT 10 reached the range limit which was found to be 5 mm and it was then corrected for the 3rd load cycle by extending the range limit.
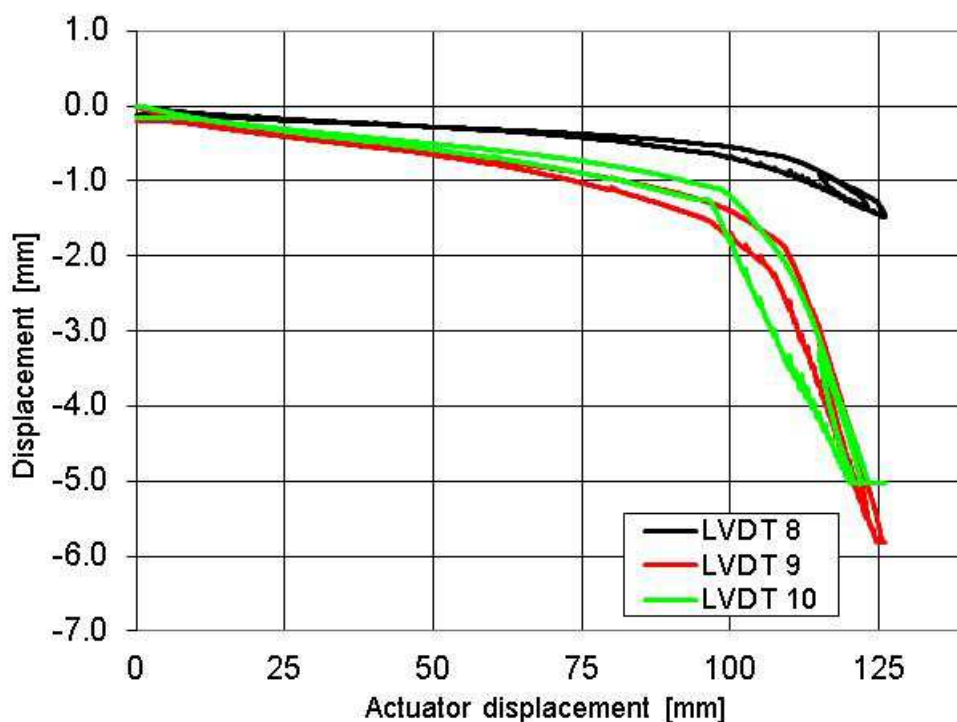
Figure 63. Displacement of LVDTs 8, 9, 10 vs. actuator displacement

The strain gauge readings in the shear tie webs are presented in Figure 64. The linear reaction of the panel was obvious as expected. The relaxing process was performed in order to check whether the shear ties were still alive. The reload curve showed that the shear ties exhibited a large buckling wave, but they were still capable to carry further loads. As mentioned before, at approximately 110 mm of the actuator displacement, the strain gauge 27 shows the linear response where the shear tie started to buckle. At 123 mm of the actuator displacement, there was a crack noise which was coincident with a slightly decreased stiffness as shown in Figure 61.
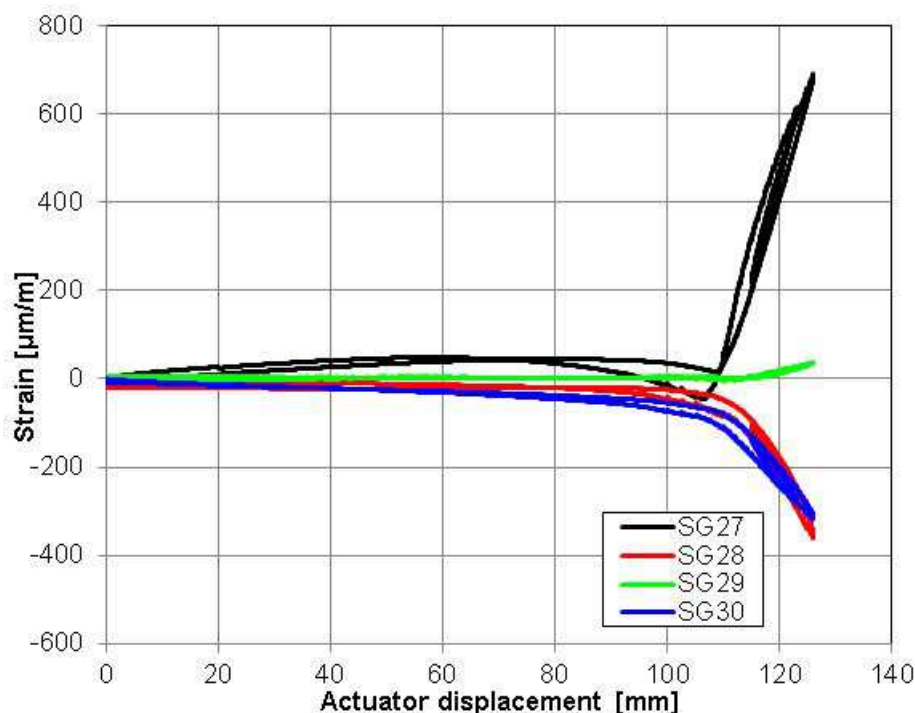
Figure 64. Shear tie strain gauges: strain vs. actuator displacement (LC2)

4.4.3.   Load Cycle 3

Clear evidence of cracks in the central shear ties was observed at around 131 mm actuator displacement. Continuous cracking noises were heard at the actuator displacement of 134 mm, 136 mm, 137 mm and 139 mm, respectively. There was no other damage except for the cracks in the center shear ties cross the radius. As the load increased, radius delaminations progressively opened. The unloading process was performed in two steps and went back to 136 mm and 130 mm. After relaxing, the panel was loaded again and the crack noise was heard at actuator displacement of 142 mm, which is much later than the first loading. A continuous cracking noise was again audible at displacement of 145 mm. Load noise at displacements of 146 mm and 150 mm indicated further damage growth. The maximum damage propagation was observed in the ST 3.3 which was found to grow to almost the entire shear tie length at a displacement of 154 mm (a load of 133.6 kN). The extent of damage was evident upon part inspection (see Section 4.4.5), which additionally revealed the first evidence of minor twisting of the center Z-profile frame. The deformation of the frames resulted in additional bending and shear load transferred to the shear ties which caused tilting of the webs. The load-displacement curve is illustrated in Figure 65, which shows the typical failure stage of the skin panel after 131 mm of the actuator displacement, where the linearity ends.
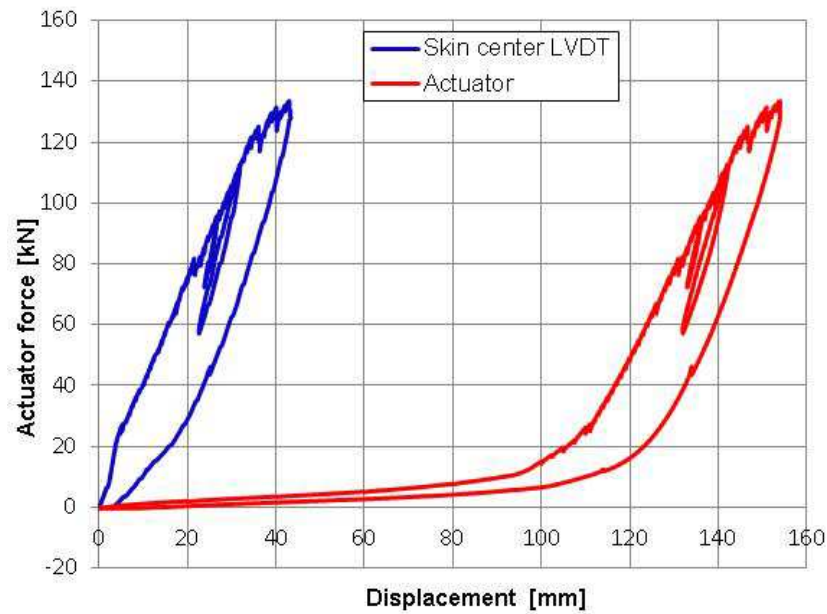
Figure 65. Load-displacement curve: skin & actuator displacement vs. actuator force (LC3)

The visual damages of the shear ties 3.3, 2.3 are depicted in Figure 66. The cracks occurred along the whole shear tie radius due to the unfolding between the shear tie and frame. The damage in the radius was caused by opening moment.
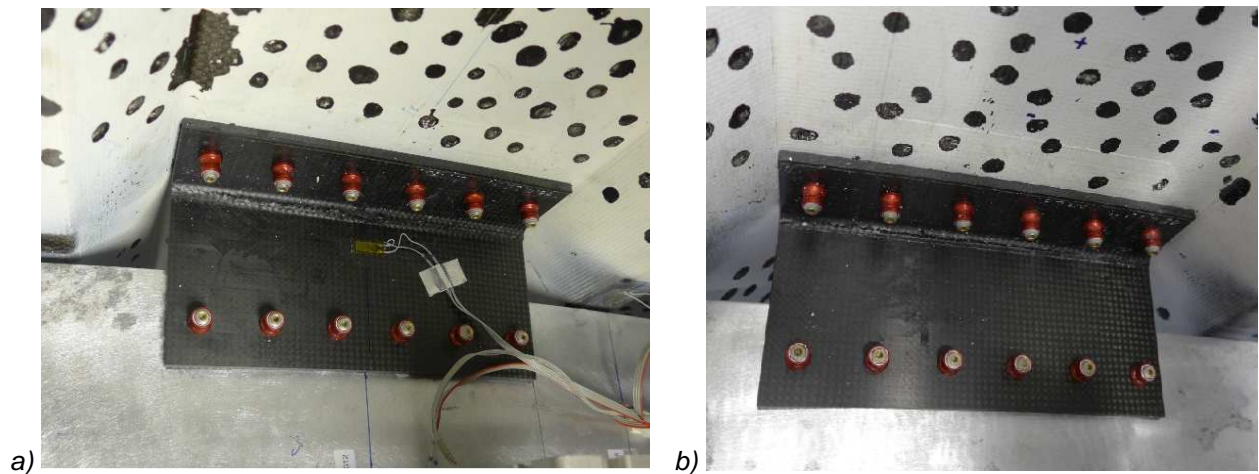
Figure 66. Shear tie damages after the third load cycle: a) shear tie 3.3; b) shear tie 2.3

The readings of the strain gauges in the shear tie web are depicted in Figure 67. According to previous studies, the shear ties were the first parts to fail and the current testing reconfirmed this statement.
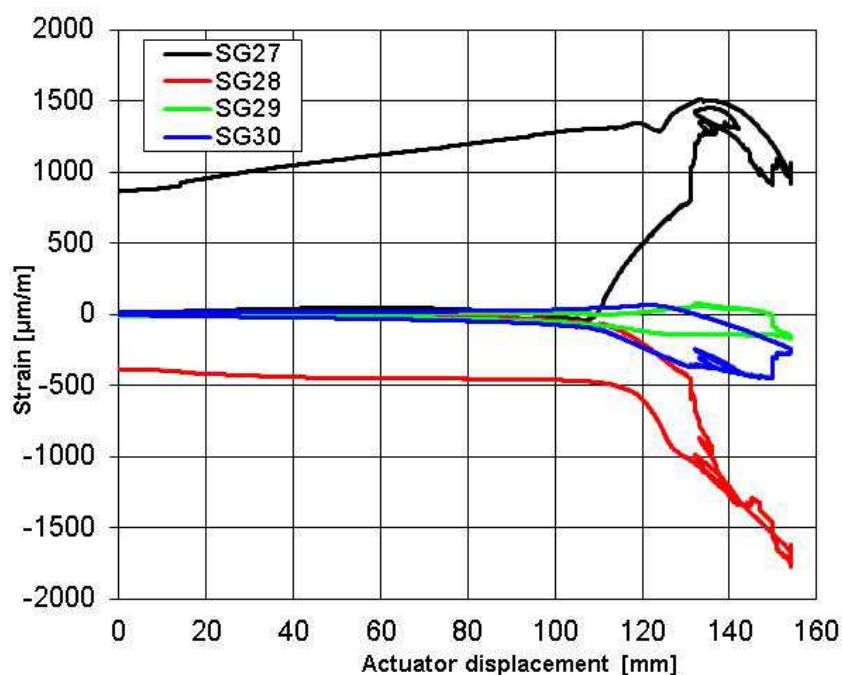
Figure 67. Shear tie strain gauges: strain vs. actuator displacement

The readings of strain gauges 6, 8, 9 and 10 are displayed in Figure 68. As described in Section 4.3, the strain gauges 6 and 8 are installed in the inner skin surface. Strain gauge 6 presented a sudden change from compression to high tension strain (approximately 2300 μm) at an actuator displacement of 135 mm. These readings are significant for the further indication of skin cracking.
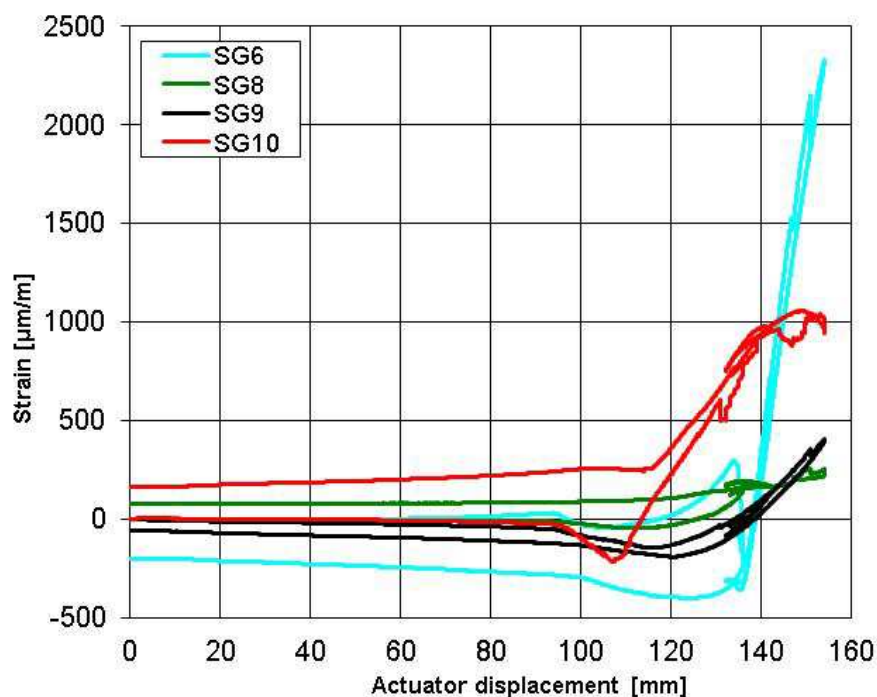
Figure 68. Skin & stringer axial strain gauges: strain vs. actuator displacement

The other strain gauge readings from frame are displayed in Figure 69 and Figure 70.
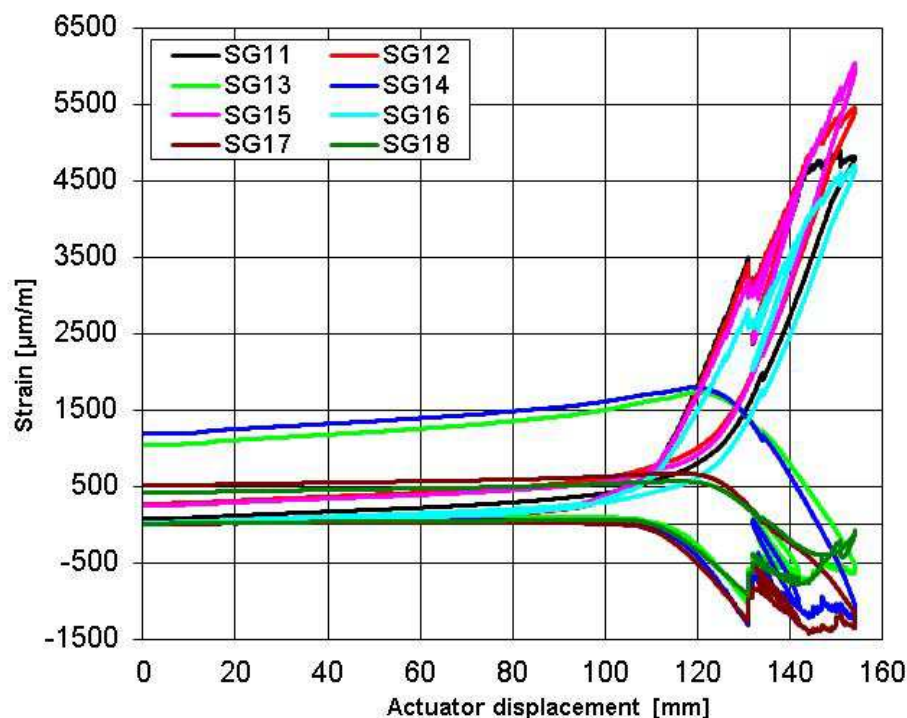
Figure 69. Frame flange axial strain gauges 11 -18: strain vs. actuator displacement
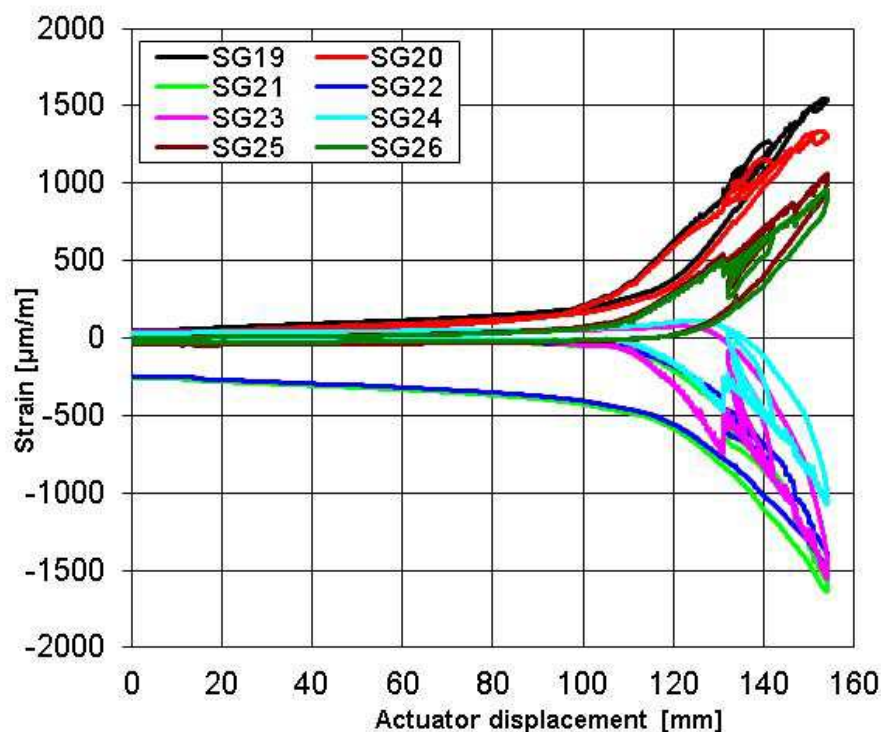
Figure 70. Frame flange axial strain gauges 19 -26: strain vs. actuator displacement

As mentioned earlier in Equation 1, the bending strain provides information about the bending direction of the frame and shear ties shown in Figure 71, Figure 72 and Figure 73. This is helpful to understand the tendency of the structural behavior, especially for the unfolding between the shear tie and frames. Therefore, as shown below in Figure 71, the bending strain measured from strain gauges 15,16 were under tension, which is in the same direction as the individual strain reading from strain gauge 15 and 16.
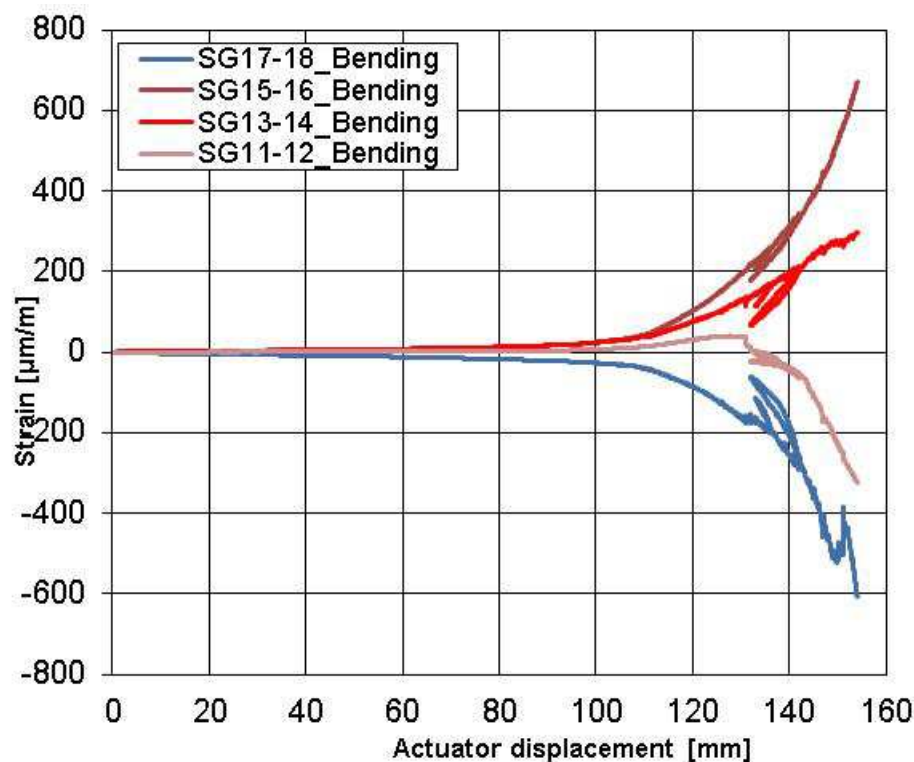
Figure 71. Frame flange axial strain gauges 11 -18: bending strain vs. actuator displacement
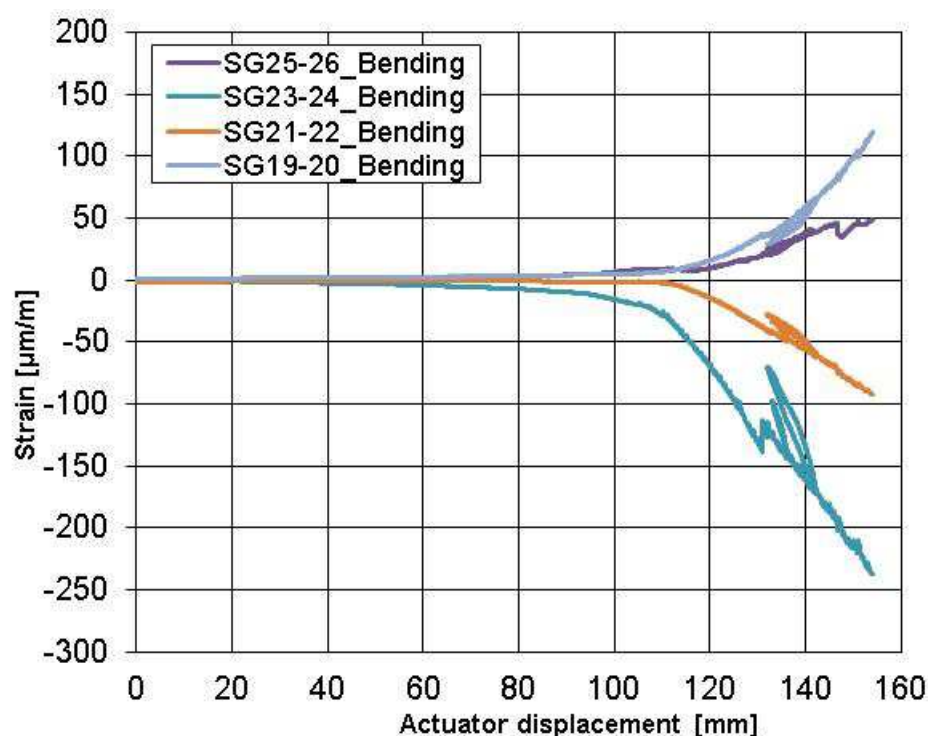
Figure 72. Frame flange axial strain gauges 19 -26: strain vs. actuator displacement
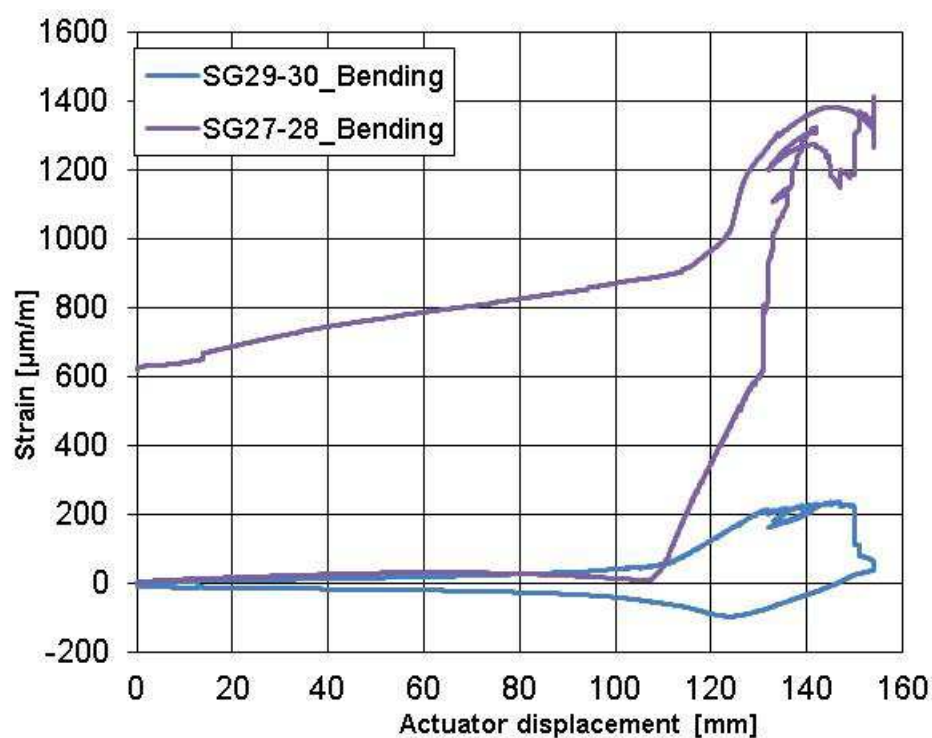
Figure 73. Shear tie strain gauges: bending strain vs. actuator displacement

4.4.4. Summary of Load Cycles

The measured force vs. actuator displacement in Figure 74 shows the panel lost overall stiffness with increased damage level beyond 131 mm of the actuator displacement. These three separate load cycles followed the testing methodology well, the slight panel setting is visible as an offset towards a higher displacement in the two latter load cycles. Moreover, the first damage is visible as a load drop and decreased stiffness in the third load cycle.
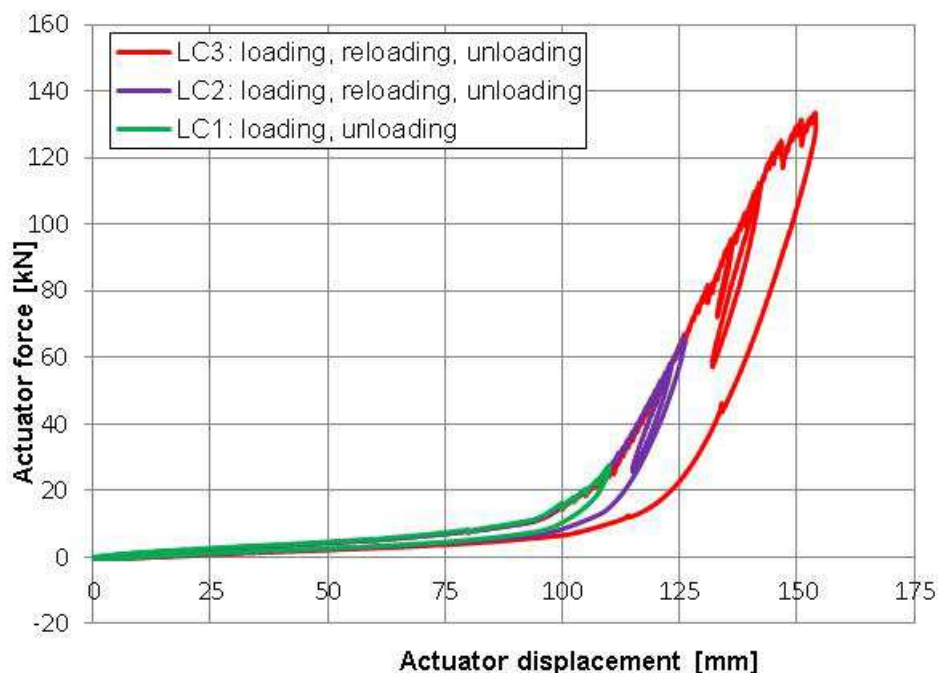
Figure 74. Force comparison vs. actuator displacement: three load cycles

The energy that was applied to impact the test panel was calculated using the actuator force and the corresponding displacement. Figure 75 shows the energies that were needed to load the entire system consisting of the test panel and the rubber bumper. The second type of energy curve displayed is related to the displacement of the skin centre of the panel and thus excludes the compression of the rubber bumper. At an impactor displacement of approximately 110 mm during the test, the rubber bumper was fully compressed and the panel started to deform. The point of full compression of the rubber bumper was indicated by the FEA at higher actuator displacement of approximately 125 mm. This matches the offset that was found in the load-displacement charts of the actuator and skin measurements of the test and FEA. Thigh might be related to the simplified linear isotropic representation of the rubber material in the FEA, due to the absence of appropriate material parameters for the rubber. The energy absorbed by the bumper was found to be approximately 726 J in the full compression status.
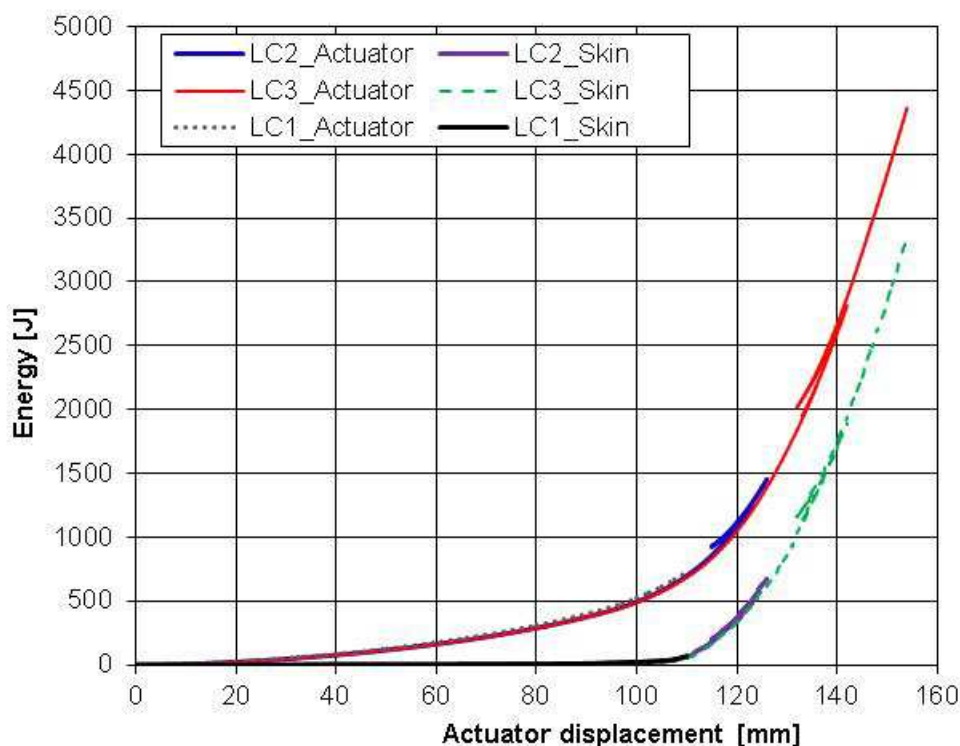
Figure 75. Energy levels in three load cycles

The energies achieved in the three load cycles associated with the initiation of buckling, occurrence of nonlinearity and shear tie failure, are reported in Table 7. The actuator deformation is not taken into account here.

Table 7. Energy levels of the test load cycles

	1st Load cycle	2nd Load cycle	3rd Load cycle
Energy at first indication of damage	723 J (elastic buckling onset)	1409 J (nonlinearity)	2020J (shear tie failure and skin crack)

4.4.5. Inspection

The panel has been inspected visually and by NDT prior to testing and after the second load cycle and the final load cycle.

The scan pattern for the A-Scan is displayed in Figure 76. In the pre-test scan, also the outer edges of the panel were scanned for damage from manufacturing or transport. The A-Scan was performed on the flat and all the shear ties and the protruding parts of the two center stringers.
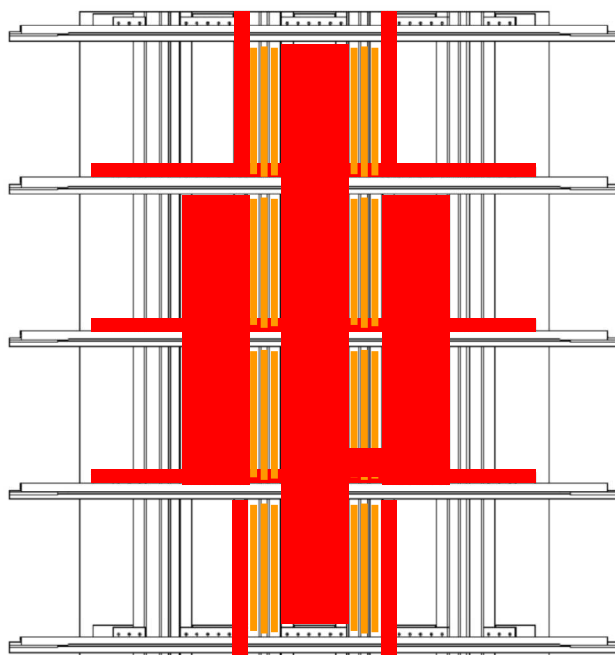
Figure 76. A-Scan inspection pattern

The frames and shear ties were numbered, as illustrated in Figure 77.
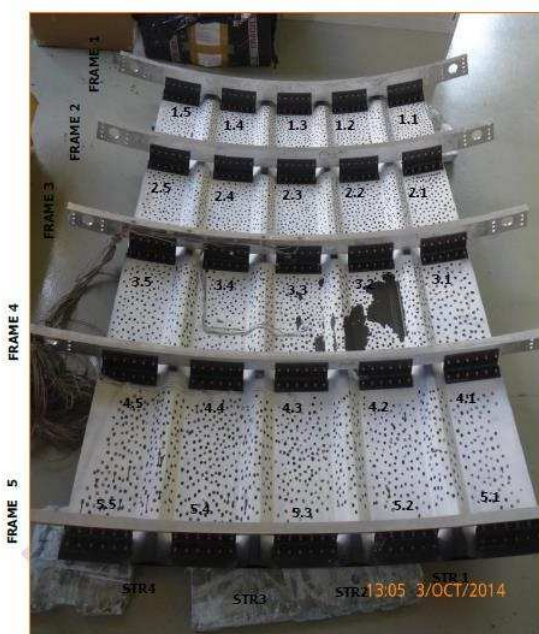
Figure 77. Panel inside and shear tie numbering [Bergo Soto 2014]

The scanned shear tie damages are displayed in Figure 78. The damage that was visually found in the radii of three shear ties (2.3, 3.3, 4.3), could not be reached by the NDT due to the curvature of the surface. None of these damages reached the flat regions of the shear ties which were scanned. Shear tie 2.3 presents the crack across 3/5 of the radius length and delamination in the edge about 10 mm

length and 7 mm width. Shear tie 3.3 cracked along 4/5 of the radius length direction, and cracks can also be observed in the flange. Moreover, this shear tie had delaminations on both edges close to the shear tie radius. Shear tie 4.3 cracked along the entire length of the radius.

In addition, damage was observed through NDT in the radius of shear tie 4.2 and 5.2. Shear tie 4.2 showed no crack but a delamination of dimension 36.7 mm by 10.4 mm. Shear tie 5.2 had similar delamination as shear tie 4.2, with larger dimensions of 39.3 mm by 30.1 mm.
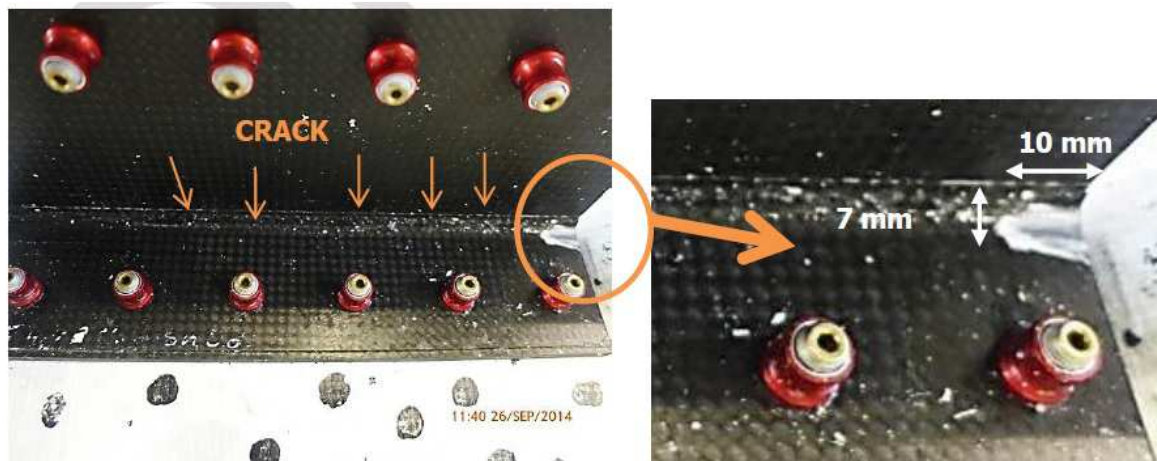
a)
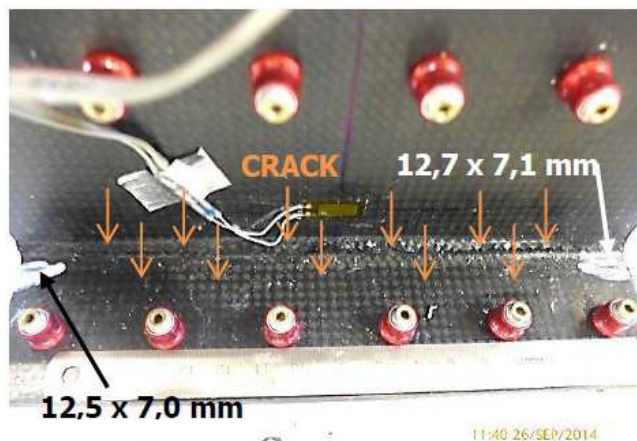
b)
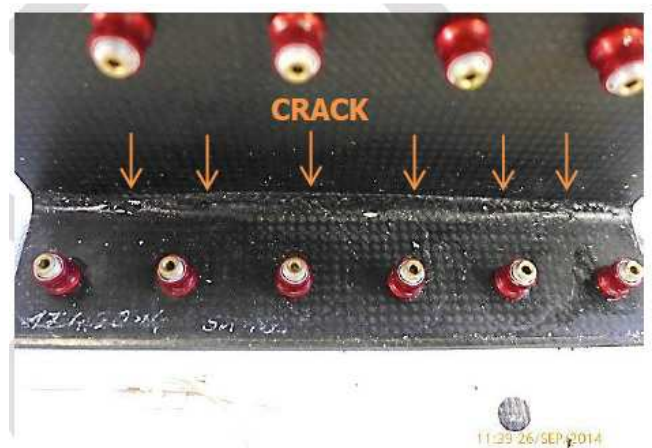
c)
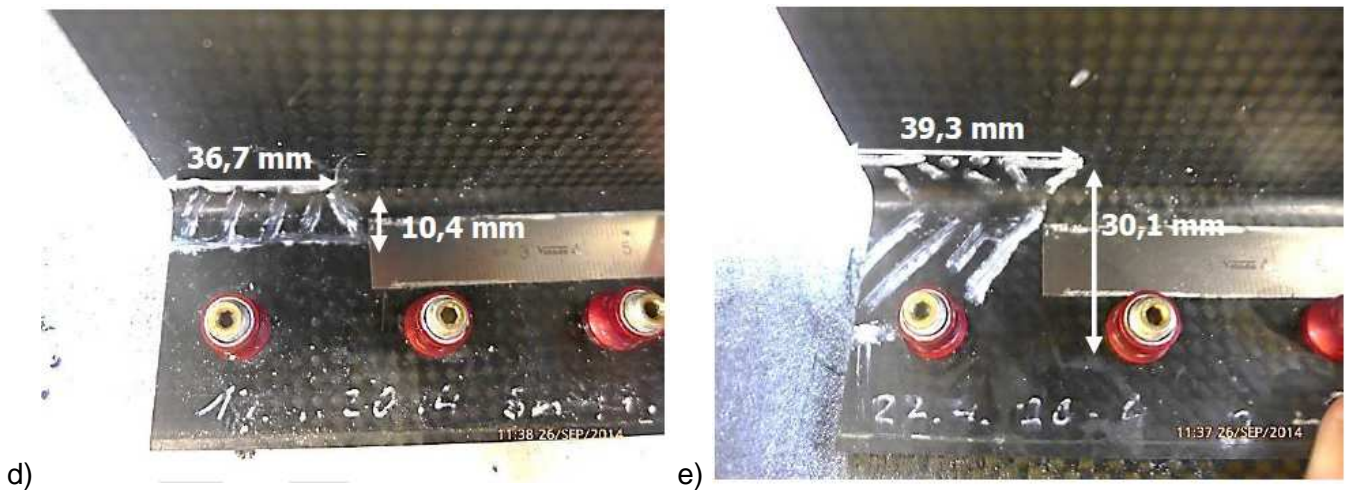
Figure 78. Damages detected in shear ties: a) shear tie 2.3; b) shear tie 3.3; c) shear tie 4.3; d) shear tie 4.2; e) shear tie 5.2 [Bergo Soto 2014]

The overall delamination, as determined by manual pulse-echo ultrasonic inspection is illustrated in Figure 79. The NDT inspection, after the three performed load cycles, revealed only damage on the skin panel. No delamination was detected between the skin and the stringer foot flange.
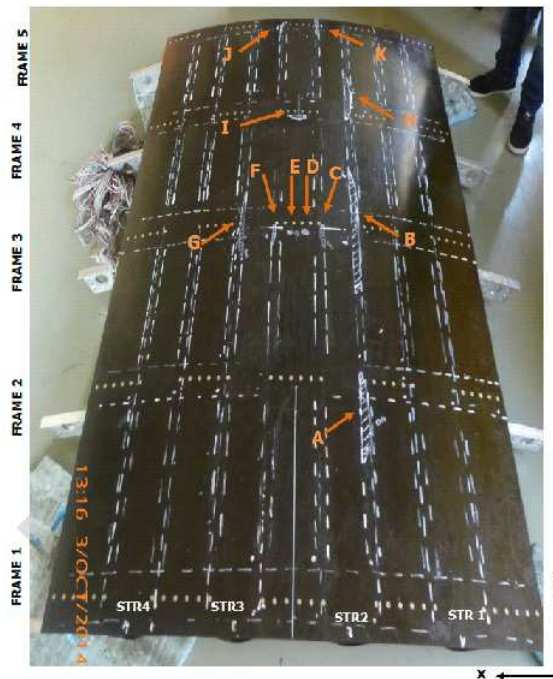
Figure 79. Locations of the delaminations after inspection [Bergo Soto 2014]

The detailed images for the detected delamination areas are described from Figure 80 to Figure 83.
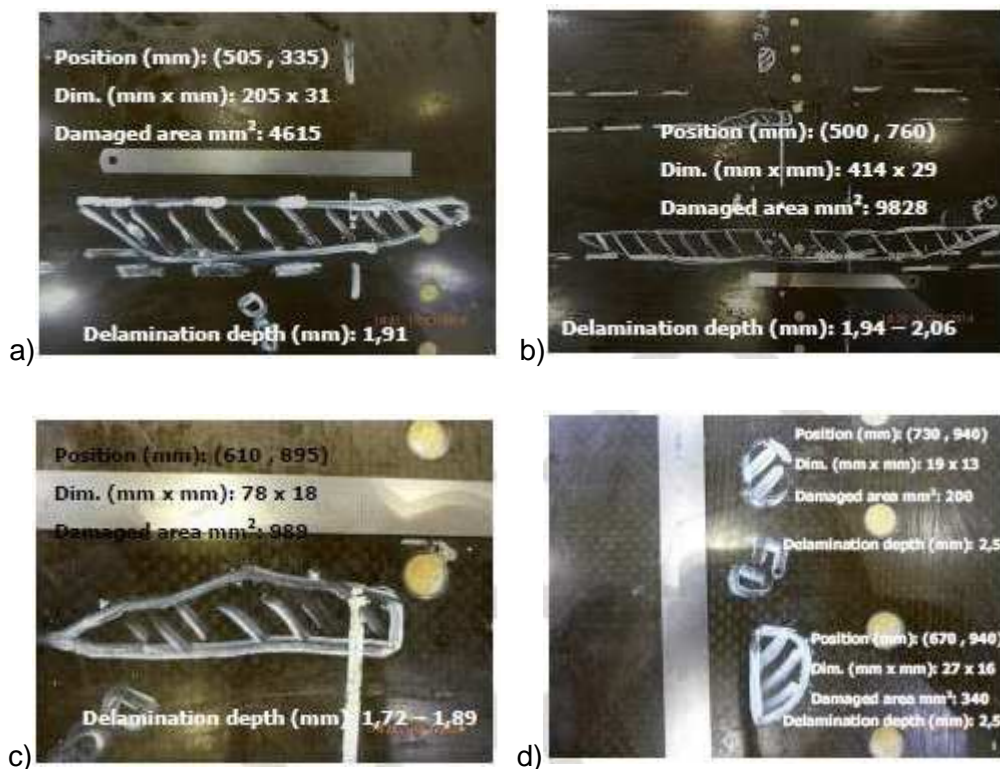
Figure 80. Characterization of delamination: a) Damage A; b)Damage B; c) Damage C; d) Damage D,E [Bergo Soto 2014]
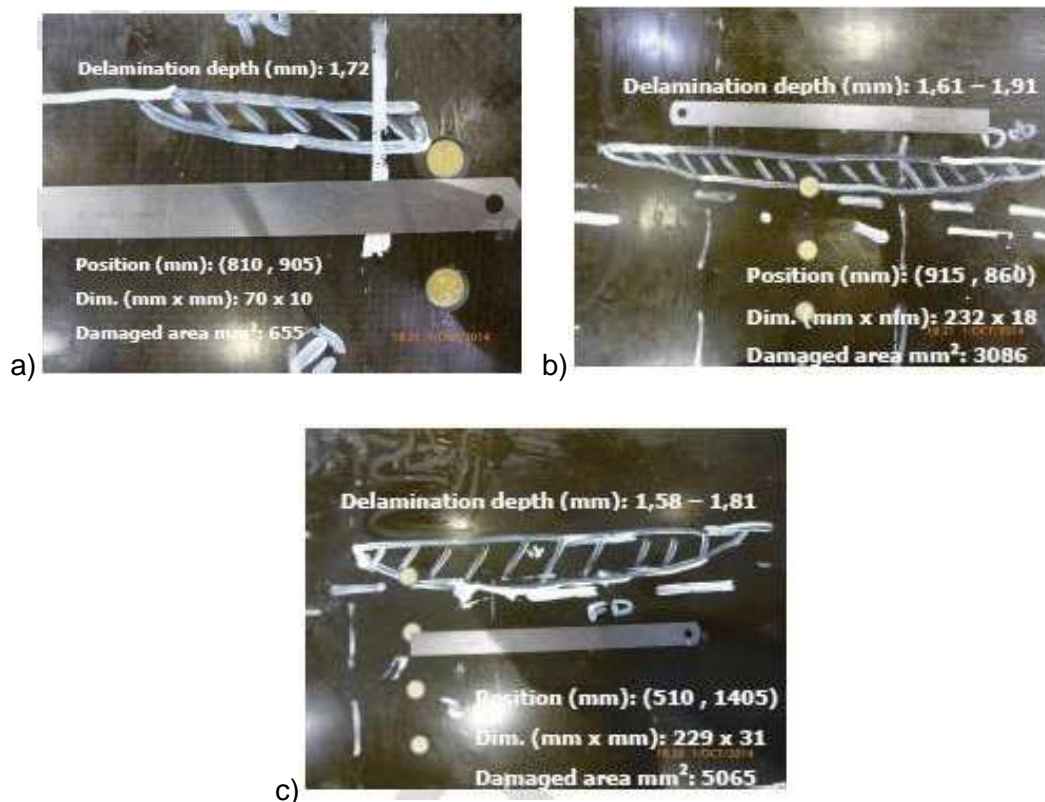
Figure 81. Characterization of delamination: a) Damage F; b) Damage G; c) Damage H [Bergo Soto 2014]
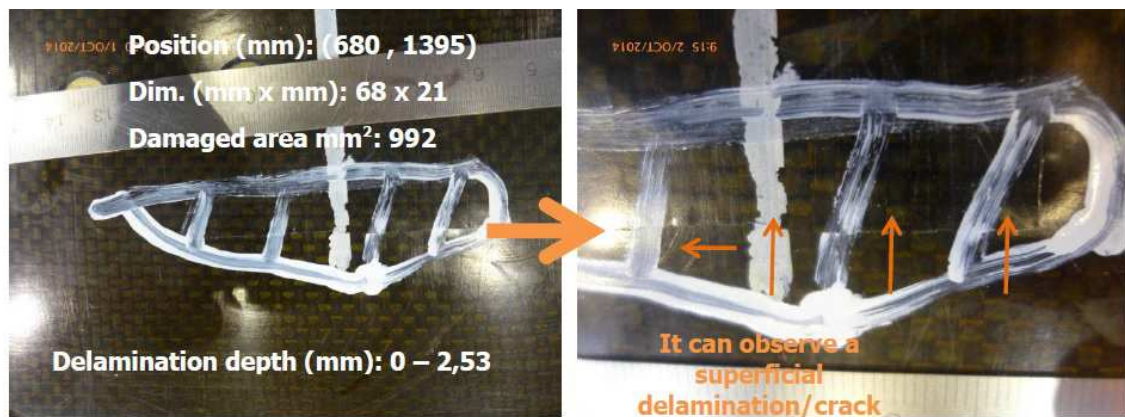
Figure 82. Characterization of delamination: Damage I [Bergo Soto 2014]
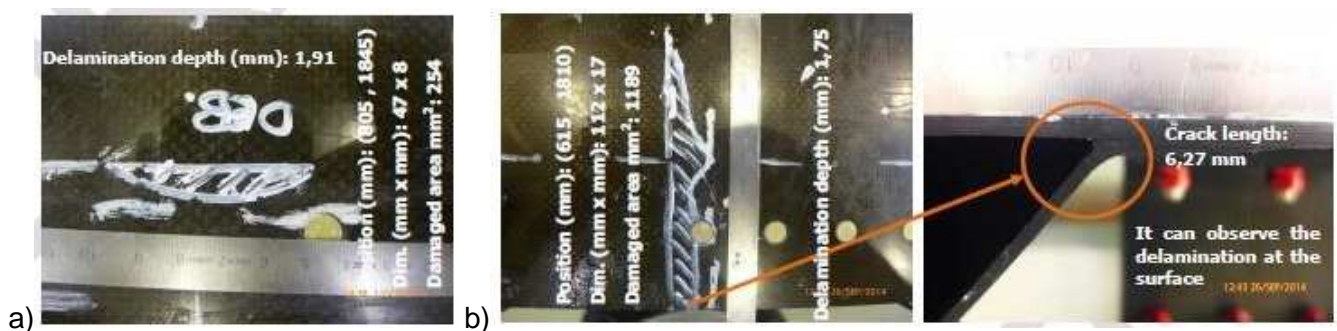
Figure 83. Characterization of delamination: a) Damage J; b) Damage K [Bergo Soto 2014]

From the inspections, there are two visible damages (damage D and damage K) at different degrees of visibility. Damage D is barely visible and damage K is clearly visible. Damage D showed 2.5 mm depth. Damage K appeared at the end of the panel in axial direction along the interface between the skin and stringer flange. Damage I induced 0 mm - 2.53 mm delamination depth. Compared to the nominal skin thickness of 2.69 mm, damage D and I is regarded as the internal delamination between the composite layers.

4.4.6. Comparison of the CODAMEIN Test Results

The last load cycles of the CODAMEIN I, CODAMEIN II and CODAMEIN III tests are compared using the global load-displacement readings in Figure 84. At loads above 25 kN, the CODAMEIN II panel behaved softer which indicates faster damage growth in the shear ties.

The load-displacement curves of the actuators indicated different compression behavior of the rubber bumper in comparison with the skin displacement chart. It was compressed for the first time in the first load cycle of all the tests which possibly made it behave softer in later compressions. The slopes rather indicate a stiffer response of the rubber bumper in the CODAMEIN III test than CODAMEIN II test and CODAMEIN I test.
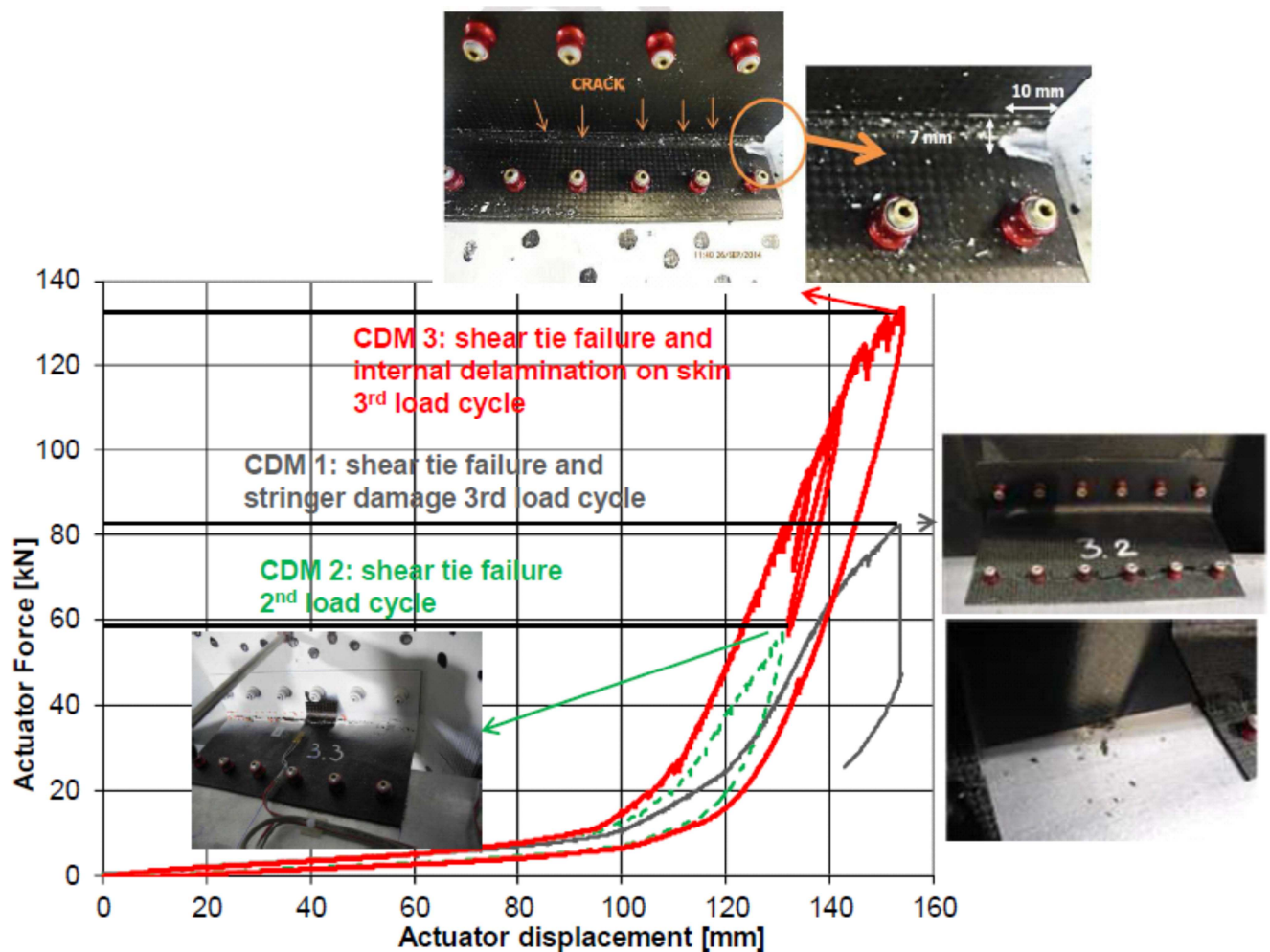
Figure 84. Load-Displacement curves comparison of the last load cycles: CODAMEIN I, CODAMEIN II and CODAMEIN III

All the CODAMEIN projects show the similarity of the typical three stages (pre-contact stage, contact stage, failure stage) as described before. In the contact stage, the stiffness of the CODAMEIN III panel is higher than that of the CODAMEIN II panel due to the use of stronger shear ties, five frame attachments instead of three and the additional rotational stiffness.

Moreover, the damage onset of shear ties was of interest to compare the three tests. In CODAMEIN I test, the shear tie failure happened at 46.7 kN (see Figure 85) at the second load cycle. The threshold energy for the failure was calculated to be 1140 J, which represents a vehicle with a mass of 2280 kg impacting the fuselage with a velocity of 1 m/s.

During the first load cycle of CODAMEIN II, the shear tie 3.3 had visible crack in the radius which covered ¾ of the width of the shear tie, at the load level of 39.5 kN. The failure threshold energy for the first damage onset was 969 J, which is lower than the failure threshold energy level of CODAMEIN I test.

a)   *b)*
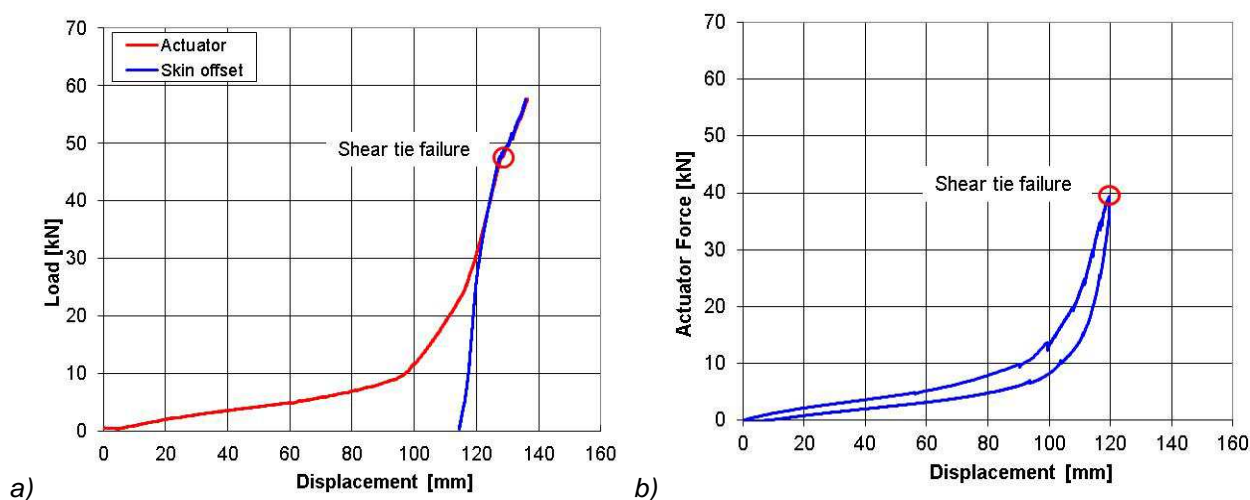
Figure 85. Shear tie failures: a) CODAMEIN I 2nd load cycle; b) CODAMEIN II 1st load cycle

The CODAMEIN III test indicated that the shear tie failure occurred much later than previous tests, at a load level of 82.1 kN at the third load cycle. The energy level for the tested damage onset was listed in Table 8.

Table 8. Energy levels of damage onset

	Energy at first indication of failure	Load level at first failure
2nd Load cycle (CDM I)	1140 J	46.7 kN
1st Load cycle (CDM II)	969 J	39.5 kN
3rd Load cycle (CDM III)	2020 J	82.1 kN

4.4.7. Comparison with UCSD Results

The CODAMEIN III testing with 4 stringers and 5 frames was in conjunction with the research activities of the UCSD's research group with 4 stringers and 3 frames in terms of the harmonized test panel design (the UCSD used all composite test panels while CODAMEIN III uses a hybrid design with high similarity) and the same rubber bumper used to impact the same location on the panel. The test fixtures of CODAMEIN III that were different to those of the UCSD were adopted from the CODAMEIN I and CODMEIN II test. The characteristic damage sequence of the CODAMEIN I test and the UCSD tests was already confirmed by the CODAMEIN II test and the associated numerical analyses.

The experiments of CODAMEIN I, II and III of Bishop GmbH are compared with Frame01 and Frame02 of UCSD in Table 9 and Table 10.

Table 9. GSE Blunt Impact Tests by UCSD [Kim 2013]

Specimen ID	Panel Config	Loading Details	Intermediate Failure Modes	Final Failure Mode	Externally Visible?	Max Load (kN)	Max Indent (mm)
Frame01	4 Stringers, 3 Frames	Long Cyl. Bumper Spans 2 Frames, Between Stringers, Q-Static	Shear Ties Crush, Stringer Sever & Flange Delam	Frame Crack	N	57.4 (28.7/ Frame)	75.5
Frame02	5 Stringers, 3 Frames	Long Cyl. Bumper Spans 2 Frames, at Stringer, Q-Static	Shear Ties Crush, Stringer Sever & Flange Delam, Skin Crack	Frame Crack	Y	71.0 (35.5/ Frame)	55.9

Table 10. GSE Blunt Impact Tests by Bishop GmbH

Specimen ID	Panel Config	Loading Details	Intermediate Failure Modes	Failure Type	Externally Visible?	Max Load (kN)	Max Indent (mm)
CODAMEIN I 3 LC (2LC)	4 Stringers, 5 Frames	Long Cyl. Bumper Spans 3 Frames, Between Stringers, Q-Static	Shear Ties (ST) Crush	Frame Twist Stringer Failure	N	83 (46.7 ST Crush)	38.8 (13 ST Crush)
CODAMEIN II 2 LC (1 LC)	4 Stringers, 5 Frames	Long Cyl. Bumper Spans 3 Frames, Between Stringer, Q-Static	Shear Ties Crush	Significant Shear Ties Crush	N	57 (39.5 ST Crush)	21.5 (12.5 ST Crush)
CODAMEIN III 2 LC	4 Stringers, 5 Frames	Long Cyl. Bumper Spans 3 Frames, Between Stringers, Q-Static	Shear Ties Buckling	No Failure	N	66.3 ST	17.7 ST
CODAMEIN III 3 LC	4 Stringers, 5 Frames	Long Cyl. Bumper Spans 3 Frames, Between Stringers, Q-Static	Shear Ties Crush & Stringer delamination & Skin Crack	Significant Shear Ties Crush & Skin Crack	Y	133.6 (82.1 ST Crack, 125 Skin Crack)	43 (23.2 ST Crack, 38.1 Skin Crack)

In the UCSD tests that were run up to panel failure, the centre shear tie failed first. In Frame01 due to load redistribution, the centre shear ties of the adjacent frames failed at the same impactor displacement which made the centre frames contact to the centre stringers, creating a direct load path to the frames and finally cracking the frame.

A comparison of the CODAMEIN I, II and III tests with Frame01 and Frame02 of UCSD tests shows the similarity of the failure. These tests all indicated that the shear ties are the first parts to fail within the test panel.

In CODAMEIN III (Table 10) the loaded centre shear ties at 17.8 mm indentation 66.3 kN started to bend/buckle first, then while the L-shape of these shear ties opened and initiated damage in the radii. The centre region of the Z-profile frame shows minor twisting due to load redistribution. Delamination and cracking on the skin panel as well delamination between the skin and the stringer foot flange was detected. This behavior can also be observed in Frame01 and Frame02 of UCSD. The maximum damage propagation was observed in the center shear tie which was found to grow to almost the entire shear tie length at a displacement of the skin 43.1 mm (a load of 133.5 kN) during the third load cycle.

5. Correlation between Tests and FE Prediction

The FEA predictions correlated well the CODAMEIN III test results, especially the predicted shear tie failure displacement which varied by only 6.8%. The predicted post shear tie failure (after 122 mm) was plotted in dotted line in black as shown in Figure 86. The frame exhibited large bending as plastic failure at 154 mm actuator displacement in both test and simulation. The detailed comparisons are reported in Table 11.
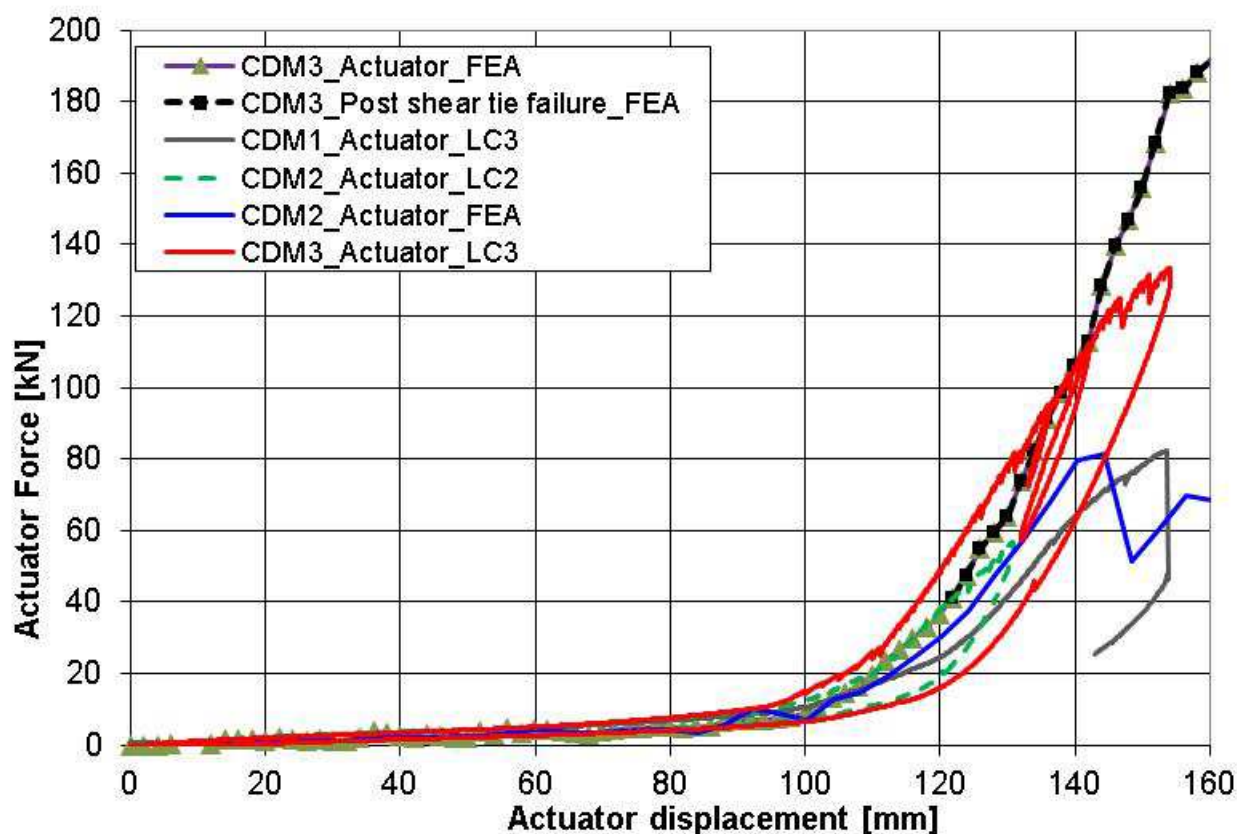
Figure 86. Load-Displacement curves comparison of tests and FE predictions: CODAMEIN I, CODAMEIN II and CODAMEIN III

Table 11. Comparison between FE and Tests

	FE Prediction	Test
Shear tie failure initiation	122 mm	131 mm
Large frame rotation	154 mm	154 mm (test stop)

5.1.   LVDT Comparison

A comparison of the load-displacement measured in the test and generated by the FEA is shown in Figure 87, where the additional skin center displacement is included. The slope of the load-displacement curves relating to the actuator displacement show good agreement. The FEA result exhibits minor dynamic influence on the results in the low load phase. The displacements measured at the skin centre, next to the shear tie ST3.3, show an offset between the test and the FEA which is expected to be caused by the material properties assumed for the rubber bumper. The rubber bumper was modelled using dimensions measured from the test bumper and the material was represented by simplified linear elastic material whose stiffness was adjusted within the FEA sensitivity study. Further adjustments were not done to the rubber bumper representation.
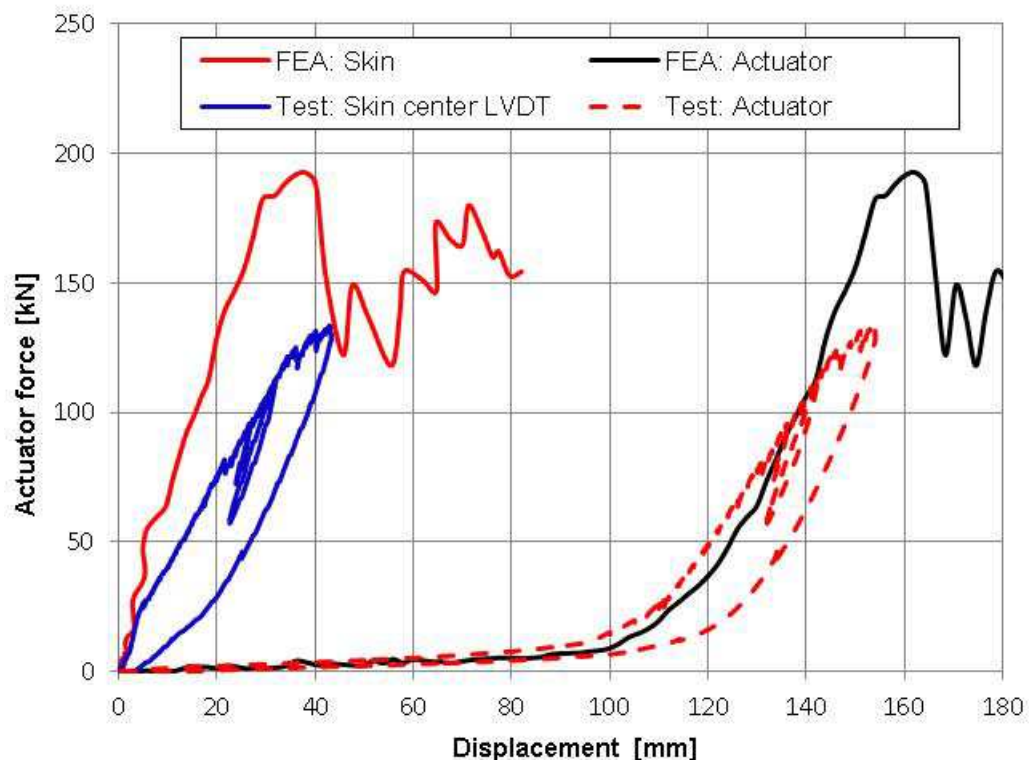
Figure 87. Load-Displacement curves comparison: skin and actuator displacement from tests and FE prediction

A first comparison of the detailed readings of displacements and strains of the test and the FE analysis is given below. In this comparison, the FEA results are compared to the readings of the 3rd load cycle of the CODAMEIN III test.

The positions of the LVDTs that were used in the test, as well as their numbering are described in Section 4.3. In the comparison of the displacements measured by LVDTs (see Figure 53), the offset of the skin centre displacement is shown in Figure 88, which was also indicated by the global load-displacement charts of the test and the FEA. The displacement of the end of frame 5 in the impact direction showed good agreement with FE prediction and it is close to zero.
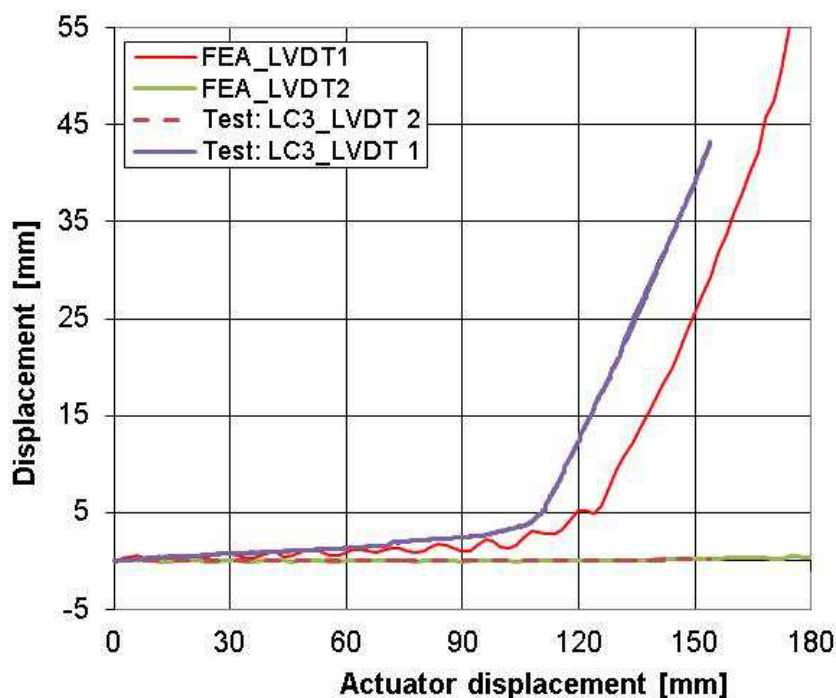
Figure 88. Test and FEA: Displacements of LVDTs 1 and 2

The LVDTs 3, 4 and 7 which assessed the rotation of the frame ends 3 and 4 were underestimated by the FEA, with an offset of up to 15 mm actuator displacement. The general magnitude of rotation was found to be very low (see Figure 89) with a maximal rotation angle 1.7 degree. However, the safety factor of 3 was introduced to design for the test fixture.
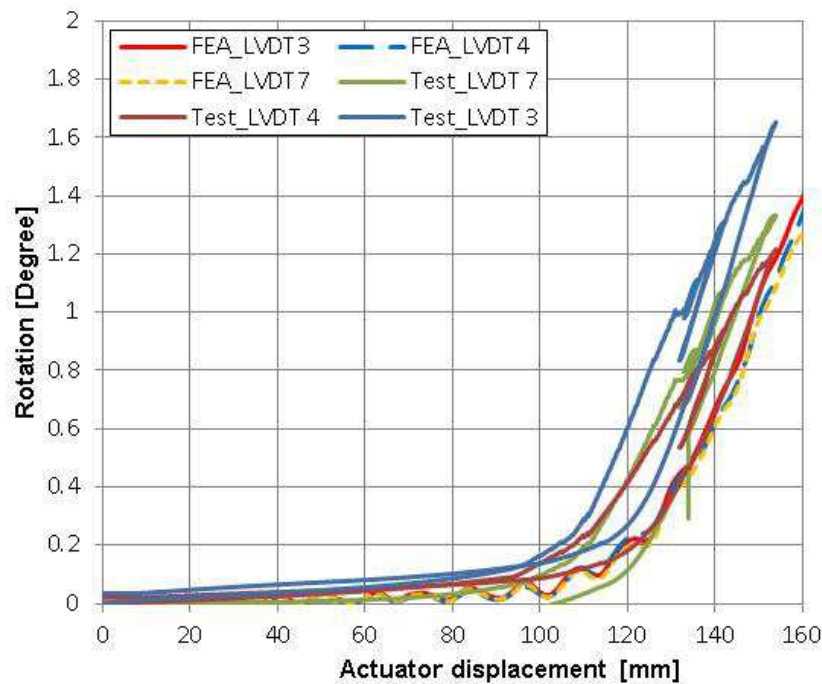
Figure 89. Test and FEA: Rotation of LVDTs 3,4,7

The LVDTs 8, 9 and 10 in Figure 90, which indicated the out-of-plane deflections of center frame 3. The displacement of LVDT 8 was overestimated by FE analysis while the displacements of LVDT 9 and 10 were underestimated by FEA analyses.
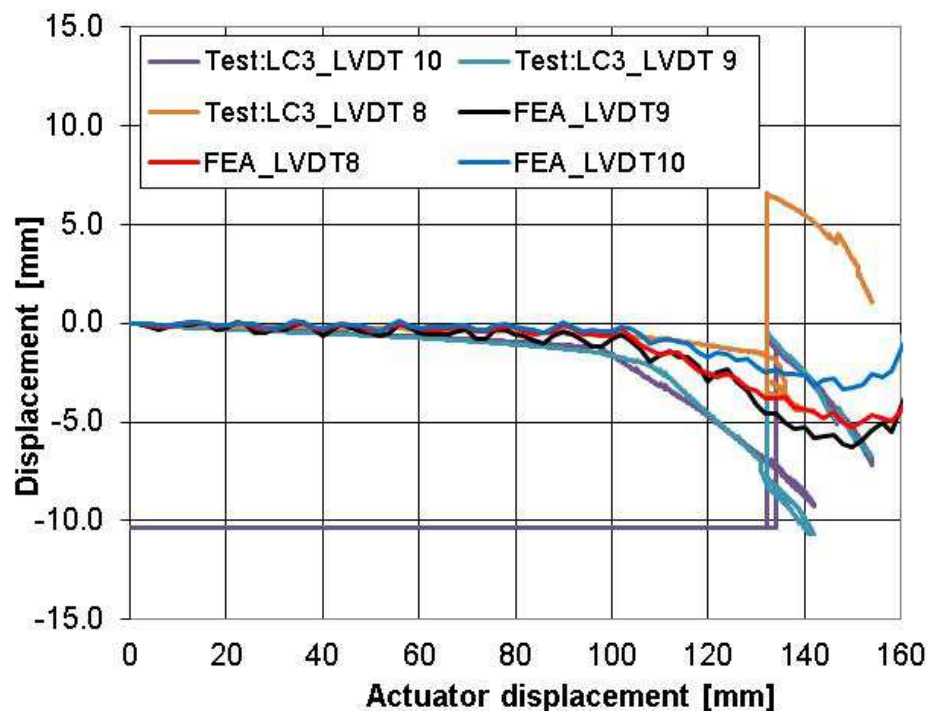
Figure 90. Test and FEA: Deflection of LVDTs 8, 9 and 10

The compression of the spring-based test fixtures presented poor correlation between FEA prediction and testing results of LVDTs 5 and 6, as shown in Figure 91. The compression less than 4.5 mm is regarded to be low and they showed quite similar compressed level by both the prediction and test results.
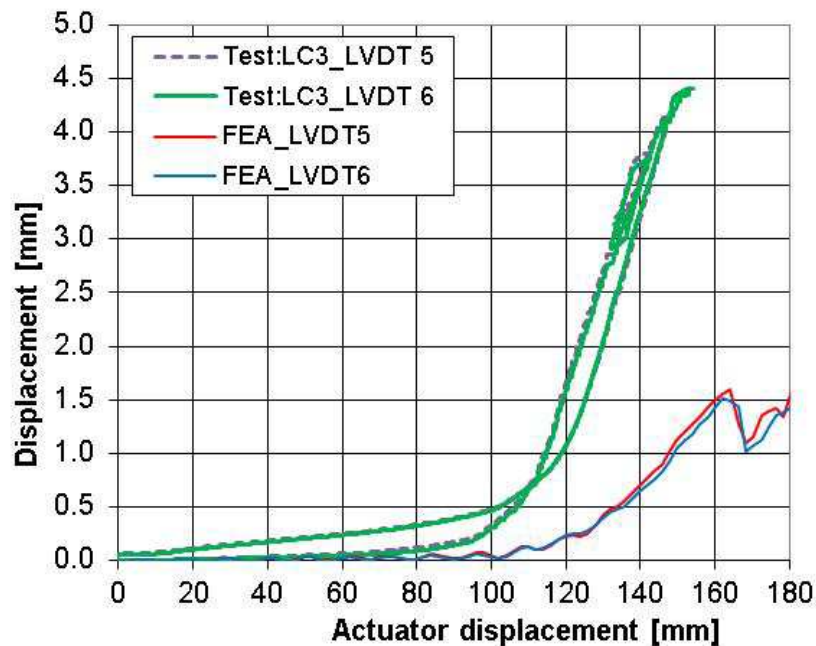
Figure 91. Test and FEA: Compression of LVDTs 5 and 6

The deviations in the measured boundary displacements and rotations between the test and the FEA enable an assessment of the friction and damping behaviour of the massive test fixtures which were modelled as perfectly elastic and frictionless in the FEA. The mass of the test fixtures would cause friction when the test fixture is compressed since it is not carried by the gliding pads but by the guiding pins of the springs. Independent from the effect of the test fixture' mass, the described deviations may also indicate that linear motion within the test fixtures causes friction. As a result, the effective compression stiffness of the test fixtures was obviously increased beyond the spring stiffness. For clarification of the assumed friction influence, a partial 3D model of the test fixture is displayed in Figure 92. The mass of the movable part of the test fixture and the mass of the panel may generate significant friction at the guide pins. The actuator load is transferred through the gliding pads where also friction may occur corresponding to the actuator load.

Figure 92. Test fixture: mass influence and friction

5.2. Strain Comparison

The strain gauge positions and numbers can be found in Figure 55. The skin strains in circumferential direction and in axial direction, in the loaded skin bay (frame 3-4, stringer 2-3) show good agreement. The results are displayed in Figure 93. Only at high load the circumferential strain gets underestimated by the FEA.
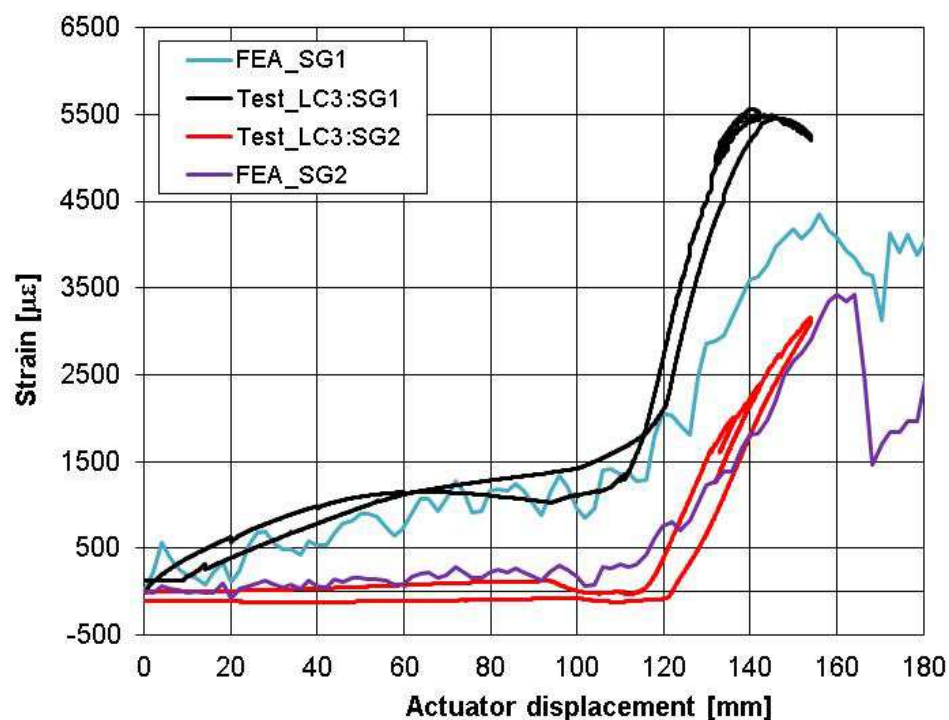
Figure 93. Test and FEA: Strain gauges 1 and 2

The strains of the skin strain gauges 3 and 4 show very good agreement between test and FEA (see Figure 94), while the FEA outputs clearly show dynamic effects due to the high loading rate used in the simulations. However these dynamic effects are limited and are obvious only at low measured strains.
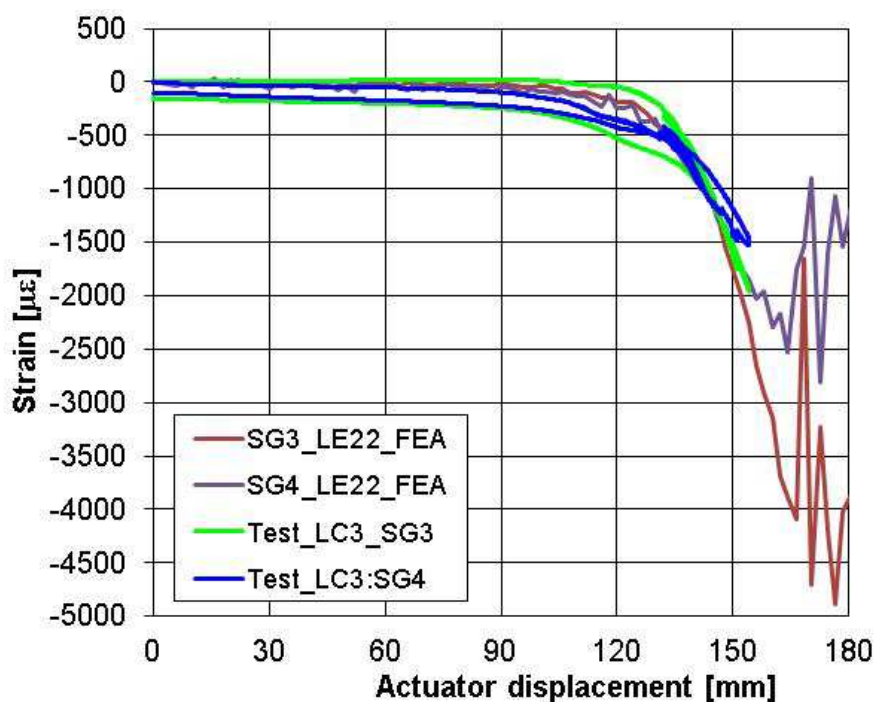
Figure 94. Test and FEA: Strain gauges 3 and 4

The strain of the skin strain gauge 5 was predicted accurately up to the actuator displacement of 133 mm, as depicted in Figure 95. At this point, the skin suffered sudden change from compression to tension at the next loading stage in the test. The FEA predicted the sudden change of strain at the actuator displacement of 152 mm, where the compression strain had reached 3250 µm.
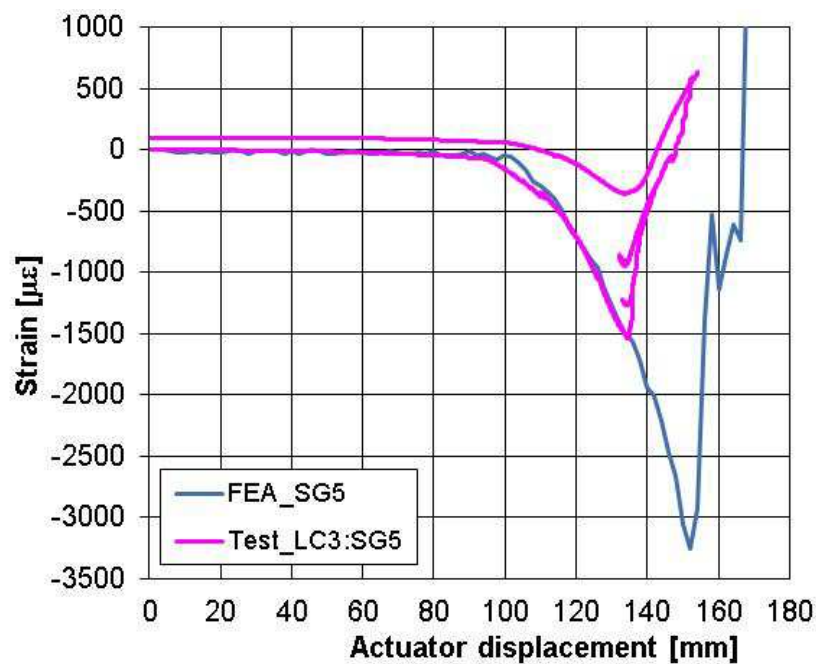
Figure 95. Test and FEA: Strain gauge 5

The strain of the skin strain gauge 6 was overestimated by FE analyses in Figure 96. However, it is visible that the sudden drop of the tension strain at the actuator displacement of 133 mm from the testing. Moreover, the sudden reduction of the tension strain from FE analyses was anticipated after 160 mm of the actuator displacement.
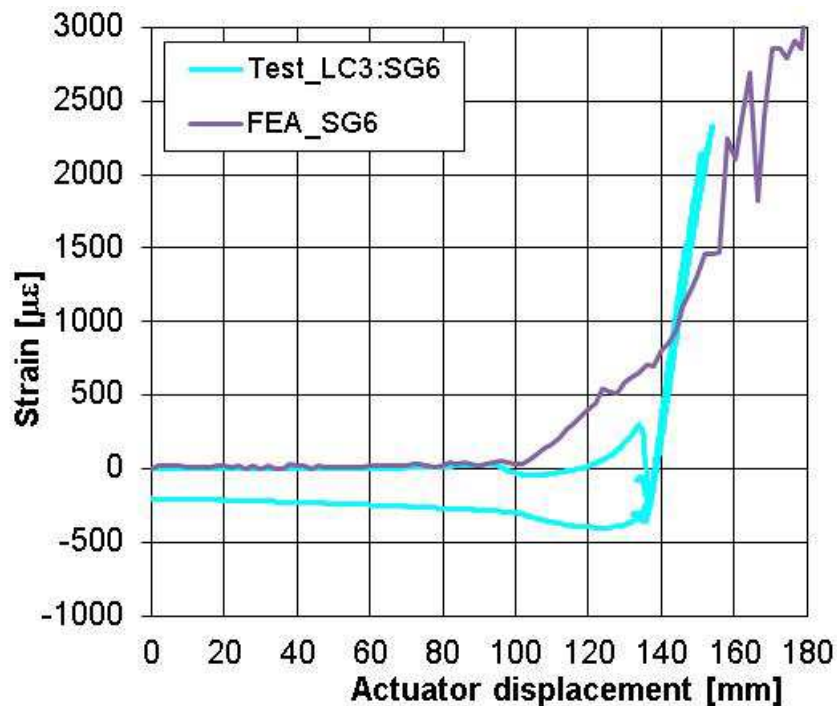
Figure 96. Test and FEA: Strain gauge 6

The strains of the skin strain gauges 7 and 8 slightly deviated from the FEA prediction, as shown in Figure 97 and Figure 98. The FEA underestimated the load for the sudden strain change.
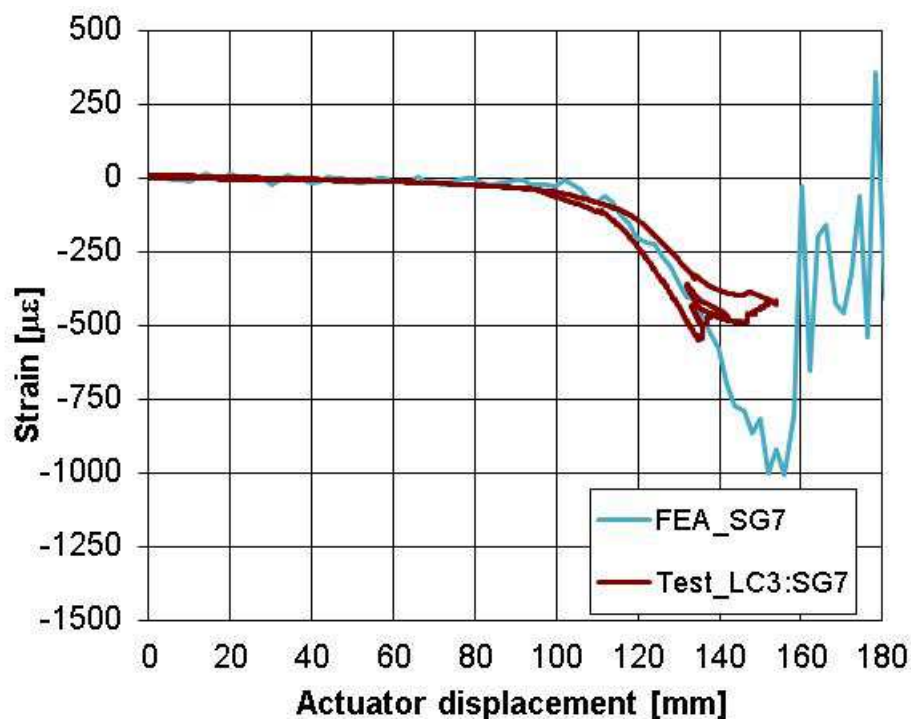
Figure 97. Test and FEA: Strain gauge 7
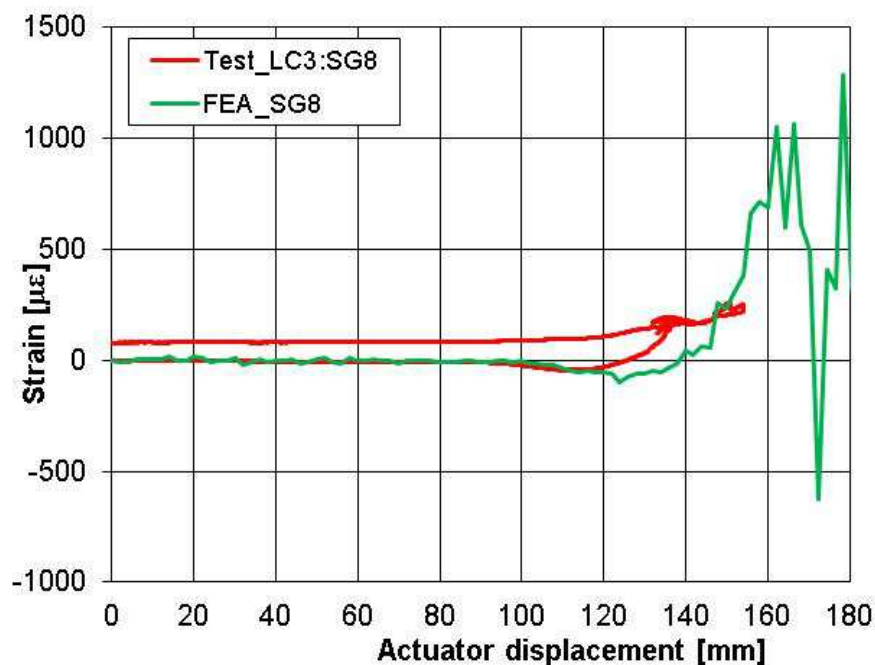
Figure 98. Test and FEA: Strain gauge 8

The strains of the strain gauges 9 and 10 at the stringer were underestimated by FE analyses (see Figure 99). Strain gauge 9 was positioned in the stringer flange and strain gauge 10 located in the stringer cap. Before the actuator displacement of 158 mm, FE analyses predicted small compressive strain. From the reading of strain gauge 10, the stringer cap was experiencing from compression to tension at the actuator displacement of 112 mm.
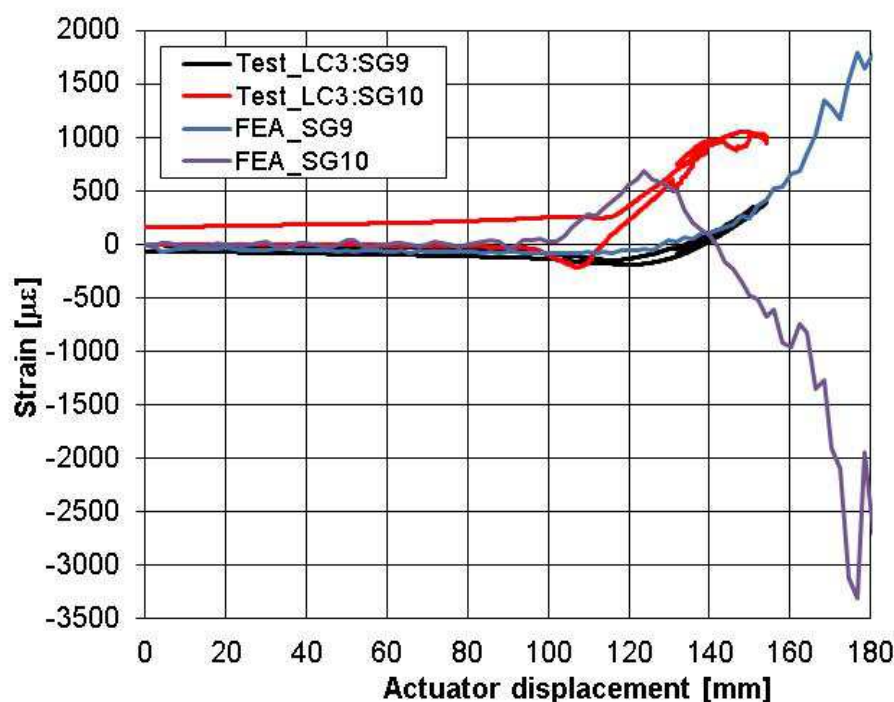
Figure 99. Test and FEA: Strain gauges 9 and 10

The strain gauges on the flanges, in the centre region of frame 3, which are all aligned in circumferential direction, show general good agreement between the test and the FEA in Figure 100 - Figure 107. It is interesting to note that the predicted strains of the inner flange in the thinner frame thickness (0.1 in) zone (SG11-12, 15-16, 19-20) were slightly underestimated, while the strains in the reinforced parts were slightly overestimated (SG23-24) by the FE analyses. However, the predicted strains in the outer flange (SG13-14, 17-18) showed the same tendency in terms of the structural response. Moreover, the predicted strains of strain gauge 25 and 26 were taken from an element in the transition region from 0.15 in thickness to 0.2 in thickness where the element size in the FE model is 15 mm. For these reasons, the measurement from test deviated from the FEA prediction as shown in Figure 107. Generally, the FE analyses were able to predict the results accurately.

The strains in the boundary region of frame 3 are represented by the FEA (Figure 107) and proven to be very low in comparison to the test field in the centre of the panel. The different regions with varied thickness were illustrated in Figure 17.
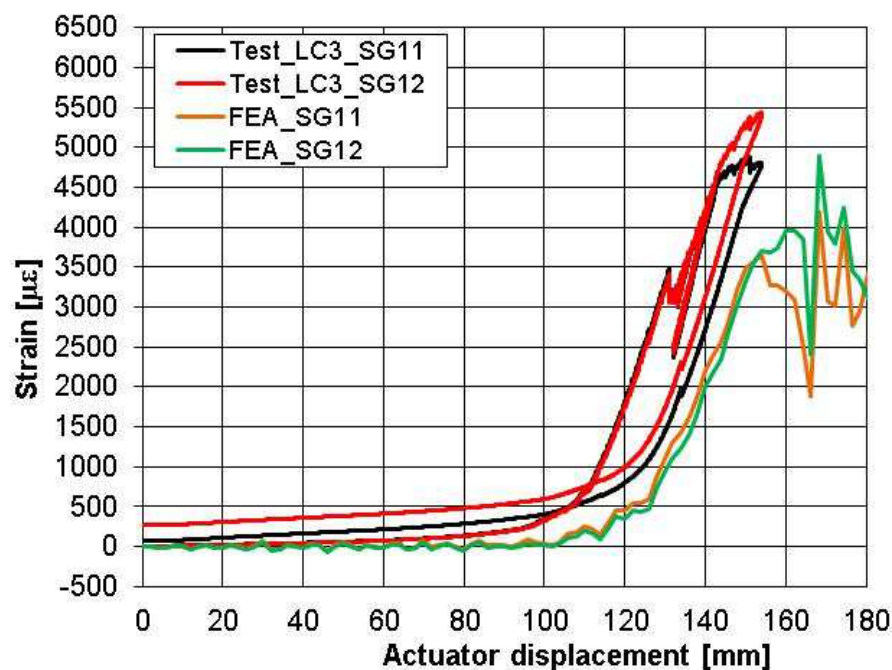
Figure 100. Test and FEA: Strain gauges 11 and 12
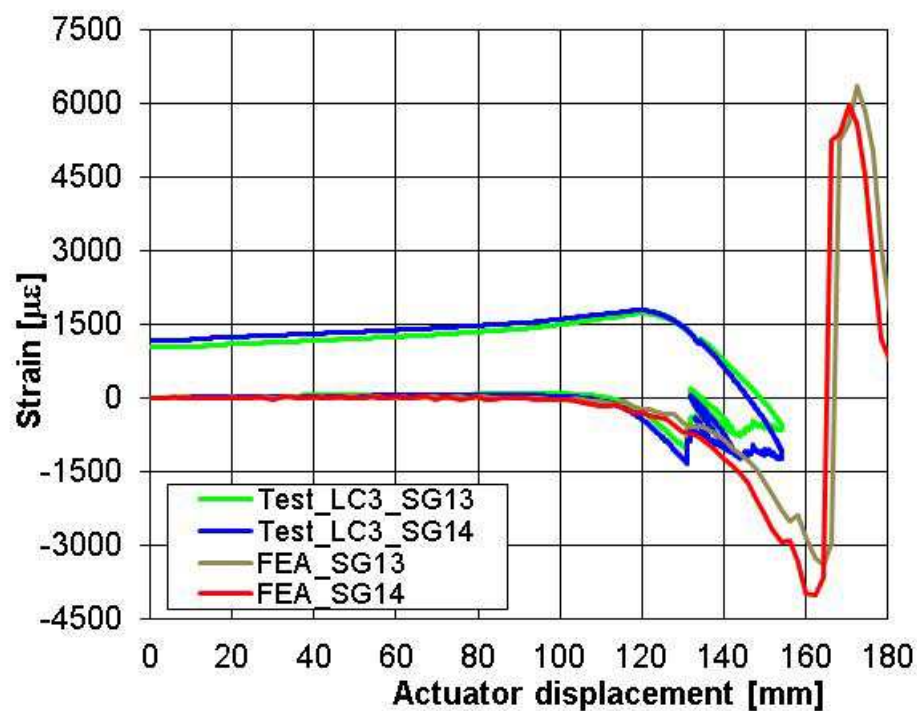
Figure 101. Test and FEA: Strain gauges 13 and 14
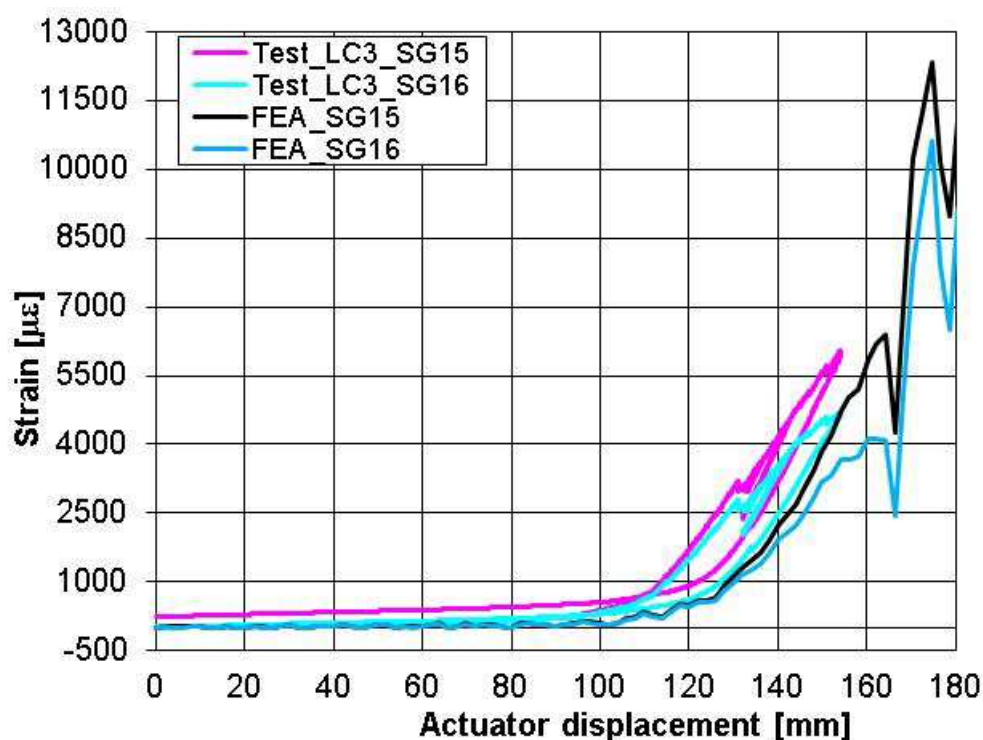
Figure 102. Test and FEA: Strain gauges 15 and 16
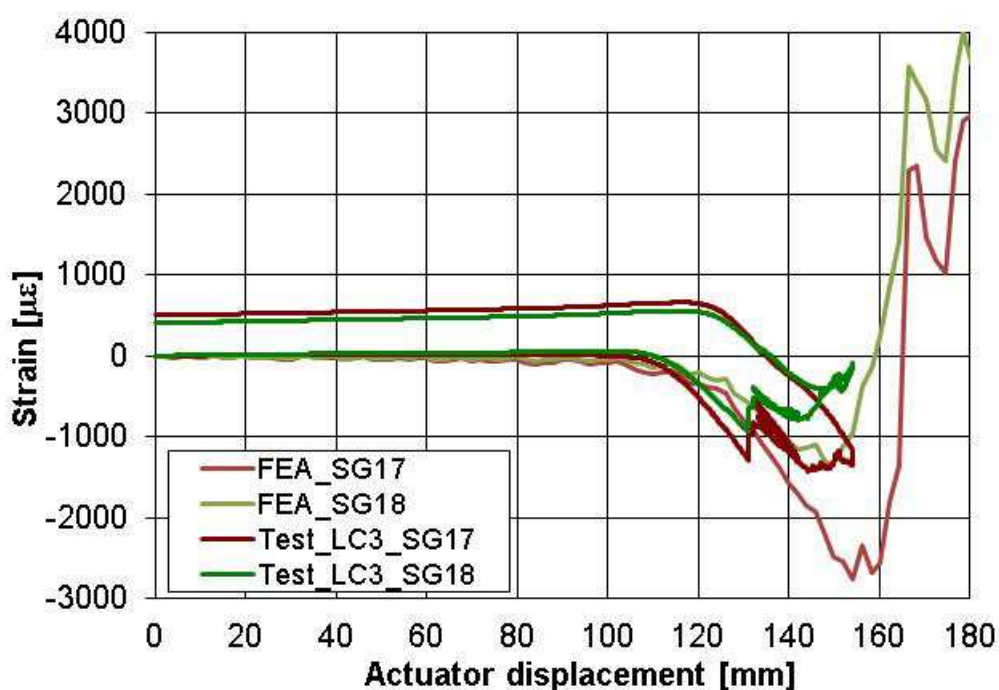
Figure 103. Test and FEA: Strain gauges 17 and 18
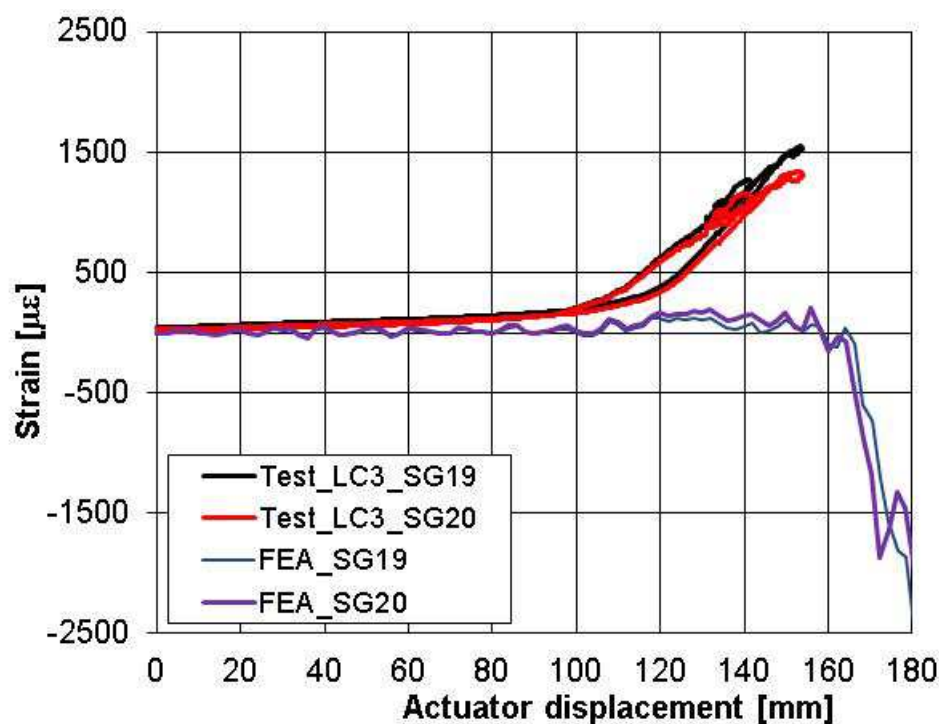
Figure 104. Test and FEA: Strain gauges 19 and 20
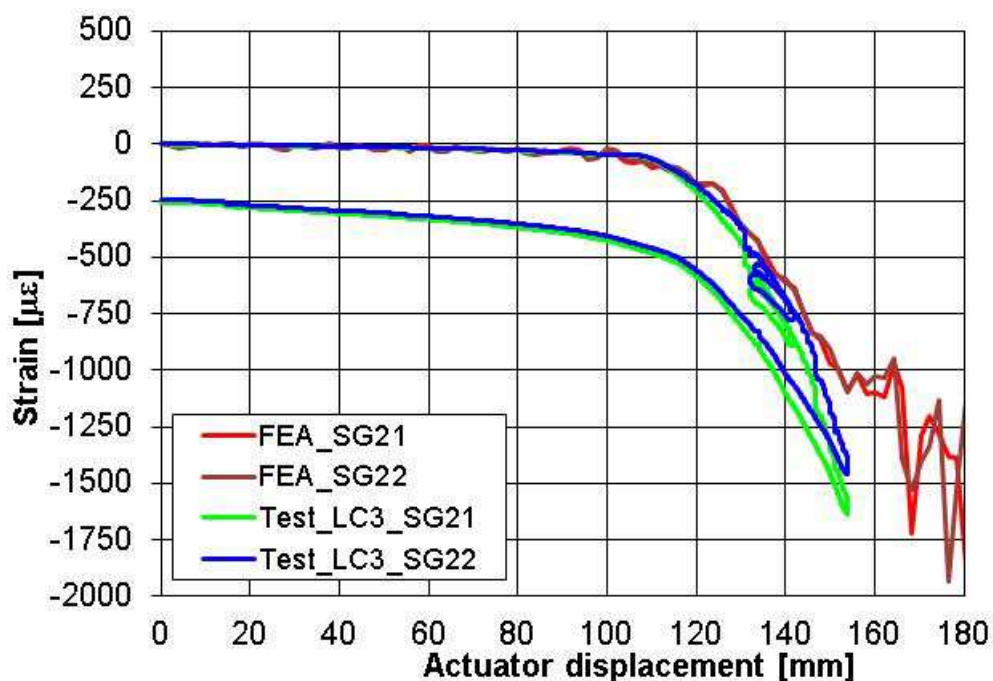
Figure 105. Test and FEA: Strain gauges 21 and 22
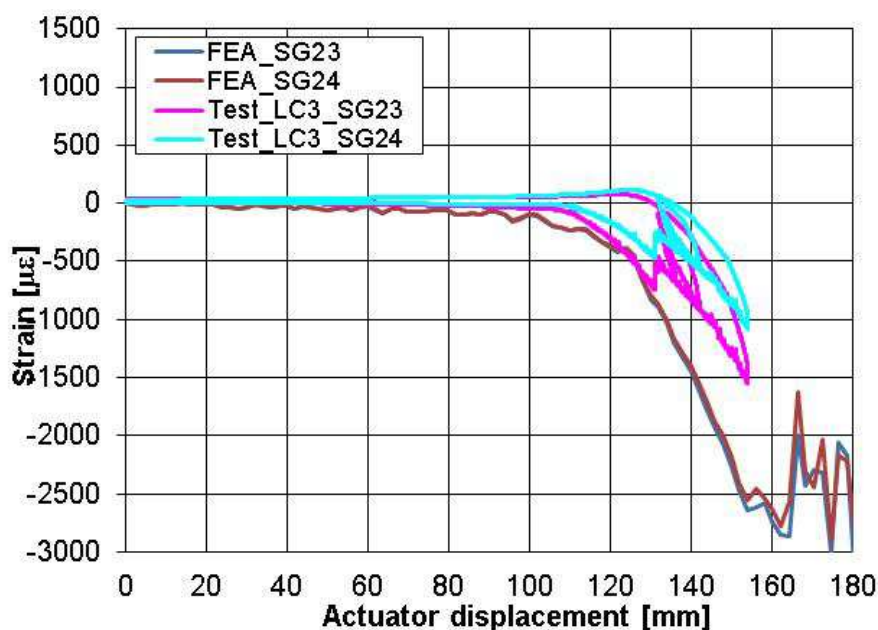
Figure 106. Test and FEA: Strain gauges 23 and 24
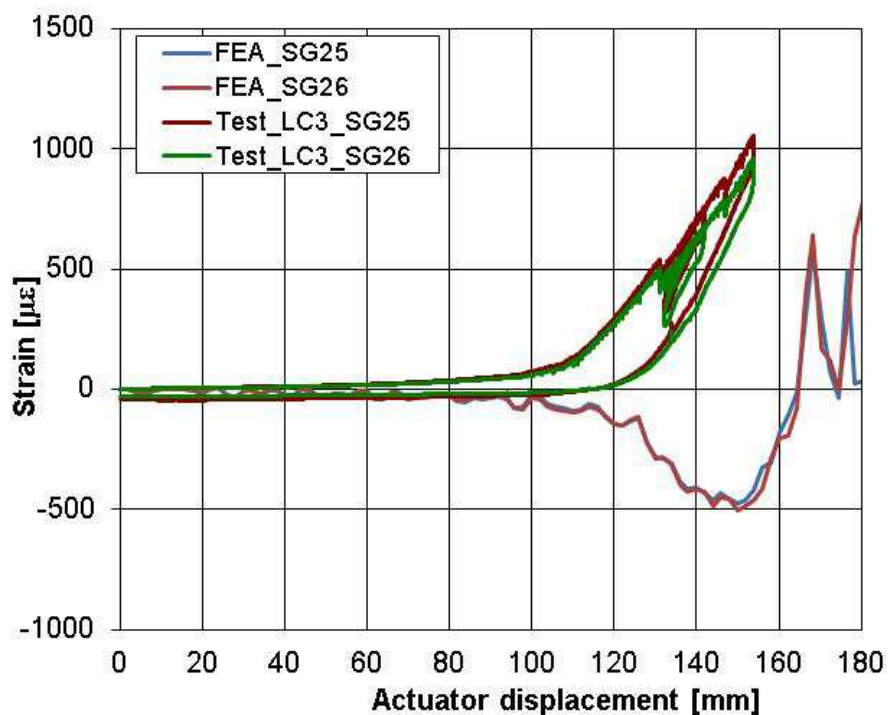
Figure 107. Test and FEA: Strain gauges 25 and 26

The strain gauges applied in the radial direction on the flanges of the two shear ties ST3.3 and ST3.4, reflect the observed bending in both the test and the FEA readings (see Figure 108, Figure 109). The strain level is in line with the FEA at these positions, although the post shear tie failures were not

observed from tests. This might be related to the high deformation level in combination with damage sequences in these regions and the limitation of the single element outputs from the FEA.
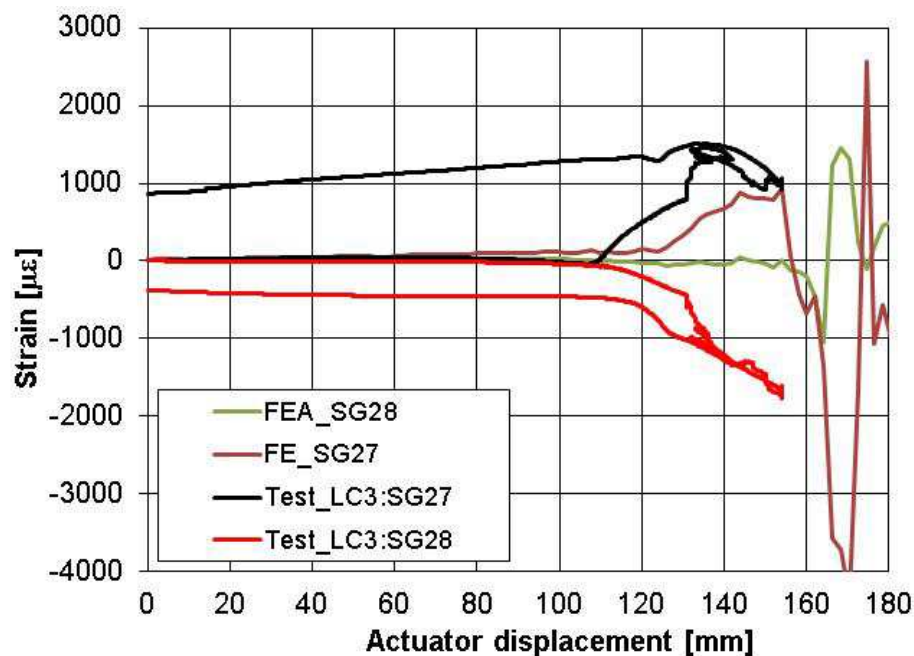
Figure 108. Test and FEA: Strain gauges 27 and 28
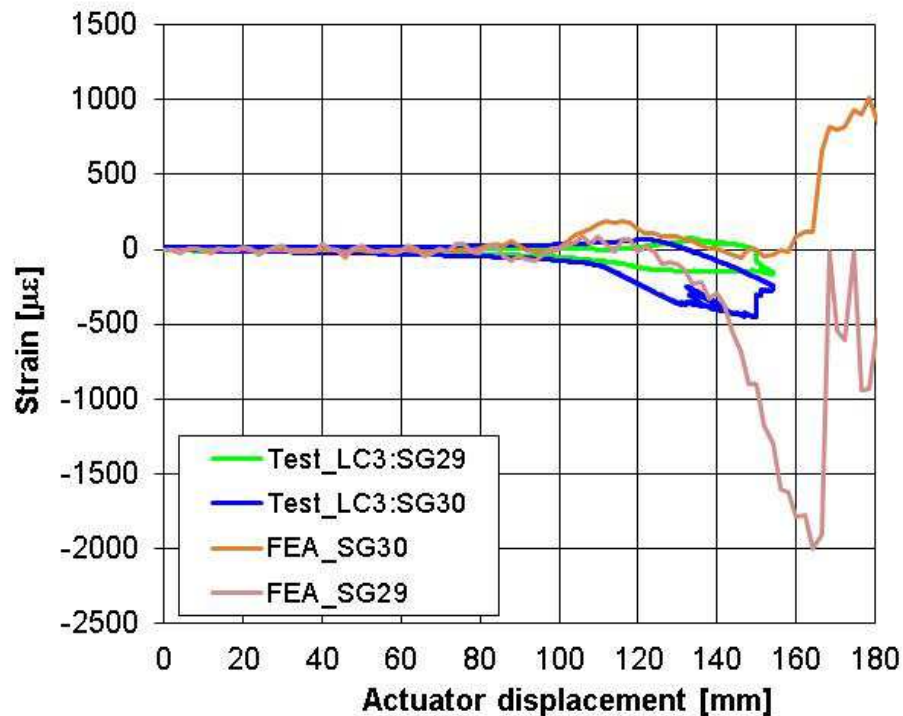
Figure 109. Test and FEA: Strain gauges 29 and 30

For a direct comparison of the strains that were measured in the test and in the FEA, the strains at the maximum load that was reached in the test are plotted at their respective position on the panel. The strains that were measured on the skin inside and on stringer 3, give a differentiated picture. Since the mesh of the FE model was not adjusted to provide nodes at the exact positions of the strain measurement, the accuracy of the strains that were extracted from elements or as interpolated output from nodes, was limited. The highest strain in the skin was measured in the impacted skin bay between the frames 3 and 4 and between the stringers 2 and 3. The skin crack was indicated by the strain reading from strain gauge 5 at the 3200 µm, between frames 4 and 5 and between the stringers 2 and 3.

This circumferential strain was underestimated by the FEA while the axial strain was well represented. The strains in the skin bay between the frames 4 and 5 and between the stringers 2 and 3 indicate a slightly different shape of the zones of circumferential skin bending outside the impact region, between the test and the FEA. While the axial component in the test shows compression that indicates a higher level of bending, the whole skin bay is under tension in the FEA and therefore undergoes less bending. The strain gauges between the stringers 3 and 4 show a similar behaviour in circumferential direction.

The axial strain on the top of stringer 3, under frame 3 shows only a short phase of compression in the test, before it undergoes more significant tension. This position stays under tension in the FEA. The strain measurements from the test in the stringer flange showed good agreement with FE analyses.

The strain measurements at the flanges of frame 3 and at two shear ties attached to frame 3 show a good agreement between the test and the FEA. The main deviation for this group of strain gauges is the different bending behaviour of the two shear ties. The bending tendency for the strain gauges 11-22 is the same, while the bending tendency near the frame clamping area for the strain gauges 23-26 is the opposite. Yet the strain levels are increasing at a lower load level in the test. As the shear tie buckling and failure, which was directly predicted by the strain measurements in the shear ties, were represented by the strain change. These results were found to be overestimated by the FEA, the damage behaviour of the centre shear ties was found to be not identical.

6. Residual Strength Analysis

The goal of EASA CODAMEIN III Program is to develop a verified nonlinear structural analysis methodology for stiffened structures with damage and subjected to axial compression and shear loading. The approach to accomplish this goal has been to: develop modelling strategies required to represent the damage modes after impact tests; develop material and geometric nonlinear shell analysis capabilities and conduct nonlinear analysis of stiffened shells subjected to mechanical loads.

The present work is concerned with the residual strength and with the determination of degraded stiffness and stresses for the damaged panel with respect to the undamaged state. From the testing results as shown in Figure 78, the three shear ties in the center were completely damaged so that in the current finite element model, the center three shear ties are removed in order to investigate the residual strength of panel after impact. The undamaged model is equivalent to the intact model as a reference later and the model with removed three shear ties is regarded as damaged model in the current study. Bending load should be modelled in a simplified way which might represent a maximal vertical bending of a fuselage, so that the panel is subject to longitudinal compression (as might be experienced in dynamic landing when cabin is unpressurised).

Compression loading case:

The translational and rotational displacements on the skin and the stringer (feet and hat) in circumferential direction are clamped, while at the opposite side, the compressive loading in longitudinal direction is applied in the skin and stringer feet. Furthermore, the potting constraints of displacements in the radial and circumferential direction ensure even application of the compressive load. Both free edges of the skin panel are supported by constraining the circumferential displacement and rotation around the longitudinal axis. As the first step, the eigenvalue analysis is performed for both undamaged and damaged finite element models. At the free end of the panel, 2.5 mm compressive load is applied to investigate the load level when the skin panel buckles. The buckling displacements for these two models are reported in the table below.

Table 12. Eigenvalue analysis for undamaged and damaged models under compression

	Undamaged model	Damaged model
Buckling displacement	0.429 mm	0.430 mm

The typical buckling mode 4 from the intact model and buckling mode 5 from the damaged model are illustrated in Figure 110. The nonlinear calculation considers the failure behaviour and the results are

presented in Figure 111. The buckling displacement of 0.43 mm corresponds to the buckling load of 88 kN. The pre-buckling stiffness is equal to 220 kN/mm in the linear stage. The loading and displacement is measured at the free edge of the panel.
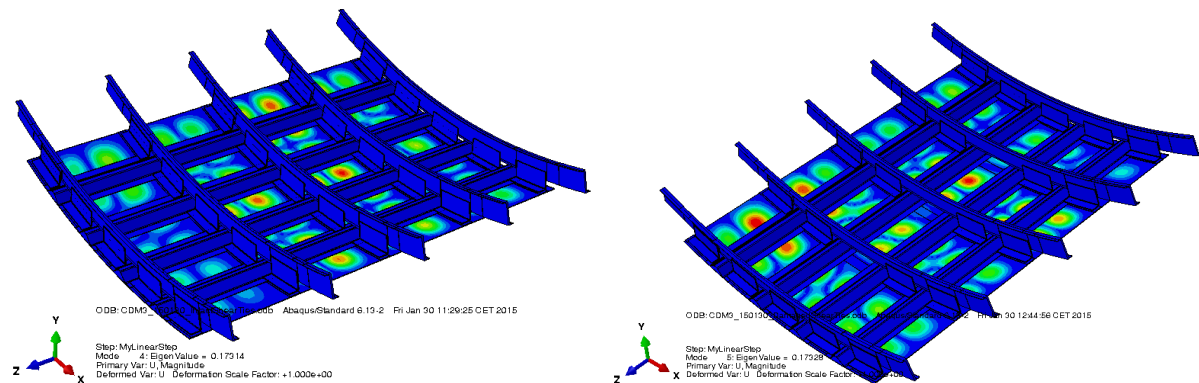
Figure 110. Buckling mode shapes in the skin-inner surface: undamaged model (left); damaged model (right).
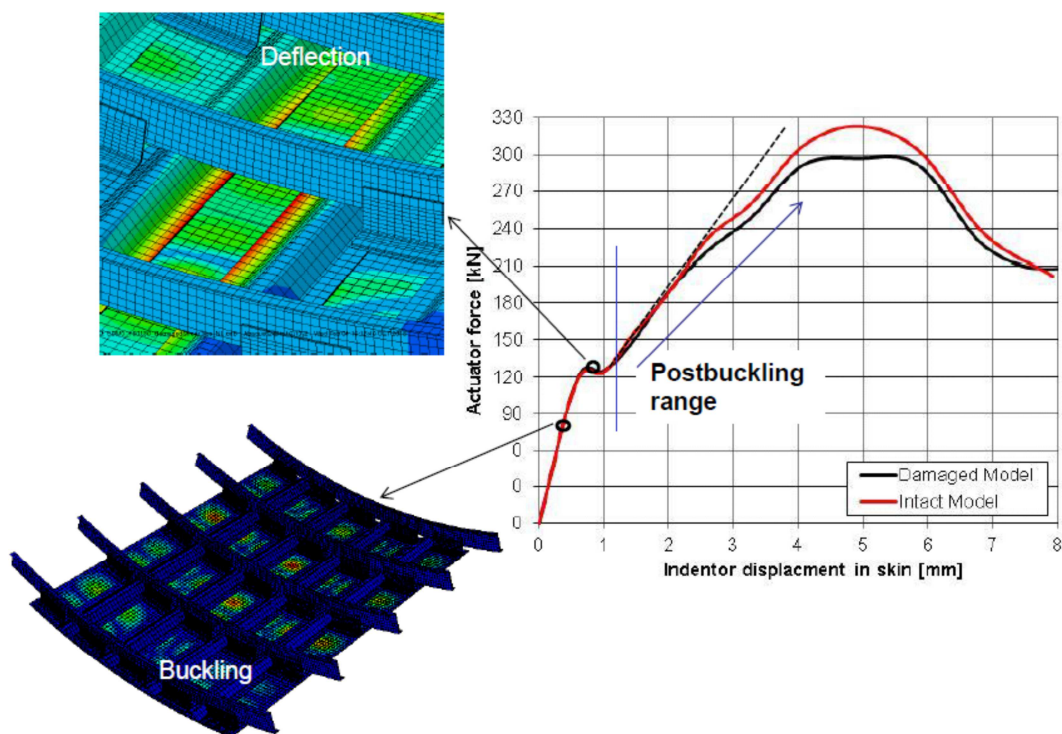
Figure 111. Load-shortening curve under pure compression

As a further explanation, the skin buckling initiates at the load level of 88 kN and local buckling cross the whole skin area, as shown in Figure 111. With the increasing load at the free edge, the stringer feet started to debond from the skin surface mainly in the middle two stringers as highlighted in the curve at the load level of 125 kN, as illustrated in Figure 112. Meanwhile, the skin exhibits the overall buckling and it is obvious to observe the reduction of stiffness. After this event, the load is redistributed entirely in

the substructure and the panel is still capable to carry more loads. The stiffness increases again after the load redistribution and the panel therefore undergoes post-buckling deformation. Up to the load level of 195 kN, the damaged panel collapse earlier than the intact panel due to the collapse of substructure (shear ties). If 1.5 is taken as the safety factor, it is indicated that the panel is safe for the load level of 83 kN as a limit load. It is also reasonable that it generally does not allow the panel to buckle before the limit load. As the further discussion

a)   *b)*   *c)*
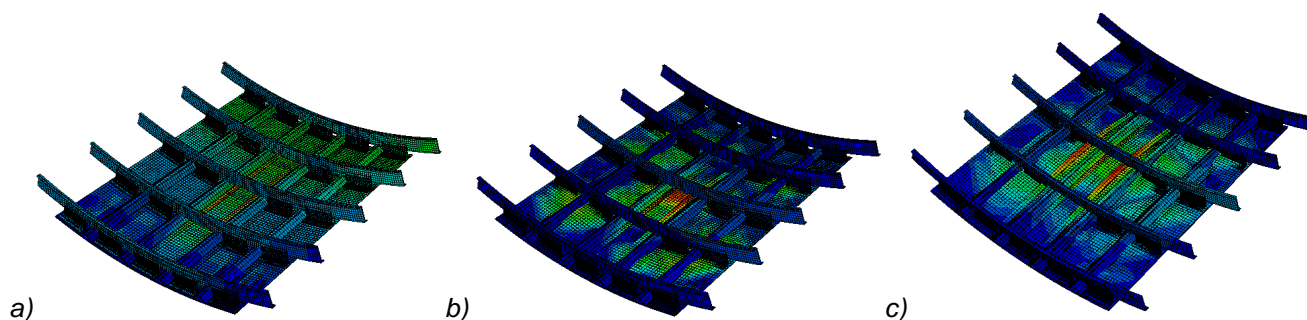
Figure 112. Deflections of the panel at different load levels: a) 88 kN; b) 125 kN; c) 292 kN

7. Discussion of the Results

A summary of the failure progress is provided in Figure 113. Failure initiated in the radius of center shear tie 3.3. With the increasing loads, widespread delaminations formed in several shear ties in the center radius region. A slight loss of stiffness was caused by the accumulated damage both in the shear ties and skin. Finally, the shear ties were completely cracked at the actuator displacement of 154 mm, when the test was stopped since the shear ties were not able to carry any more load. This was exactly monitored during the test through the strain gauge reading.
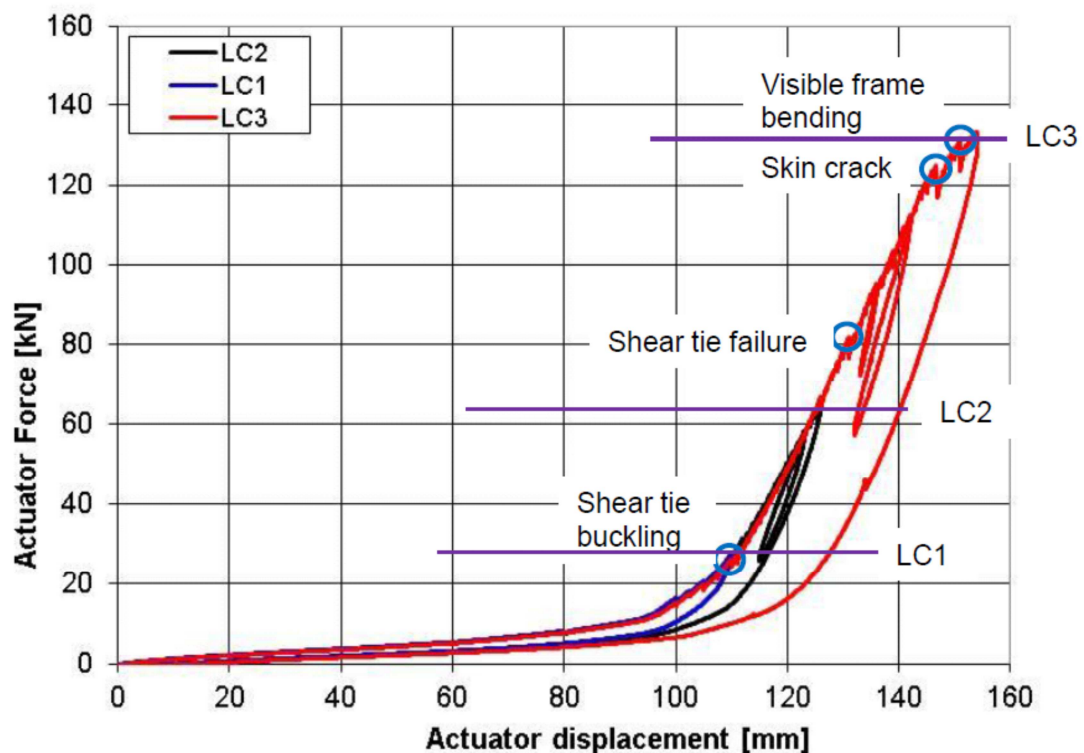
Figure 113. Damage progression during testing

The impact energy levels achieved in the three performed load cycles are reported in Table 13.

Table 13. Energy levels of three load cycles

	1st **Load cycle**	2nd **Load cycle**	3rd **Load cycle**
Maximum energy of three load cycles	726 J (end of load cycle)	1445 J (end of load cycle)	4319 J (end of load cycle)

Moreover, beyond 152 mm, the skin cracked on the outer surface with visible fiber damage. This damage is regarded to be clearly visible, its development in relation to the internal "non-visible" damage is based on the following observations made during the testing:

- After 2nd load cycle up to 66 KN external load, NDT inspection provided no indication of damage in this location.
- Therefore, this crack occurred during the 3rd load cycle.

Based upon strain measurement of SG6 (100 mm distance from crack location, see Figure 114) and nonlinear calculation, the damage development in this location can be summarized as follows:

- onset of elastic buckling at 27.6 kN load level
- Shear tie cracking at 82.1 kN
- skin crack at 125 kN (first sharp of SG6 reading in Figure 96 followed by load reduction)
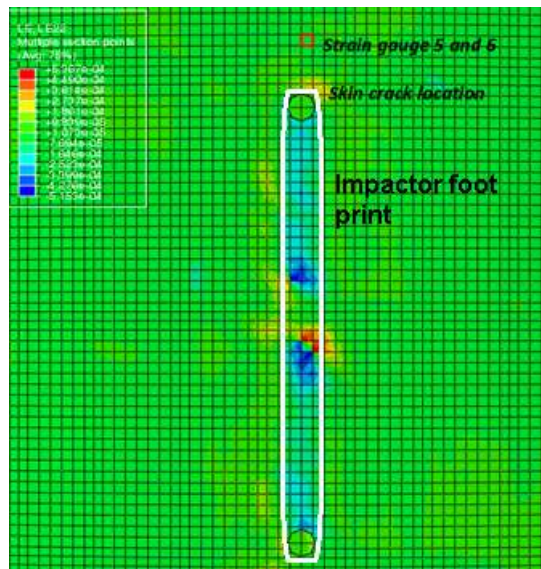
Figure 114. Skin crack, bolt and strain gauge locations

The strains of SG6 rose sharply to 2200 µm in a very high gradient, due to good correlation with the FEM, the crack position was also found in the finite element model. Skin strain beyond 6000 µm that is above its normal capability. The crack was considered to have been caused by a sharp stiffness change in the structure (pure skin to skin with substructures, shear tie and frame).

Moreover, the bumper attachment bolt also contacted the skin, resulting in high stress concentrations in the skin impact region.

The crack depth of 2.53 mm in skin damage I indicated the crack had not progressed fully through the skin thickness 2.69 mm. In this case, it can be inferred that circumferential inner skin layers are still intact.

8. Conclusions

The three phases of the CODAMEIN project have investigated the effects of ground service equipment impacting the new hybrid fuselage construction used in CS-25 aircraft. Such events usually transferred some typical phenomena to the ground crew, (i.e. loud or unexpected aircraft movement, etc.), and it should be reported immediately. In case of missing reporting or the ground crew neglected those impact effects due to no external visibility, high energy low velocity blunt impact can initiate significant internal damage that may not be detected by visual inspection of external surfaces. Therefore, it is important to demonstrate the safety level in the design change from metallic to advanced composite structures in order to detect such an event earlier and adapt the appropriate maintenance and operational procedures.

The panel design showed the good compromise in terms of realistic representation of a typical CS-25 fuselage construction harmonized with the research activities of UCSD. A hybrid composite-metallic test panel consisted of four stringers that were co-cured to the curved skin panel and five metallic frames. It is regarded as an intermediate pyramid level and it is recognised that higher pyramid testing is required to capture more realistic boundary condition in conjunction with the representative damage mechanisms.

The CODAMEIN III fuselage panel test set up introduced load via an external vertical low velocity high mass impactor, which was similar to previous test set-ups of the CODAMEIN I and CODAMEIN II test. Evaluating all aspects of the different test methods, the quasi-static displacement controlled test was selected for the three series of CODAMEIN tests. This method was in agreement with the existing research program and due to enhanced control of test parameters and simple damage monitoring solutions, involved relatively low project risk. Moreover, a design with stiffer shear ties is introduced for the CODAMEIN III panel in agreement with EASA in order to investigate potentially different failure modes, in line with UCSD. The stiffness of the spring arrays within the test fixtures was increased to 9.5 kN/mm at each of the five frames instead of three. Additional rotational stiffness 1.36e8 N*mm/radian was also introduced to both frame ends. This approximate value has been chosen by accessing the real fuselage case and budget limitations for the test fixture.

The maximal load applied during testing was intended to cause initial, non-catastrophic failure of the panel, while retaining the capability of the structure to carry more loads. In order to avoid damage in the panel caused by contact of frames and stringers as a result of shear tie failure, the test was stopped at a state where complete shear tie damage is noticed, yet prior to overall structural failure. Following the reduction of the external load, the panel relaxed fully to its original shape without visible failure on the

surface except for a small crack on the skin surface outside. Therefore, damage with low external visibility was generated in the test panel.

The test confirms the expected general behaviour. Compared to the CODAMEIN II test, the early damage events (shear tie failure) were recorded at higher loads (82.1 kN) due to the improved boundary stiffness and shear tie reinforcement. Cracks were mainly generated in the centre shear ties of the three inner frames and delamination was detected in the outer shear ties. The visual inspection, the NDT scans and the instrumentation readings provides the detailed structural behaviour. In accordance with the UCSD research, the similar failure was found to be the shear tie damage which failed first. However, UCSD panels showed severe contact between the stringer and frame due to the failure of shear tie, but the inner frame of CODAMEIN III rotated with plasticity and did not get in contact with the stringer.

The energy levels 726 J, 1445 J and 4319 J were reached at the end of three load cycles, respectively. The shear tie failure was found in the 3rd load cycle at the energy level of 2020 J. The review of the actual incident data and previous test results supported the determination of reasonable failure energy threshold boundaries for high energy blunt impact which was estimated in a range between 1000 J and 3000 J. These failure threshold levels are above the energy levels considered typical of such impact events in design.

Moreover, the FEA results of CODAMEIN III correlated with the testing in an acceptable way. In particular, the predicted shear tie failure load varied from the test results by only 6.8%. The LVDTs and strain gauge predictions show good agreement with the test results. Deviations between the testing and finite element analyses could be attributed to limitations of finite element models. It can be concluded that the FE modelling is able to predict the structural behaviour accurately. In this case, the changed boundary conditions improve the correlation between the panel and barrel. Based on the results of CODAMEIN I, CODAMEIN II and UCSD tests, it provides valuable information about the range of applicable boundary conditions. The objectives have therefore been fulfilled.

Possible Interpretation of CODAMEIN relative to current certification expectations and robust design practice - based only upon the configuration used in this study and the associated results:

Comparing the CODAMEIN I, II, & III results, as reported in Table 7 and Table 8, with certification reference points, it should be noted that, largely as determined by a process of 'reverse engineering' from the existing metallic fleet [18], high energy impact events with impact energy larger than 140 J occur at a failure rate $< 10^{-9}$ per flight hour and represent the limit of typically current certification expectations (although significantly higher energies (larger than 200 J), have been considered at

frequently impacted locations for existing projects in order to provide further confidence regarding the design of a robust structure).

It is noted that the lowest damage initiation energy recorded during phase I, II, or III, i.e. 969J, is significantly above the energy level expected at 10^{-9} per flight hour, i.e. it is very unlikely, but it is not externally visible if it does occur. However, also noting that such impact events can, and do, occur, this project also suggests that a blunt impact energy larger than 2000 J could become externally visible. Therefore, if this test panel formed part of an aircraft level structure, such that the damage between 969J and 2000J resulted in internal damage which was only visibly detectable by internal inspection, and this resulted in residual strength capability below UL (but > LL), then this could potentially be addressed by some adaptation of AMC 20-29 category 2 damage tolerance.

9. Recommendations

As concluded from all test cycles within CODAMEIN I, CODAMEIN II and CODAMEIN III, different aspects of panel reactions were found with respect to the geometry of the specimen. What was not changed from one to the next test was the impactor size and the static test approach meant with different cycles and load intensity.

A general outcome is that a threshold of visible and non-visible damage on the outer CFRP skin surface can be generated for a particular impactor load level.

The CODAMEIN III test was performed in three load cycles increasing the external load from 27.6 kN in the first load cycle up to 66.2 kN in the second load cycle until specimen failure at 133.5 kN during the third load cycle. The first two load cycles could be performed without any damage inside and outside the specimen while the impactor elastically deformed the skin and internal structure approximately 18 mm.

Reviewing all tests that have been performed, is there a dependency on the type of backup structure composition?

Examining the events facing the different geometries and materials of the backup structures (shear ties thickness, frame material and geometry), there is a substructure failure intensity depending on its strength.

Normally built structures in areas where ground service equipment (GSE) will collide with the aircraft are typically strong due to its lower fuselage area, which must also withstand high ground/flight compression loads mainly in the aft fuselage (location of bulk and cargo). This structure has been tested within the CODAMEIN work packages.

It can be observed that the shear tie strength versus frame, its geometry and capability to prevent frame tilt is vital. Specially, the CODAMEIN I shear tie (2.5 mm) collapsed at 46.7 kN of the 2nd LC, CODAMEIN II shear tie (2.5 mm) collapse at 39.5 kN, while the CODAMEIN III shear tie (4.7 mm) collapsed at 82.1 kN. The strength of the fastening also plays an important role. The carbon frames tested by UCSD crack, while metal frames tested in CODAMEIN deform plastically.

There is also a clear influence how the frame lateral movement is supported or better prevented to move. Typical fuselage structures include structural elements build in, so called cleat elements, to support the frame against tilting. These have not been included in the test specimens.

To understand how this will change the capability, a deeper investigation is needed to clear the structure health against external collision. Two different events should be considered:

1. Collision of a GSE with a certain threshold that results in no visual damage can be detected on the outer surface while:
   a. Fully intact substructure remains (CODAMEIN III first and second load cycle)
   b. Entire delamination / failure of inner elements (CODAMEIN II)
2. Collision of a GSE at a higher velocity incurring a small visible surface scratch but significant inner structure failure as per CODAMEIN III third cycle.

There is a question of the airframe residual capacity in cases where a collision has occurred but not detected or declared by the crew or ground service people, which means the plane will continue to fly.

No catastrophically failure can be evaluated on basis of:

1. Analysis implementing different grades of substructure residual capacity using the test results of CODAMEIN I, CODAMEIN II and CODAMEIN III detected delaminations and part failures.
2. Analysis investigating the influence of different types of structure elements (cleats, shear ties, frame profiles material and part thicknesses).

A first analysis on basis of a full fuselage barrel, representing the part of the aft fuselage wide-body airframe to be evaluated containing the test panel with all effects of defects using NL-FEM.

A second analysis on basis of the NL-FEM analysis should be conducted on a panel that correlates with test readings as such of strain and displacement implementing different types substructures and materials. The results from this analysis can be used to create a sort of tabular that demonstrates impact velocity against failure threshold.

The CODAMEIN III work package put us into the position to be ready to investigate such questions, based on the demonstrated correlation between NL-FEM and test in terms of overall structural response and failure prediction. This subject area is worthy of further study, and the next logical step would be to investigate a half barrel.

Furthermore, NL-FEM shows good conformity of representing a local structure part that behaves similar as a full size fuselage barrel, through the appropriate definition of the panel boundary conditions.

Recommendations relative to current certification expectations and robust design practice – based upon the configuration used in this study and the associated results:

Building upon the principles of AMC 20-29, and other philosophies which may help to ensure that a design is robust, e.g. the need to show that appropriate residual strength can be maintained following a 2 frame bay and frame notch damage or a single disbonded stringer between arrest features etc, a

structure which, when subject to blunt impact with a 1000mm long 180mm diameter impactor (or impactor geometry, as appropriate to the structure and impact threat being considered) could be expected to show that it:

- generates dominant and predictable internally visible damage mode(s) in the internal structure directly under the external contact area of the impactor dimensions (as determined by test or analysis supported by test)
- retains >LL when damaged as described above
- shows no damage growth during a substantiated inspection period

Although this would not address structures with local strong design details at the impact locations which could displace damage initiation to other remote points in the likely impact load transfer path, it could provide a book case reference point which would help to increase confidence regarding the design of a robust structure.

10. References

[1] Bishop, P. CODAMEIN II (Composite Damage Metrics and Inspection), EASA-funded research project, Aerospace Structural Impact Dynamics International Conference, Wichita, 6-9 November 2012.

[2] Bishop, P. CODAMEIN II (Composite Damage Metrics and Inspection), EASA-funded research project, 14th Annual Ground Handling International Conference, Milan, 26-29 November 2012.

[3] Bergo Soto, R. Non-destructive Testing Inspection Report, Report No. 14/31706675, 8 October 2014.

[4] EASA Certification Specifications: General Acceptable Means of Compliance for Airworthiness of Products, Parts and Appliances, AMC 20/6, Annex II- AMC 20-29, 26 July 2010.

[5] Hernandez, O. Proposal for "Testing of the CODAMEIN III Panel", Offer Ref. 2013_5810209430_ACB_347, Issue 5, 15 Jan 2014.

[6] Hernandez, O. Applus LGAI Mechanical Testing Laboratory, Fcilities Breakdown, 2012.

[7] Haase, P. Composite Damage Metrics and Inspection (CODAMEIN II). EASA.2011.NP.24, Final Report, 14 February 2013.

[8] International Air Transport Association: Ground damage prevention programme targets 10% cost reduction, Industry Times, Edition 7, Article 4, September 2005.

[9] Kim, H. Impact Damage Formation on Composite Aircraft Structures. FAA Joint Advanced Materials & Structures (JAMS) 6th Annual Technical Review Meeting, Seattle, WA, 19-20 May 2010.

[10] Kim, H. Impact Damage Formation on Composite Aircraft Structures. FAA Joint Advanced Materials & Structures Center of Excellence Meeting NIAR/WSU, Wichita KSTechnical Review Meeting, Seattle, WA, 21-22 July 2010.

[11] Kim, H, DeFrancisci, K.G, Chen, Z.M., Rhymer, Delaney M., Le J. Impact Damage Formation on Composite Aircraft Structures, FAA (JAMS) 2013 Technical Review Meeting, San Diego, CA, Everett, WA, 09-10 April 2013.

[12] Kim, H, DeFrancisci, K.G, Chen Z.M. Ground vehicle blant impact damage formation to composite aircraft structure. *Advanced Composite Materials*. Vol. 23, No. 1, pp. 53-71, 2014.

[13] Mikulik, Z., Haase, P. CODAMEIN (Composite Damage Metrics and Inspection). EASA.2010.C13, Final Report, 31 Jan 2012.

[14] Mikulik, Z. Blunt Impact on Composite-Metallic Aircraft Structure: Overview of the EASA / Bishop GmbH Research Project, 2011 FAA / EASA / Industry Composite Transport Fatigue, Damage Tolerance, Maintenance & Crashworthiness Workshop, Atlanta, 18 May 2011.

[15] Mikulik, Z. Damage Criticality and Inspection Concerns of Composite – Metallic Aircraft Structures subjected to high Energy, low Velocity Blunt Impact, 4th European Conference on Materials and Structures in Aerospace, Hamburg, 8 February 2012.

[16] Pringle, T. Preventing ramp and ground accidents, Transport Canada, 2010. www.tc.gc.ca

[17] Zou, D. EASA.2013.OP.12 "Composite Damage Metrics and Inspection (CODAMEIN) III - Test Plan". 19 September 2014.

[18] Composite Materials Handbook 17 (CMH-17). Volume 1, 2. https://www.cmh17.org/

Appendix A   Hardware, Software

- Abaqus 6.13-2 CAE, Abaqus 6.13-2 Explicit solver

- Analyses on HP LP2065 Linux workstations Intel® 4 AMD Xeon® CPUs, 24 GB RAM

- Analyses time of the panel model: minimum 54 hours

Appendix B   Drawing

EASA

European Aviation Safety Agency